PHOTOLUMINESCENCE STUDY OF ZnO DOPED WITH NITROGEN AND ARSENIC

JULIEN KOUADIO DANGBEGNON

Submitted in fulfilment of the
requirements for the degree of

PHILOSOPHIAE DOCTOR

In the Faculty of Science at the
Nelson Mandela Metropolitan University

January 2010

Promoter: Professor J.R. Botha

Acknowledgements

I would like to thank:

my thesis promoter, Prof. J.R. Botha, for his support, mentoring and the opportunity to work in his group.

the members of the physics department, Prof. A. Venter, and Prof M.C. Magnus for measurements, friendly support, constructive critics, and helpful discussions

Dr. R. Chantelle, for the corrections and helpful suggestions

Prof A.C. Bèye, for opening the door of this great journey

my colleagues, for the great team spirit

my friends and brothers, K. Talla, K.T. Roro, for the optimism, the great support throughout this journey

G. William and O. Jaco, for the SEM measurements

J. Ferreira and L. Kritzinger, for the administrative assistance

Nelson Mandela Metropolitan University (NMMU), the National Research Foundation (NRF) and DAAD, for financial support

my loving wife, Coffi Romance Laure Ophélie, for her patience and great understanding

my families, in Côte d'Ivoire, Benin and Sénégal, for their supports

TABLE OF CONTENTS

LIST OF FIGURES

LIST OF TABLES

ABSTRACT

In this work, the optical properties of ZnO doped with arsenic and nitrogen were studied. The ZnO samples were grown by Metalorganic Chemical Vapor Deposition (MOCVD). The solubility of nitrogen in the ZnO films, as well as its activation upon annealing, was also investigated. Hydrogen is known as a major source for passivation of the acceptors in ZnO:N. Therefore, it is crucial to dissociate the complex(es) formed by nitrogen and hydrogen and diffuse out the hydrogen in order to prevent the reformation of such complexes. High temperatures (≥ 600°C) are required for these purposes. In order to effectively remove the hydrogen impurities from the sample, it is important to know the optical fingerprints of hydrogen and its thermal stability. Therefore, the effects of annealing and hydrogen plasma treatment on bulk ZnO (hydrothermally grown) were first studied. The use of bulk material for this purpose was motivated by the well-resolved photoluminescence (PL) lines observed for bulk ZnO, which allow the identification of the different lines related to hydrogen after plasma treatment. Annealing at 850°C was effective for the removal of most of the hydrogen related transitions in the near-band-edge emission. Also, additional transitions at ~3.364 eV and ~3.361 eV were observed after hydrogen plasma treatment, which were ascribed to hydrogen-Zn vacancy complexes.

In this work, a comparative study of the annealing ambient and temperature on ZnO films grown on GaAs substrate, using diethyl zinc (DEZn) and tertiary butanol (TBOH), showed that arsenic diffuses in the ZnO films and gives a shallow level in the band gap, which is involved in an acceptor-bound exciton line at 3.35 eV. This shallow level is visible when annealing is performed in oxygen, but not when annealing is performed in nitrogen, and indeed only for annealing temperatures around 550°C. However, annealing in either ambient also causes zinc to diffuse from the ZnO films into the GaAs substrate, rendering the electrical properties deduced from Hall measurements ambiguous.

For ZnO:N, NO was used as both oxygen and nitrogen sources. Monitoring the concentration of nitrogen, carbon and hydrogen in the ZnO films, the formation of different complexes from these impurities were deduced. Furthermore, an investigation of the effect of annealing on the concentrations of impurities showed that their out- diffusion was strongly dependent on the

crystalline quality of the ZnO films. For porous ZnO films, obtained at low growth temperatures (≤310°C), the out-diffusion of impurities was efficient, whereas for films grown at higher temperatures, which have improved crystalline quality, the out-diffusion was practically non-existent. The out-diffusion of unwanted impurities may activate the nitrogen dopant in the ZnO films, as was confirmed by the PL measurements on the different samples grown at different temperatures. PL transitions at ~3.24 eV and ~3.17 eV were related to substitutional N_O. These transitions were more dominant in the spectra of samples grown at low temperatures. An additional transition at ~3.1 eV was assigned to a donor-acceptor pair transition involving V_{Zn}, instead of N_O, as previously reported.

1 Introduction

The semiconductor lighting technology is destined for a bright future. In particular, ultra-violet light emitting diodes (UV-LED) are expected to replace the traditional lamps which will reduce the energy consumption by 29 % (1) and will also open the door to many new optoelectronic applications enumerated in ref. 2, such as high-storage capacity optical recording medias (e.g. blue-ray discs), traffic signals, automobile interior panel lighting, high-resolution printers, video game consoles, and biophotonics (2). Already in 2008, LEDs in the UV spectrum were the dominant devices in sub-400 nm applications. More than 90% of the UV LED market was taken up by applications such as UV curing, counterfeit detection, and medical and instrumentation applications requiring UV sources. The remaining 10% was allocated to air and water purification with again a great portion of UV-based LED sources for photo-catalytic air purification (3).

This achievement has been possible due to intensive research undertaken on the crystal growth and conductivity control of large band gap semiconductors for optoelectronic devices, such as SiC (4), III-V (5) and II-VI (6) compound semiconductors. To date, the III-V nitride-based LEDs have been successful due to (i) their high quantum efficiency (35% for InGaN-based LEDs (7) compared to 0.03 % for SiC LEDs (8)) and (ii) the ability of achieving stable *p*-type III-V nitride compounds with low resistivity (9). Besides the III-V nitrides, II-VI oxide compounds continue to receive significant attention due to their low cost of fabrication, high thermal conductance and chemical robustness. In particular, the direct wide band gap semiconductor (3.37 eV at room temperature) ZnO with its high excitonic binding energy (60 meV (10) against 28 meV for GaN (11)), is a unique oxide compound which could be used for brighter LEDs in the blue-UV region. Its high exciton binding energy of 60 meV allows excitonic optically pumped lasing at and even above room temperature [(12), (13)]. Higher exciton binding energies of 90 - 100 meV is achievable by the fabrication of ZnO-related superlattices [(14), (15)]. The possibility of band-gap tuning from 3 eV to 4.5 eV in small lattice mismatched $Mg_xZn_{1-x}O$ and $Zn_xCd_{1-x}O$ alloys, while conserving the ZnO crystallographic structure, has also been demonstrated [(16), (17)]. It is clear therefore, that ZnO and its ternary alloys have the potential to compete with III-V nitrides for optoelectronic applications. However, stable *p*-type ZnO still needs to be proved. In

fact, ZnO is a naturally *n*-type semiconductor due to the high concentration of native donor defects with low formation energies (18) resulting from the non-stoichiometry of ZnO (19) and also due to the presence of the H-related donors in ZnO (20). The *n*-type conductivity of ZnO can also be improved and controlled by doping with Al, Ga and In (19) to improve its *n*-type conductivity. These impurities are present in commercially available sources of Zn and are also incorporated unintentionally during ZnO growth.

The doping asymmetry in ZnO was reported to arise from the low solubility of the acceptor dopants [(21), (22)] and the self-compensation of the acceptor dopants (23). These represent the main difficulties for achieving *p*-type material. Also, doping is known to induce point and extended defects in ZnO that could affect the optical efficiency of the ZnO samples. These different problems linked to the *p*-type doping will be explained in chapter 2.

Since the early 90's (24) to date, despite the efforts dedicated to improve the quality of *p*-type ZnO grown by various techniques, such as pulsed laser deposition (25), molecular beam epitaxy (26), sputtering (27), chemical vapor deposition (28) and metalorganic chemical vapor deposition (MOCVD) (29), the quality of the *p*-type ZnO achieved to date suffers from instability and irreproducibility.

Using the MOCVD technique, highly crystalline and optically efficient *n*-type ZnO has been achieved (30). However, the presence of H and C in most of the metalorganic sources used unfortunately introduce high concentrations of defects related to these impurities into the ZnO films and constitute a major obstacle for *p*-type doping [(31), (32)], especially for ZnO:N. The concentrations of these defects may be controlled by optimizing the oxygen to zinc (VI/II) ratio and the growth temperature. Up to now, only few reports studied the effect of the growth temperature, the VI/II ratio, as well as post-growth annealing on the solubility of nitrogen in ZnO grown by MOCVD.

An element such as arsenic, which has a large size-mismatch with the constituent atoms of ZnO, has been reported as a good *p*-type dopant, by forming the shallow As_{Zn}-$2V_{Zn}$ acceptor complex (33). In particular, post-growth annealing of ZnO grown on GaAs substrate was reported as *p*-type (34), but the electrical properties remain ambiguous, since Zn could also diffuse into the

semi-insulating GaAs substrate, also producing *p*-type conductivity. Such diffusion will also affect the optical properties of the ZnO films.

Moreover, the interpretation of the different photoluminescence (PL) lines appearing in ZnO:N and ZnO:As and respectively assigned to N and As acceptors, is still controversial.

This thesis focuses on the optical properties of MOCVD-grown ZnO/GaAs annealed in oxygen and nitrogen at different temperatures. Also, the effect of the growth parameters (VI/II ratio and the growth temperature) on the solubility of the nitrogen in ZnO films grown by MOCVD, with NO as dopant and oxidizing agent, will be investigated. Furthermore, the effect of post-growth annealing on the activation of the nitrogen-related acceptors as well as on the crystalline properties determining the out-diffusion of unintentionally incorporated impurities such as carbon and hydrogen will be investigated. The activation energies of the nitrogen acceptors will be deduced from the nitrogen acceptor related PL transitions.

The following structure is therefore adopted in this thesis: chapter 2 describes the fundamental properties of ZnO and presents an overview of the doping issues in II-VI compound semiconductors. Chapter 3 deals with the characterization and growth technique used in this study. In chapter 4 the optical properties of bulk ZnO grown by the hydrothermal method, as-received as well as annealed and/or exposed to an hydrogen plasma, are discussed. A study of the optical properties of MOCVD ZnO/GaAs films, annealed in different ambient and at different temperatures, is presented in chapter 5. In chapter 6, the solubility of nitrogen in ZnO:N films and the effects of annealing are investigated. Chapter 7 will show the effect of the growth parameters on the optical properties of ZnO doped with nitrogen. Finally, chapter 8 summarizes the results of this work.

2 Fundamentals properties of ZnO

2.1 Structural and crystalline properties

Based on ref (35), ZnO has a wurtzite crystal structure which consists of two interpenetrating hexagonal close packed (hcp) sublattices of Zn and O, displaced by the length of the Zn-O bond in the *c*-direction. The lattice constants of the unit cell are $a = 3.2500$ Å and $c = 5.2060$ Å, yielding the ratio c/a of 1.60, which is very close to the ideal value of 1.633 expected for the hcp unit cell. In the ideal wurtzite structure (figure 2.1), each sublattice consisting of either Zn or O atoms is displaced with respect to each other, along the threefold *c*-axis by $u = 3/8$ in fractional coordinates. The parameter u is known as the length of the bond parallel to the *c*-axis, in units of c, or the nearest neighbor distance b divided c. The bond angles α and β of 109.47° are also shown.

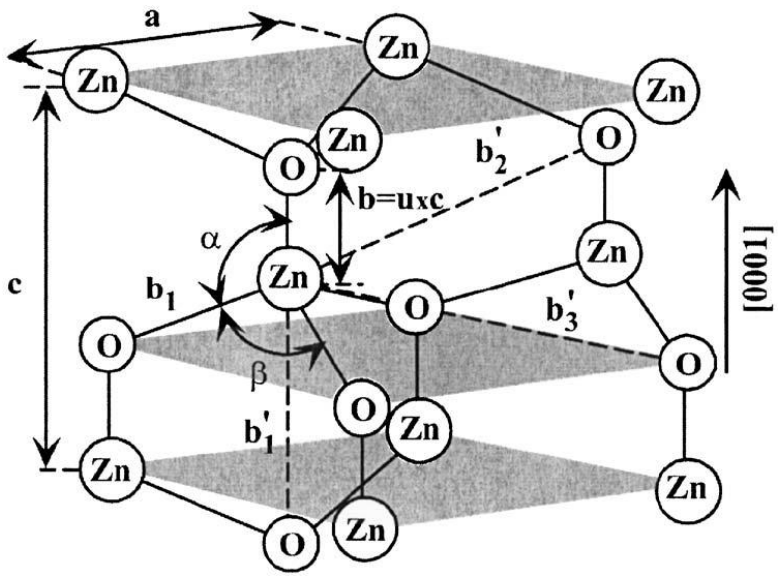

Figure 2.1: Schematic representation of the wurtzite structure of ZnO (after (35)).

Each sublattice consists of four atoms per unit cell and every atom of one kind (e.g. group II atom) is surrounded by four atoms of the other kind (i.e. group VI), or vice versa, which are coordinated at the edges of a tetrahedron. In the real ZnO crystal, the wurtzite structure deviates from the ideal arrangement, i.e. the c/a ratio (or the u value, which is correlated) slightly deviates from the ideal value. Indeed, a decrease in c/a ratio is accompanied by an increase in

the u value, in such a way that the four tetrahedral distances remain approximately constant. This is achieved through a distortion of the tetrahedral angles due to long-range polar interactions. The two slightly different bond lengths will be equal if the following relation holds:

$$u = \frac{1}{3}\frac{a^2}{c^2} + \frac{1}{4} \qquad (2.1)$$

An issue of ZnO epitaxy is the significant scattering in the measured ZnO lattice parameters. For instance, the reported values for a vary from 3.2475 to 3.2501 Å, while the c lattice parameter values vary from 5.2042 to 5.2075 Å (35). This scattering can be due to the use of different mismatched substrates and different growth techniques. However, it can also be related to deviations from stoichiometry (36).

2.2 Electronic band structure

Considering that ZnO is a candidate semiconductor for optoelectronic device applications, a clear understanding of the band structure is of critical importance to explain the optical and electrical properties (as well as many other phenomena), because it determines the relationship between the energy and the momentum of the carrier. Amongst the different techniques used to determine the band structure, namely X-ray reflection/absorption/emission techniques, photoelectron spectroscopy (PES), and angular resolved photoelectron spectroscopy (ARPES), the latter, along with synchrotron radiation excitation, are the most powerful tools that allow experimental bulk and surface electronic band-structure determination, under the assumption of k conservation and a single nearly free electron like final band (37).

The important aspect of the electronic band structure of ZnO is that it has a direct band gap. The band structure E(k) for ZnO calculated by Ivanov *et al.* (38), using an empirical tight–binding Hamiltonian, is given along some symmetry lines in the Brillouin zone in figure 2.2. The optical band gap between occupied and empty bands (represented by $\Gamma_{1,5}$) and Γ_1) and in ZnO is about 3.37 eV. This energy represents the energy difference between full and empty states. The filled states are called the valence band and the energy at the top of the valence band is called the valence band maximum (VBM). The empty states above the gap are called the conduction band with the lowest point in that band called the conduction band minimum (CBM). For ZnO, the

(VBM) and (CBM) coincide at $k = 0$, the Γ point, determining the direct band gap nature of this material.

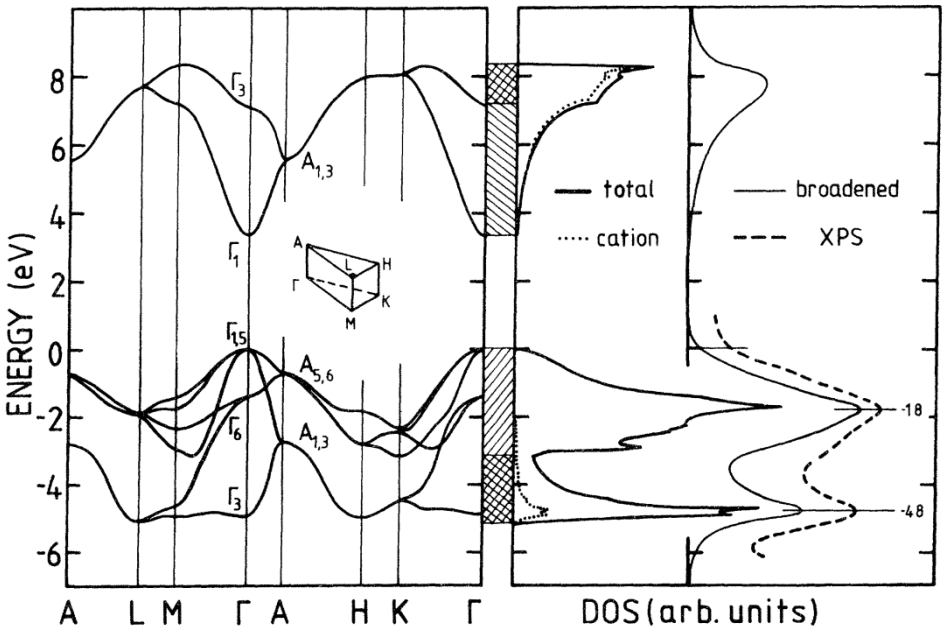

Figure 2.2: Band structure and density of states (DOS) for ZnO. The zero in the graphs is taken as the valence band upper edge (after (38)).

In figure 2.2 six valence bands can be seen between –6 eV and 0 eV. These six valence bands are derived from the 2p orbitals of oxygen. Below –6 eV, at about –20 eV, the valence band terminates with the 2s core like states of oxygen. For the conduction band there are two bands visible (above ~3 eV). These bands are strongly localized on the Zn and correspond to the unoccupied Zn 3s levels.

2.3 Optical properties

According to Kaldis *et al.*, ZnO is noted as a material with high luminescence intensity from the beginning of the 20th century (39). For example, ZnO powders served as a material for short

Table 2.1: Properties of wurtzite ZnO

Properties	Values
Lattices parameters at 300 K a_0 c_0	 3.2495 Å 5.2069 Å
$\frac{a_0}{c_0}$	1.602 (1.633 for ideal hpc structure)
u	0.345
Density	5.606 g/cm^3
Stable phase at 300 K	wurtzite
Melting point	1975°C
Thermal conductivity	0.6, 1-1.2 W/K.cm
Linear expansion coefficient (/°C)	$a_0 = 6.5 * 10^{-6}$ $c_0 = 3.0 * 10^{-6}$
Static dielectric constant	8.656
Refractive index	2.008, 2.029
Energy band gap	3.4 eV, direct
Exciton binding energy	60 meV
Electron effective mass	0.24
Electron Hall mobility at 300 K (for low n-type conductivity)	200 cm^2/V.s
Hole effective mass	0.59
Hole Hall mobility at 300 K (for low p-type conductivity)	5-50 cm^2/V.s
Ionicity	62 %

decay time cathodoluminescent screens in the 1940s (40). Nowadays, very narrow excitonic recombination lines are resolved in high quality ZnO crystals at liquid helium temperature (19). Additionally, excitonic luminescence is detected at room temperature because of the large

exciton binding energy of 60 meV (10). This energy is higher than in GaN (21-25 meV), which also makes ZnO exceptionally attractive for optoelectronics. The luminescence spectrum of ZnO consists of three groups of peaks which are situated in the ultra-violet and visible region of the electromagnetic spectrum (360 nm to 720 nm). Beside others, it includes excitonic, free-to-bound and donor-acceptor pair transitions. More details on the recombination mechanisms will be given later (chapter 3). Table 2.1 summarizes the principal physical and optical properties of ZnO.

2.4 ZnO doping

2.4.1 *n*-type doping

In many III-V and II-VI semiconductor materials, bipolar doping is difficult. For instance, ZnTe can easily be doped p-type (41), whereas GaN (42), CdS (43), ZnSe (44), ZnS (45) and ZnO (22) are intrinsically n-type semiconductors with strong resistance to *p*-type doping. The exceptions are CdTe (46) and GaAs (47) which can be doped either *p* or *n*-type. Amongst the factors used to explain this asymmetric doping, native point defects [(48), (49), (50)] and unintentional impurities introduced during growth [(32), (51)] are most often the proposed cause.

The non-stoichiometry introduced during the growth of these semiconductor materials generates native point defects. In particular, the synthesis of ZnO under zinc-rich conditions could increase the concentration of donor-like native defects such as zinc interstitials (Zn_i), oxygen vacancies (V_O) and zinc antisites (Zn_O) [(18), (52)]. Reports have shown that Zn_i is a shallow donor with an ionization energy of ~ 50 meV [(53), (54)] and a migration energy of 0.57 eV (52). Moreover, a correlation between the donor bound excitonic PL line I_3 at 3.366 eV and the Zn_i was reported (55), confirming the shallow level in the band gap of Zn_i. Furthermore, the low migration energy of Zn_i renders it very mobile at room temperature and can thus form stable complexes, such as Zn_i-N_O with a binding energy of 0.9 eV (56), which can contribute to the free electron concentration. This complex between Zn_i and N_O can be a source of compensation of nitrogen acceptor in ZnO:N. On the contrary, V_O and Zn_O are located deep in the band gap, [(22), (52), (57)] and therefore cannot contribute significantly to the electron concentration. Moreover, a recent report has shown that the native defects cannot be the cause of unintentional

n-type conductivity, due to the deep nature of most the native defects (52) and possibly the high mobility of Zn_i.

For ZnO grown under oxygen-rich conditions, zinc vacancy (V_{Zn}) (a relatively shallow acceptor-energy level at ~ 0.3 eV above the valence band maximum (58)) could form in addition to Zn_i and V_O, which also have low formation energies in oxygen-rich conditions. Such hole-killers may compensate the V_{Zn} defects.

Substitutional Al, Ga or In on the zinc site also form shallow donors with the optical fingerprints being the I_6, I_8 and I_9 excitonic PL lines, respectively (19). These impurities are generally found in commercially available zinc sources and could be unintentionally incorporated into ZnO during growth. ZnO doped with Al or Ga gives rise to a transparent conductive oxide which is widely used as an Indium Tin Oxide (ITO) [(59), (60)].

Hydrogen, which exhibits amphoteric behaviour in most semiconductor materials and often compensates the dominant carriers (61), is, according to Van de Walle *et al.* (62), solely a shallow donor in ZnO. Recently, a different configuration involving hydrogen and giving rise to a shallow donor was reported by Lavrov *et al.* (63). They assigned the I_4 line (at 3.3628 eV) to hydrogen in an oxygen site (H_O), while a transition at 3.3601 eV was correlated with hydrogen at the bond-centred site (H_{BC}). They also mentioned the possible involvement of hydrogen in two shallow donor levels with ionization energies of 35 and 42 meV. Hydrogen could also form shallow donor complexes with V_{Zn} defects (64), which annihilate the compensation effect of the isolated V_{Zn}. Moreover, hydrogen could also enhance the solubility of nitrogen acceptors in ZnO films by forming N_O-H complexes, which have smaller formation energies than N_O (28). This complex passivates the active N_O acceptors. Therefore, its dissociation and the resultant out-diffusion of hydrogen are important for possible *p*-type doping. Hydrogen incorporation is significant in metalorganic chemical vapor deposition (MOCVD) growth of ZnO, and its minimization in the films during growth is crucial in order to achieve *p*-type doping (29).

2.4.2 *p*-type doping

Possible p-type dopants in ZnO include the group I and V elements. According to the Hume-Rothery rules for metals (65), the dopant has more chance to substitute in the lattice if it only size-matches with the host atom. Table 2.2 lists the ionic radii of the different *p*-type dopants for ZnO. The size mismatch of the dopant atoms with respect to the host atom is also presented. Large-size dopants are unlikely to form substitutionals when there is appreciable elastic strain energy. In principle, therefore, only Li_{Zn} and N_O substitutions are favourable, because Li and N on the Zn and O sites in the lattice cause less strain. Substitution of Na on the Zn site and P, As and Sb on the O site are unfavourable due to the large size mismatch with the host atom. The small size mismatch of the group V element (P, As and Sb) with the Zn host atom is striking. This could favour the formation of the X_{Zn}-$2V_{Zn}$ acceptor complex (X=As, Sb or P) (33) involving group V antisite and could partly explain the *p*-type conductivity found when ZnO is doped with P, As or Sb.

Table 2.2: Ionic radii and size mismatches with host atoms of potential acceptor dopants in ZnO (66). The ionic radii correspond to a coordination number of 4. The elements in italic introduce acceptors upon substitution of the host element in bold. Percentage mismatch is defined as $\frac{r_{dopant}}{r_{host}} - 1$).

Elements	Ionic Radius (Å)	Size mismatch (%)
Zn (+2)	**0.60**	
Li (+1)	0.59	-2
Na (+1)	0.98	63
P (+3)	0.58	-3
As (+3)	0.60	~0
Sb (+3)	0.76	27
O (-2)	**1.38**	
N (-3)	1.71	24
P (-3)	2.12	54
As (-3)	2.22	61
Sb (-3)	2.45	78

2.4.3 Doping limitation in II-VI compounds

For effective doping, it is necessary to meet a number of requirements for good electrical conductivity.

1) An adequate concentration of doping atoms must be incorporated into the crystal, which implies a good solubility of the dopant under both equilibrium and non-equilibrium conditions.
2) The dopant must be able to substitute the host atom.
3) The dopant must be shallow, i.e. its energy level must be close enough to the corresponding band-edge so that it can ionize at room temperature and contribute to the free carrier concentration.
4) The spontaneous formation of defects with opposite charges must be minimized. Such defects could deactivate the dopants by pairing with them or by compensating their electrical activities.

Briefly, the compensation effect in the case of *n*-type doping, for example, will occur when unintentional acceptors are introduced in conjunction with the incorporation of the donors. These acceptors present a lower energy state for electrons otherwise trapped in the donor levels. The electrons can lower their energy state by dropping down into the acceptor levels. The immediate consequence is the reduction of the free carrier concentration, which reduces the conductivity of the material (67). The following model explains how different mechanisms could hamper the doping efficiencies of various dopants.

Using the phenomenological "doping pinning rule" [(68), (69)], the *p*-type pinning energy $\varepsilon_F^{(p)}$ and *n*-type pinning energy $\varepsilon_F^{(n)}$ can be derived. These two Fermi levels determine the maximum doping limit at which oppositely charged, compensating defects form. Consider *p*-type doping. This model implies that the doping asymmetry is related not only to the nature of the wide band gap of the II-VI compounds, but because intentional doping by acceptors moves the Fermi level E_F, towards the valence band maximum (VBM). This lowers the formation energy of spontaneously formed donors, which compensates the intentional acceptor dopants. The formation energy ΔH, of spontaneously formed defects, α, with charge q, is given by:

$$\Delta H(\alpha, q) = \Delta H_0 + qE_F \qquad (2.1)$$

where ΔH_0 is a constant on the order of a few eV. It is independent of E_F and depends only on parameters such as the atomic chemical potential during growth (70). For a donor-like defect, q is positive. Doping with acceptors lowers E_F towards the VBM, and thus ΔH (α, q) for q > 0 (α = donors) is lowered. Lower formation energies result in higher donor concentrations, thus compensating the intentionally introduced acceptors. This leads to the pinning of E_F near the CBM at an energy, $\varepsilon_F^{(p)}$. Similarly for *n*-type doping, a pinning of the Fermi energy near the VBM at an energy $\varepsilon_F^{(n)}$ can also be deduced.

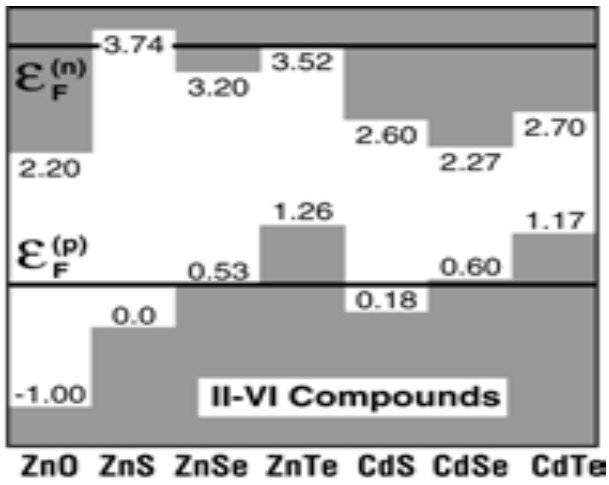

Figure 2.3: The *n*-type pinning energy $\varepsilon_F^{(n)}$ and *p*-type pinning energy $\varepsilon_F^{(p)}$ are shown relative to the absolute band-edge energies (from (71)) of II-VI semiconductors. The positions of the conduction and valence band edges are given relative to the valence band edge in ZnS.

Figure 2.3 compares the trends in dopability of different II-VI compounds using the natural valence band offsets and the experimental band gap energies, which determine the conduction band offsets. For ZnO, $\varepsilon_F^{(n)}$ is inside the conduction band at E_C + 0.6 eV (72) or E_C + 1.3 eV (71). Therefore, high *n*-type doping in ZnO could rely on the fact that electron killers like V_{Zn} start to form when E_F is in the conduction band, so that the material is already highly doped before compensation occurs. The low CBM energy (large electron affinity) of ZnO could also explain the difficulty in forming electron killers during *n*-type doping. In contrast, *p*-

type ZnO doping remains impossible according to this diagram, since $\varepsilon_F^{(p)}$ lies at E_V + 1.5 eV (71) and the formation of hole killers like Zn_i and V_O occur readily during *p*-type doping. Nonetheless, a new report has shown that the $\varepsilon_F^{(p)}$ level could be inside the valence band at E_V – 0.1 eV (72). This could lead to the formation of relatively good *p*-type ZnO, provided that the dopants have small ionization energies. However, doping with acceptors which have relatively small ionization energies is generally difficult in materials with large ionization potentials such as ZnO.

The lack of appropriate shallow donors (acceptors) cannot solely explain doping asymmetry. For instance, a comparison of acceptors in CdTe and ZnTe shows that, despite a much stronger inclination of ZnTe for *p*-type doping, the ionization energies of potential acceptors in both materials are practically the same. Also, doping ZnSe with a very small concentration of P results in a strong incorporation of P into the substitutional site, where it has quite a low ionization energy (73). There must thus be other reasons to explain the doping difficulty.

The solubility of dopants remains an issue for II-VI compound semiconductors. The level of conductivity achieved is determined by how the dopants incorporate into the host lattice. The chemical potentials of the dopant and the elements forming the lattice, determine the solubility of the dopant. However, a low concentration of free carriers could be the result of the formation of a second phase (74), precipitation (75) and substitution of the dopant on the wrong lattice site (76), especially in highly doped material. Various solutions have been proposed to increase the dopant solubility. For instance, in the case of *in-situ* doping of ZnO with nitrogen, growth under Zn-rich conditions will, in theory, decrease the chemical potential of the nitrogen dopant and consequently increase its solubility (47). Techniques such as co-doping (77) and cluster-doping (47) present alternatives for increasing the dopant solubility. The co-doping method consists of simultaneously doping the host material with a balanced concentration of acceptors and donors. Using this method for *p*-type doping could increase the incorporation of the acceptor dopant by minimizing the ionic potentials and lowering the Madelung energy (electrostatic energy of an ionic crystal given by the sum of pairwise interactions between ions treated as point charges) (77). These techniques predict that acceptor solubility in ZnO can be increased by introducing donors, which will lower both the lattice energy and the formation energy of the acceptor defect.

When the dopant is soluble, however, it may form complexes with native point defects. Indeed, the efficiency of foreign atoms in the host lattice to act as dopant could be strongly influenced by the relative ease of formation of a native vacancy in one of the sublattices. Theory suggests that the strong lattice relaxation around the vacancy when it is doubly positively charged could reduce its chemical potential and allow its formation in high concentration. This propensity to generate vacancies could lead to the formation of dopant-native vacancy complexes (A-centers) when the doubly positively charged vacancy pairs with the singly negatively charged dopant (78). The resulting pair acts as a singly ionized donor which then compensates one more single acceptor. These A-centers have lower formation energies than isolated vacancies and could be one of the major compensating defects in II-VI compound materials.

The lattice relaxation can also generate deep centers involving the dopant. Incorporation of a foreign atom of different size into the host lattice can induce relaxation of the surrounding atoms, which has a direct effect on the total energy of the crystal. For strong relaxation, broken bonds in the vicinity of the foreign atoms can occur, leading to the formation of a charged, compensating defect center [(79), (80), (81), (82)]. This phenomenon leads to the conversion of a normal substitutional atom, which is expected to behave as a shallow dopant, into a deep level where the dopant is displaced from its lattice site. If this happens upon binding with a point defect X, the resulting deep center is called a DX (or AX) center.

Some dopants may be introduced at different sites in the crystal and this could lead to opposite charge states, resulting in mutual compensation. The best example comes from the doping of II-VI compounds with a group I element, particularly Li [(76), (83)]. The small size mismatch between Li and Zn (see table 2.2) indicates that Li should be a good *p*-type dopant for II-VI compounds. The formation energy of Li_{Zn} is reasonably low (0.51 eV in ZnSe (83)) with a relatively shallow acceptor level in the band gap [(0.09 eV in ZnO (76) and 0.114 eV in ZnSe (84)]. This substitutional defect induces negligible distortion (83) and lattice relaxation in its vicinity [(21), (79)]. However, Li could also be located at the interstitial site (Li_i), which has a low migration barrier and formation energy compared to that of Li_{Zn} (83). The Li_i can therefore migrate through the crystal and readily pairs with Li_{Zn} to give the neutral Li_{Zn}-Li_i complex. This amphoteric behaviour was also reported in ZnSe:N where a N_{Se}-N_i complex was suggested (75). In addition to this complex, N_2 molecules could be generated in the crystal when the growth is

done under generally anion-rich conditions (75). This electrically inert molecule annihilates the electrical activity of the N_O acceptor. Under cation-rich conditions, the split interstitial N-N pair at the anion site is generated and behaves like a double donor [(75), (85)].

Crytal defects (threading dislocations and stacking faults) arising from the large lattice mismatch between the substrate and the thin films could also hinder the *p*-type doping process by interacting with the dopant. In particular, the strain and the electrostatic fields introduced by the dislocations could scatter the free carriers, reducing the mobility. Distinctive optical transitions have been related to crystal defects. Bound excitons (BE) localized at stacking faults (86), surface defects (87), and screw dislocations (88), have been observed in GaN (89), ZnSe (90), ZnTe (91), and ZnO (92). In ZnO in particular, transitions at ~3.33 eV and ~3.31 eV were related to excitons bound to structural defects (93), and free to bound acceptor recombinations (FA) related to the stacking fault (92), respectively. These transitions relating to the crystal defects are strongly localized and can cause malfunction of optical devices. In general, dislocations are non-radiative centers with a deep level in the band gap (94). Moreover, the energy released into the material upon non-radiative recombination can be the driving force for diffusion and the promotion of defect reactions. For example, In ZnSe-based devices, degradation occurs by the propagation of misfit dislocations into the active region (95). Therefore, the reduction of the imperfections introduced by the mismatch between the substrate and the ZnO thin film is also fundamental for enhancing the properties of the ZnO sample. The choice of a suitable substrate with a small lattice mismatch is thus important.

2.5 Choice of substrate

In order to reduce strain, crack and dislocation densities in an epitaxial film, a substrate with an analogous crystallographic structure, the smallest lattice mismatch and similar in-plane linear expansion coefficients should be chosen. Also, epitaxial perturbation arising from chemical reactions on the substrate surface should be minimized. Taking this into consideration, no suitable substrate for epitaxial growth of ZnO exists. This complicates the growth mechanism of the initial nucleation layer and a high concentration of imperfections in this initial layer is possible.

Table 2.3: Lattice parameters of substrates for ZnO

Substrate	Crystal structure	Lattice parameters	Lattice mismatch (%)	Thermal expansion coefficient $\alpha(K^{-1})$
		a (Å)		$\alpha_a(10^{-6})$
		c (Å)		$\alpha_c(10^{-6})$
GaAs	Cubic	5.652	42.4	6.0
Al_2O_3 (0001)	Hexagonal	4.757	18 % (after 30^0 in-plane rotation)	7.3
		12.983		8.1
$ScAlMgO_4$	Hexagonal	3.246	0.09	
		25.195		
GaN	Hexagonal	3.189	1.8	5.17
		5.185		4.55
Si	Cubic	5.430	40.1	3.59
ZnO	Hexagonal	3.252	0	2.9
		5.213		4.75

Several substrates for ZnO growth have been used and their different parameters are summarized in table 2.3. The most suitable substrate is ZnO itself, but this is not cost effective. Furthermore, the quality of bulk ZnO is strongly dependent on the growth technique used. Diverse quality and properties have been reported for bulk ZnO grown by hydrothermal [(96), (97), (98)], vapor phase [(99), (100), (101)] and melt growth [(102), (103)] methods. Depending on the bulk ZnO polarity, different pre-growth surface treatments are required for better homo-epitaxy (104).

The formation of silicon dioxide renders the growth of high quality ZnO on Si difficult since this amorphous layer degrades the crystallinity of the films. Despite the pre-treatment of the Si substrate in HF, which etches away the SiO_2 layer, a total removal of the amorphous SiO_2 layer

is not guaranteed. In addition, high growth temperatures can favour the formation of a SiO_2 layer since its enthalpy of formation (910.7 kJ/mol) (105).

The large lattice mismatched *r*-, *a*- and *c*-plane sapphire (Al_2O_3) have also been used for the growth of ZnO because the oxygen sublattice of sapphire has the hexagonal symmetry of ZnO. In fact, epitaxial growth on these large lattice mismatched substrates may begin with a post-nucleation phenomenon involving rotation, migration and rearrangement of stable clusters, which are generally single crystalline (106). During such a complex process, the single-crystalline layer, epitaxially aligned with respect to the rigid substrate, would elastically strain to reduce the difference between its normal lattice parameter and that of its substrate.

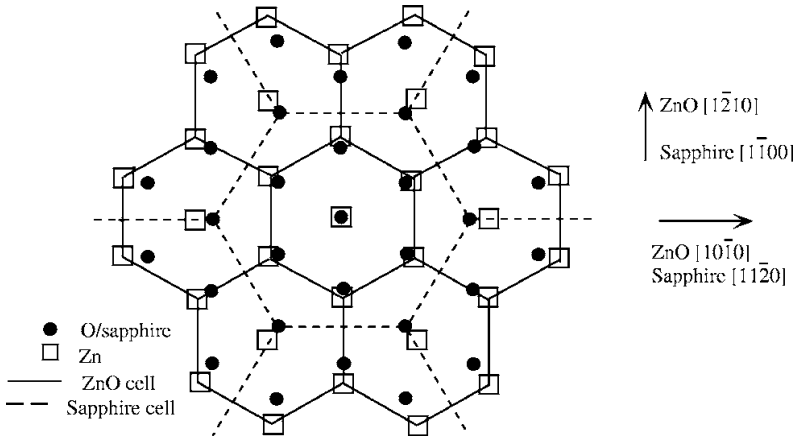

Figure 2.4: Schematic diagram for the epitaxial relationship of ZnO (0001) grown on c-plane Al_2O_3

The *c*-plane of sapphire consists of alternating layers of (sixfold symmetric) oxygen and (threefold symmetric) Al atoms. The wurtzite structure of ZnO consists of O and Zn which are both sixfold symmetric about the ZnO **c**-axis. In principle, when ZnO is deposited on a *c*-plane sapphire substrate, ZnO oxygen atoms would bond to the underlying sapphire Al atoms to form a structure with a mismatch of 31.8%. However, presumably due to the large ionic radius of the O ions (~1.40 Å) versus the Al ions (~0.53 Å), the Zn preferentially bonds with sapphire O atoms, resulting in a 30° *a*-axis rotation. This in-plane rotation decreases the lattice mismatch to ~18 %.

Epitaxial growth can therefore be achieved. The growth of ZnO films on *c*-plane sapphire substrate generally results in the epitaxial relationship ZnO (0001)//Al_2O_3 (0001) and ZnO [10-10]//Al_2O_3 [11-20]. This relationship is shown in figure 2.4. Moreover, low cost high quality Al_2O_3 wafers are commercially available. Therefore, for non-optoelectronic applications, sapphire is often used as a substrate. Nonetheless, the in-plane rotation could induce a high density of imperfections during the nucleation phase. In fact, the epitaxial growth of ZnO on sapphire shows a high dislocation density and low mobilities. Even so, sapphire was the main substrate used for the ZnO:N growth in this study.

Despite the large lattice mismatched between ZnO and GaAs (42 %), good quality ZnO films on GaAs substrate have been achieved (107). This could be due to the interfacial reactions and recrystallization of extrinsic phases in epitaxially grown ZnO/GaAs heterostructures [(107), (108)]. Single crystalline Zn_3As_2 and $ZnGa_2O_4$ can be formed at the interface and decrease the lattice mismatched to ~26 % and ~9.4 %, respectively (108), thus, enhancing the crystalline quality of the ZnO films. Furthermore, the ability of As atoms to diffusion from the substrate into the ZnO films is interesting for *p*-type doping. Agouram *et al.,* (107) showed that in ZnO grown on GaAs at 390˚C by MOCVD, As atoms diffuse up to ~1µm into the ZnO films. However, for efficient *p*-type doping with As in such heterostructures, the diffusion of Ga into the films needs to be prevented. Further details will be given in chapter 5.

In order to eliminate the in-plane domain rotation, lattice-matched $ScAlMgO_4$ substrate has been used to grow high crystalline quality ZnO, with the epitaxial relationship ZnO (0001) // $ScAlMgO_4$ (0001) and ZnO [11-20] // $ScAlMgO_4$ [11-20] (109). However, the availability of this substrate remains an issue. As an alternative, GaN, which has a small lattice mismatch (1.8 %) may be used.

2.6 Conclusion

The fundamental properties of ZnO as well as the difficulties associated with p-type doping of ZnO were summarized in this chapter. Briefly, ZnO has a wurtzite structure and is a direct wide band gap semiconductor material with the highest exciton binding energy ever reported. Although *n*-type doping is easily achieved, *p*-type doping is still controversial. The different reasons summarized above may explain this doping asymmetry, which seems common for II-VI semiconductor material.

3 Characterization and growth techniques

In this chapter, the techniques used to characterize the ZnO samples will be presented. In particular, the possible radiative recombination mechanisms giving rise to the PL will be discussed. In the last section of this chapter, the growth technique used will also be briefly explained.

The properties of the ZnO samples were investigated using photoluminescence (PL), timed-resolved photoluminescence (TRPL), secondary ion mass spectroscopy (SIMS), scanning electron microscopy (SEM) and X-ray diffraction (XRD). The samples studied in chapter 5, 6 and 7 were grown by MOCVD.

3.1 Photoluminescence

In photoluminescence (PL) experiments, electron-hole (e-h) pairs are photo-excited by absorption of light. These e-h pairs diffuse and relax into a quasi-equilibrium distribution while they are depleted by radiative and non-radiative recombination (110). The efficiency of photon emission through radiative recombination in the material is crucial in PL. A critical parameter in determining the PL efficiency is the total lifetime τ_{tot} (110):

$$\frac{1}{\tau_{tot}} = \frac{1}{\tau_{nr}} + \frac{1}{\tau_r} \qquad (3.1)$$

where τ_{nr} is the non-radiative lifetime and τ_r is the radiative lifetime. In doped samples in the low injection limit (i.e. when the photo-excited e-h density is smaller than the doping density), τ_r is related to the dopant density ($N_A \gg N_D$) by (111):

$$\tau_r = \frac{1}{BN_A} \qquad (3.2)$$

where N_A is the acceptor doping concentration and B is the radiative recombination coefficient, which is slightly dependent on the doping concentration. If the donor doping concentration $N_D \gg N_A$, one can replace N_A by N_D in Eq.(3.2).

The minimization of non-radiative recombinations is therefore important for high quantum efficiency. Different processes can contribute to τ_{nr}: (i) Auger recombination, (ii) trapping and

recombination at impurities and defects, (iii) surface recombination and (iv) diffusion of carriers away from the region of observation (110).

For reasonable efficiency, the photoluminescence can be defined as a three step process:

1. Photo-generation of e-h pairs by absorption of incident radiation near the surface
2. Radiative recombination of the e-h pairs
3. Emission of photons due to radiative relaxation

This three step PL process generally requires an excitation source with an energy greater than the band gap energy of the semiconductor.

3.1.1 Photoluminescence setup

A closed-cycle He cryostat was used to control and monitor the temperature of the sample between ~2 and 300 K. Copper clamps rather than vacuum grease were used to hold the ZnO samples on the dip tube, thus eliminating unwanted luminescence from the vacuum grease. Prior to cooling, the cryostat was evacuated for 24 h to 2×10^{-5} mbar and then the compressor was switched on. Luminescence from the sample was excited by a Kimmon, IK 3252R-E He-Cd laser with λ= 325 nm and a maximum power P_{max}=35 mW. The laser was focused through the entrance slit of a 0.5 m SPEX 1870 monochromator and detected by a Hamamatsu R3896 photomultiplier tube (PMT) with a GaAs photocathode, operating in lock-in mode. A grating with 1200 grooves/mm and a maximum resolution of 0.02 nm (in the first order) was used in order to select wavelengths that would reach the PMT. An optical chopper was used to pulse the laser and to serve as a reference for the lock-in amplifier. The incoming current from the PMT was amplified by converting it to a voltage using a resistor placed at the entrance of the lock-in amplifier. It should be mentioned that the laser penetration depth is estimated to be ~ 60 nm. However, due to the polycrystalline nature and resulting surface roughness of the ZnO films, as well as the diffusion of photo-excited carriers, this value is an underestimate of the depth probed in PL measurements.

For high resolution of the near-band edge emission, which contains information on the excitonic transitions, the measurements were taken in the second order diffracted PL. A long wave pass edge filter was placed in front of the entrance slit of the monochromator to reduce laser light

scattered/reflected into the monochromator. Neutral density filters of different optical densities were used to vary the laser power and the temperature of the sample was varied using a LakeShore 331 temperature controller.

Some measurements were taken with a 1 m SPEX monochromator in the Semiconductor Group at the Institute for Applied Physics, TU Dresden in Germany. A continuous flow He cryostat was used to vary the temperature of the sample between 2 K and room temperature. A Hamamatsu PMT (R943-02) with a GaAs photocathode was used to detect the luminescence.

3.1.2 Radiative recombination processes

The different radiative recombination processes described in the book by Landsberg (112) are presented in the following sections and are illustrated in figure 3.1.

3.1.2.1 Free exciton

The free exciton (FE) can be seen as a quasi-particle in which coulombic interaction binds the electron and the hole (113). This bound e-h pair falls into the Effective Mass Approximation (EMA). In other words, the bound e-h pair is similar to an electron bound to a proton to form a hydrogen atom. This metastable complex can move freely in the crystal and its lifetime is inversely proportional to the spatial overlap of the electron and hole wave functions. Therefore, if viewed as a hydrogen-like atom, free excitons can generate discrete energy levels, E_{Xn}, below the band gap, which are described by the following equation:

$$E_{Xn} = E_G - \frac{R_X}{n^2} \qquad (3.3)$$

where

$$R_X = \frac{\mu}{m_o}\frac{1}{\kappa_o^2}R_H \qquad (3.4)$$

In Eq's (3.3) and (3.4), E_G is the band gap energy, R_X is the exciton Rydberg also known as the exciton binding energy, R_H is the hydrogen atom Rydberg, n is the principal quantum number, κ_o is the static dielectric constant, m_o is the free electron mass and μ is the exciton reduced mass, given by:

$$\mu = \frac{m_e m_h}{m_e + m_h} \qquad (3.5)$$

where m_e and m_h are the effective masses of the electron and the hole, respectively.

The small value of the exciton binding energy makes it difficult to observe the recombination of excitons in excited states (n > 1). At low temperatures, n = 1 ground state exciton recombination dominates the band gap luminescence spectrum in relatively pure material. The ground state energy of the FE is thus smaller than the band gap energy by the exciton binding energy. The ground state exciton binding energy in ZnO is ~60 meV (114). This is the highest reported for any semiconductor material. For $m_e = 0.24m_o$ and $m_h = 0.59m_o$ (115), an excitonic Bohr radius $a_B(ZnO)$ of

$$a_B(ZnO) = \frac{\kappa_s}{\mu/m_o} a_B \approx 1.4\, nm \qquad (3.6)$$

may be calculated. The Bohr radius of such a free exciton, also called a Wannier exciton, is significantly larger than the lattice constant of ZnO, and hence the EMA is valid.

The valence band in ZnO splits into three sub-bands, which result from the combined effects of spin-orbit interaction and the crystal field. These three sub-bands, commonly named A, B and C, have energy separations of $\Delta E_{AB} \approx 5$ meV and $\Delta E_{BC} \approx 44$ meV (19).

3.1.2.2 Bound excitons

The free exciton can be localized on a neutral or ionized donor or acceptor, giving rise to a bound exciton. An exciton bound to an ionized donor (acceptor) (D^+X) ((A^-X)) is a complex consisting of a donor (acceptor) ion, an electron and a hole. A neutral donor (acceptor) bound exciton ($D^\circ X$) (($A^\circ X$)) consists of a donor (acceptor) ion, two electrons (holes) and a hole (electron). Exciton bound transitions become the dominant recombination processes in the near-band-edge region with increasing donor or/and acceptor concentrations into the material. The emitted photon energy E_{BX} from an exciton bound transition is:

$$E_{BX} = E_X - E_{loc} \qquad (3.7)$$

where E_{loc} is the exciton localization energy, which is the energy required to remove the exciton from the impurity. It has been shown that E_{loc} depends on the electron and hole effective mass ratios [(116), (117)], which can be used to estimate the impurity binding energy E_i (i = A when the impurity is an acceptor, and i = D when the impurity is a donor). Furthermore, Haynes (118) showed empirically that E_{loc} is linearly dependent on E_i for the neutral donor impurities:

$$E_{loc} = a + bE_i \qquad (3.8)$$

More recently, Meyer *et al.* (119) showed that this rule is also applicable for ionized donors. However, the validity of this rule for acceptors in ZnO is yet to be demonstrated.

3.1.2.3 Two-electron satellite transitions

During the recombination of an exciton bound to a neutral donor, the donor's final state can be the 1s ground state (normal D^0X line), or the excited (n > 1) 2s, 2p state (TES-line). The energetic distance between the D°X and its TES is consequently the difference in energy between the 1s and 2p donor states. According to the hydrogenic effective-mass approach (EMA), the energy level, $E_{(TES)}$, of the TES is given by:

$$E_{(TES)} = E_{(D^{\circ}X)} - E_D\left(1 - \frac{1}{n^2}\right) \qquad (3.9)$$

Therefore, for n = 2 and knowing the energy positions $E_{(D^{\circ}X)}$and $E_{(TES)}$ of the D°X and its corresponding TES transition, the related donor binding energy, E_D, can be obtained. The same formulation holds for A°X, but the A°X transition and consequently its corresponding TES are seldom observed in ZnO.

3.1.2.4 Donor-acceptor pair transitions

When donor and acceptor impurities are present in the material, the loosely bound additional donor electron can lower its energy by moving to a neutral acceptor site, where an electron is missing. This results in the donor and acceptor wave functions overlapping. This process is called donor-acceptor pair (DAP) recombination. The emission energy of the DAP is a function of the inter-pair distance (r) through the initial and final state interactions between the donor and the acceptor. The emitted photon energy $E_{(DAP)}$ of a DAP transition is given by (120):

$$E_{(DAP)} = E_G - (E_D + E_A) + \frac{e^2}{4\pi\kappa_s\kappa_o r} \qquad (3.10)$$

where the third term on the right is the Coulombic energy of the ionized donor and acceptor pair after recombination. Since acceptors and donors are located in a lattice, only discrete values of *r* can be assumed. Consequently, for close pair, the DAP transitions will appear as discrete lines for allowed values of *r*. However, in general, the DAP transition involves the distant pair which gives rise to a broad band in the PL spectrum.

3.1.2.5 Free to bound transitions

As the lattice temperature increases, the donor involved in the DAP transition releases its electron into the conduction band. A transition between an electron in the conduction band and the neutral acceptor A° can occur. This transition is known as a free to bound transition (FA). At a temperature T, the energy, E_{FA}, of the FA is:

$$E_{FA} = E_G - E_A + \frac{kT}{2} \qquad (3.11)$$

where k is the Boltzmann constant. This transition therefore allows one to estimate E_A and, depending on this value, the FA transition may be visible at room temperature.

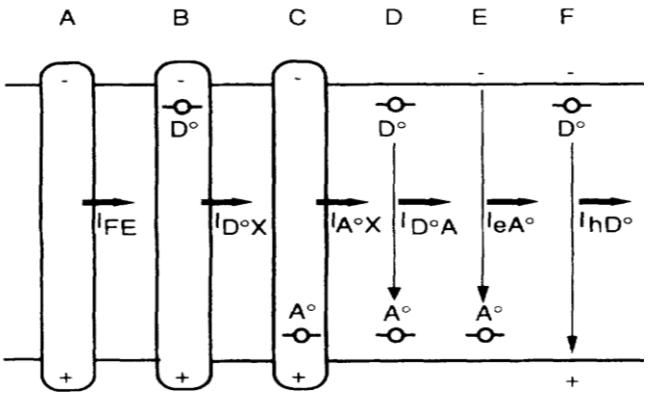

Figure 3.1: Radiative recombinations, after ref (121). (A) Free-exciton transition (FE), (B) and (C) transitions of donor- and acceptor-bound excitions (D°X, A°X), (D) donor-acceptor pair (DAP), (E) free electron and a neutral acceptor (FA) transition , (F) free hole and a neutral donor.

3.1.2.6 Phonon replica transitions

For an optical transition accompanied by a phonon, the photon emission energy, $h\omega_{(n,m)}$, is given by:

$$h\omega_{(n,m)} = E_{ZPL} - nE_{LO} - mE_{TO} \qquad (3.12)$$

where E_{ZPL} is the transition energy of the zero-phonon line (ZPL), n is the number of longitudinal optical (LO) phonons, E_{LO} is the energy of the LO phonon, m is the number of transverse optical (TO) phonons and E_{TO} is the energy of the TO phonon. In ZnO, the coupling to TO phonons is negligible and only LO phonons are visible in the spectra. The LO phonon energy for ZnO is ~72 meV (115).

The strength of the electron-phonon coupling of the LO phonon can be expressed in terms of the Huang-Rhys factor, S, which is determined by a Poisson distribution (122):

$$I_n = I_{ZPL}\frac{S^n}{n!} \qquad (3.13)$$

where I_n is the intensity of the n^{th} phonon and I_{ZPL} that of the ZPL.

3.1.2.7 Excitation-intensity dependence of the photoluminescence spectrum

The nature of the different PL transitions may be deduced using the variation in the excitation intensity. The intensity dependence of the PL emission can be described in general by a power law:

$$I \propto I_{ex}^{\alpha} \qquad (3.14)$$

where I is the intensity of the line, I_{ex} is the excitation intensity and α is a coefficient which depends on the nature of the recombination process.

For free and bound exciton emissions, when $h\omega_{ex} > E_G$, the coefficient α is generally $1<\alpha<2$ and becomes equal to unity when $h\omega_{ex} \sim E_G$ (121). For free-to-bound and donor-acceptor pair transitions, $\alpha < 1$ (121). A characteristic of the DAP transition is to shift towards the blue side of the spectrum with increasing excitation intensity. More details will be given in chapter 7

3.1.2.8 Temperature dependence of the photoluminescence spectrum

The shrinkage of the band gap with increasing temperature can be fitted with the semi-empirical Varshni equation (123):

$$E_G(T) = E_G(0) - \frac{\alpha T^2}{T + \beta} \qquad (3.15)$$

where $E_G(0)$ is the band gap energy at T=0 K. α and β are fitting parameters.

A modified version of this equation is (124):

$$E_G(T) = E_G(0) - \frac{\alpha T^4}{(T + \beta)^3} \qquad (3.16)$$

Since free and bound exciton energies differ from the band gap by values independent of the temperature, T, they follow the trend of the band gap with increasing temperature. Furthermore, the intensity of the bound exciton may be fitted with the following equation:

$$I_{BX} = \frac{I_0}{1 + \sum_i^k C_i \exp\left(-\frac{E_i}{kT}\right)} \qquad (3.17)$$

where C_i, E_i and I_0 are fitting parameters. E_i is known as the quenching activation energy and is often a good approximation of E_{loc}.

3.2 Timed-delayed photoluminescence

Originally used to study the recombination mechanisms, the timed-delayed photoluminescence was preformed to discriminate the different recombination processes occurring in the ZnO:N samples. The 325 nm line of a He-Cd laser was pulsed using a pulse generator and an accousto-optic modulator. The time resolution was about 20 ns. The measurements were performed in the Semiconductor Group at the Institute for Applied Physics, TU Dresden in Germany.

3.3 Secondary ion mass spectroscopy

Secondary ion mass spectroscopy (SIMS) was performed to investigate the nitrogen content in the grown films, as well as to quantify the unwanted hydrogen and carbon in the ZnO:N material. H, C, and N were monitored using a 40 nA, 15 keV Cs+ primary beam raster scanned over a (150 x 150) μm area. The SIMS intensities were recorded from the centre 33 μm of a ~ (2 x 2) mm^2 sample. A mass resolution of m/dm = 1400 (medium high resolution) was employed to resolve some of the possible interferences with the N-signal. Measurements were performed by Dr. Lasse Vines, in the faculty of Mathematics and Natural Sciences at the University of Oslo, Norway.

3.4 Scanning electron microscopy

Scanning electron microscopy (SEM), invented by M. Knott and E. Ruska in 1930, uses electrons for imaging. This technique has many advantages, such as its much higher magnification and greater depth of focus in comparison to light microscopy. A Philips XL30 SEM was used to study the surface features of the ZnO samples.

3.5 X-ray diffraction

The non-destructive X-ray diffraction (XRD) technique was used to investigate the orientation of the polycrystalline ZnO material grown in this study. A Philips PW 1840 powder diffraction system, with a resolution of 0.02° for 2θ, and with a Cu-Kα x-ray tube (λ = 1.5405 Å) was used. The x-ray scans were performed between 2θ values of 30° and 80° with a step size of 0.05°.

3.6 Metalorganic chemical vapor deposition (MOCVD) technique

The MOCVD technique was developed in the early 1960's (125) and has been improved throughout the years. To date, it is a well-controlled semiconductor growth technique based on the chemical reactions of various gaseous, liquid and solid precursors. Figure 3.2 shows a schematic overview of the *Crystal Specialties, Inc* MOCVD system used to grow the samples studied in this work. Since the system had previously served for the industrial growth of III-V compounds, a number of modifications were made for better adaptation of synthesis of the II-VI ZnO compound.

Upstream from the mass flow controllers, which control the flow rate of the source vapours and carrier gas in the lines, the pressure was set to 35 psi, using pressure regulators. The inert gas N_2 was used to saturate the Zn- (DEZn) and O- (TBOH) precursors. The Zn- and O-precursors have separate inlets to the reactor to reduce the pre-reaction in the gas lines. N_2 was used as carrier gas to transport the DEZn to the reactor chamber and also to carry away the byproducts of the reaction. The DEZn and the TBOH are placed in temperature-controlled baths which were set at 25°C and 40°C, respectively. These respective temperatures control the vapor pressure P_{DEZn} and P_{TBOH} which are equal to P_{DEZn}=16.08 torr and P_{TBOH}=103.67 torr, using the equations proposed by (126) and (127), respectively:

$$\ln(P_{DEZn}) = 8.28 + \frac{2109}{T} \qquad (3.18)$$

$$\ln(P_{TBOH}) = 16.85 + \frac{2658}{T - 95.5} \qquad (3.19)$$

where T is the temperature in Kelvin.

Assuming that in the gas phase, DEZn and THOH are ideal gases, the number of moles of DEZn and TBOH sent into the reactor can be calculated using the following equation:

$$n_i = \frac{P_i V_i}{R T_i} \qquad (3.20)$$

where i≡DEZn or TBOH, n_i is the number of moles (per minute) of the i-species sent into the reactor, V_i is the volume flow rate of N_2 used to saturate the i-species and T_i is the temperature bath in which the i-species is immerged. Similarly, the number of moles of NO reaching the reactor is determined using Eq. 3.20

The $\frac{VI}{II}$ ratio during growth is then defined as:

$$\frac{VI}{II} = \frac{n_{TBOH/NO}}{n_{DEZn}} \qquad (3.21)$$

In the reactor chamber, where the pressure was set at 20 torr using a vacuum pump, the Zn- and the O-precursors mix and eventually decompose on the substrate mounted on a SiC-coated graphite susceptor. The substrate is heated by a lamp and the temperature is monitored by a thermocouple inserted in the susceptor which is connected to a temperature controller. Formation of ZnO takes place on the substrate, which is significantly hotter than any other part of the reactor. The remaining toxic exhaust gases are decomposed in a cracking furnace before being sent to the vent line.

The choice of nitrogen as carrier gas is based on many reasons. Firstly, it is commercially cheaper and safer than other gases like hydrogen. Also it was shown that the precursor molecules decompose better when nitrogen is used instead of hydrogen (see for example (128)). Furthermore, nitrogen is inert with respect to ZnO even at high temperatures.

For ZnO:N, the use of nitrogen as carrier gas could also improve the incorporation of nitrogen into the ZnO films, compared to when doping is attempted using argon or hydrogen as carrier gas instead.

For ZnO grown with THOB, the growth temperature was maintained at 380°C using an optimum $\frac{VI}{II} = 60$ (129). The effect of $\frac{VI}{II}$ ratio and growth temperature on the solubility of nitrogen was studied for $\frac{VI}{II}$ =30, 60 and 120, while the growth temperature was varied between 270°C and 370°C, in increments of 20°C.

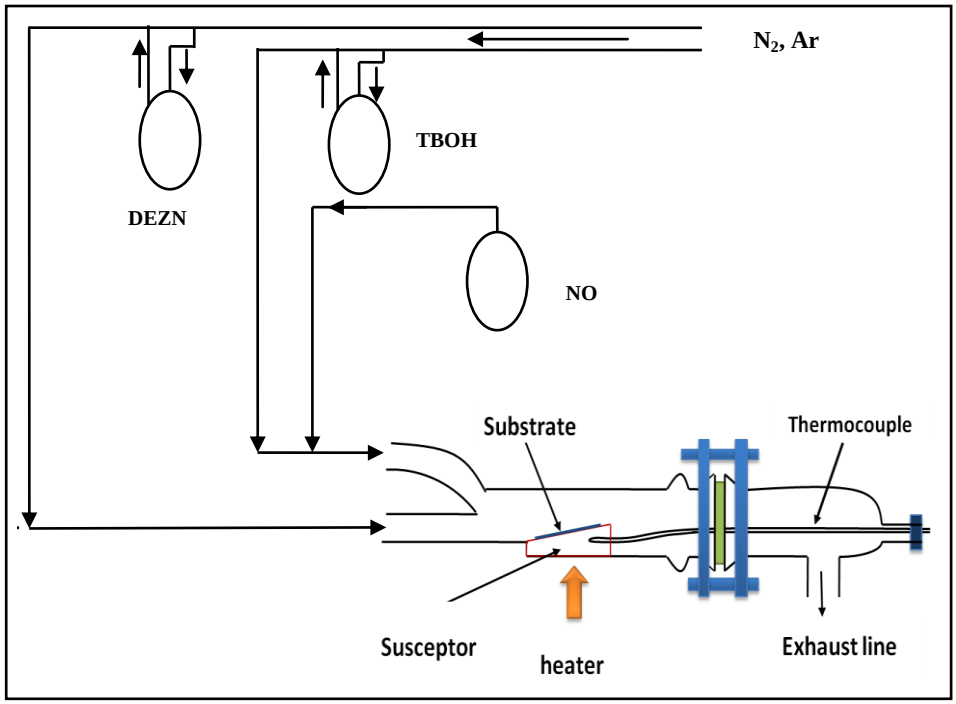

Figure 3.2: Schematic overview of the MOCVD system

4 Optical properties of hydrothermally grown bulk ZnO

4.1 Introduction

In order to better understand the optical properties of ZnO doped with acceptor impurities, an investigation of the different radiative recombination processes in n-type ZnO is necessary. Post-growth annealing is usually employed to activate the acceptor impurities. The effect of annealing on n-type material would help to single out the annealing effect on the acceptor activation. The incorporation of hydrogen into ZnO thin films during growth is known to passivate the active acceptor in ZnO. A good knowledge of the different optical transitions related to hydrogen could be correlated with its presence and behavior in the thin films. In this chapter the effects of thermal annealing and the presence of hydrogen as a dopant in n-type bulk ZnO are presented.

The first part of the chapter (sections 4.2 and 4.3) is dedicated to the effect of annealing on the radiative recombination mechanisms in the material. The evolution of the PL spectrum upon an increase in the annealing temperature is studied. The second part (sections 4.4 and 4.5) describes the effect of hydrogen plasma treatment on both the NBE emission and the DLE.

4.2 Photoluminescence of as-grown bulk ZnO

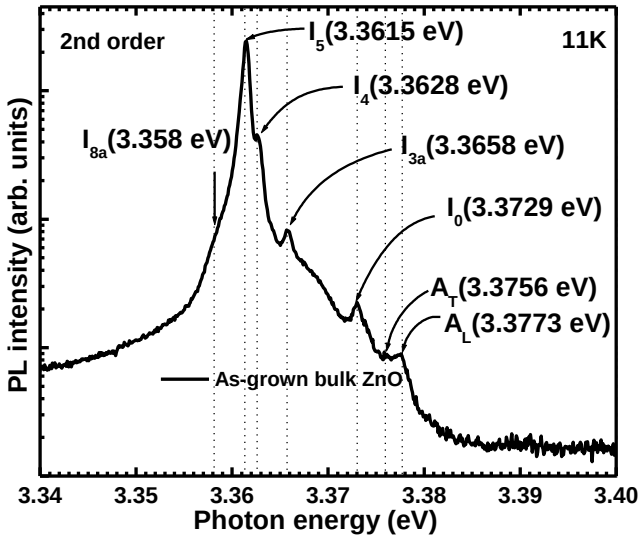

Figure 4.1: NBE PL of hydrothermally grown bulk ZnO.

Figure 4.1 shows the NBE emission of hydrothermally grown bulk ZnO. Various lines are visible and have been labeled according to the system of B.K. Meyer *et al.* (19).Relatively strong emissions from both longitudinal and transverse free excitons, A_L (3.3772 eV) and A_T (3.3759 eV) (130), are visible. Their appearance at such a low temperature indicates the as-grown sample is of high quality. The lines at 3.3628 eV and 3.3614 eV, and the shoulder at 3.359 eV, are assigned to neutral donor bound excitons which correspond in energy to the I_4, I_5 and $I_{8/8a}$ lines, respectively (19). The presence of hydrogen in the as-grown ZnO is indicated by the I_4 line (19). Additional impurities are also observed in the as-grown ZnO, with the $I_{8/8a}$ line reflecting the presence of Ga. Lines at 3.3731 eV, 3.3657 eV and ~3.364 eV are also visible and their origins will be discussed in sections 4.3

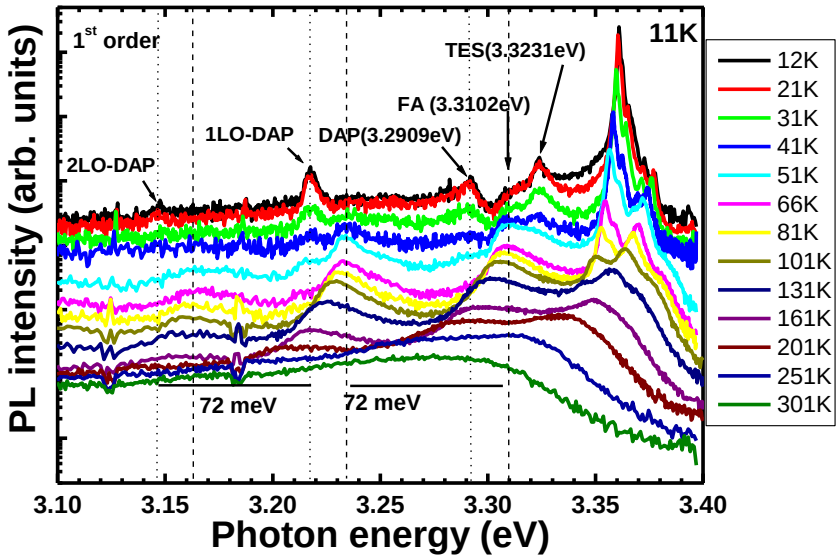

Figure 4.2: Temperature dependence (11 K - 301 K) of the PL of hydrothermally grown ZnO.

Figure 4.2 shows the temperature-dependence PL of hydrothermally grown ZnO. The temperature was varied from 11 K to 301 K. A donor-acceptor pair (DAP) band appears on the lower energy side of the NBE at 3.291 eV followed by two transitions at approximately 3.219 eV and 3.147 eV. The latter two transitions are assigned to the first and second longitudinal optical phonon replicas (LO) of the DAP band, respectively. The energy separation between them corresponds to the 72 meV LO phonon energy for ZnO (131). The assignment of the DAP

transition is based on its behavior with a variation in the sample temperature. This band rapidly quenches with an increase in temperature and is accompanied by an increase in intensity of a band which appears at ~15 meV towards higher energies in the spectra (at ~3.310 eV). This transition is assigned to free electron-to-acceptor (FA) emissions. This phenomenon is typical for DAP transitions in ZnO, where the donor easily ionizes due to its smaller binding energy. The electron freed from the donor will recombine with a hole trapped on the acceptor, thus enhancing the (FA) emission. Using Eq. (3.11), the acceptor binding energy E_A of ~127 meV is calculated. Schirra *et al.* (92) recently reported a luminescence line at 3.31 eV, which was assigned to a stacking fault-related acceptor with a binding energy of 130 ± 3 meV. This value is in good agreement with the acceptor binding energy obtained in this present work and the acceptor is therefore ascribed to stacking faults which are present even in bulk ZnO.

The thermal stability of the lines shown in figure 4.1 will now be investigated, since the out-diffusion of the corresponding donor impurities is necessary for p-type doping. Such donors can compensate the p-type dopants introduced intentionally into thin films, and it is believed that the out-diffusion of these impurities would enable more efficient p-type doping to be achieved.

4.3 Effect of annealing on the near-band-edge luminescence

Two types of annealing experiments were carried out on the bulk ZnO material – isothermal and isochronal. The results obtained are presented below.

4.3.1 Isothermal annealing

The results of isothermal annealing of ZnO at 650°C are shown in figure 4.3. Annealing at this temperature sharpens all the near-band-edge emission lines. Also new or previously unresolved lines appear after annealing. Two emission lines at 3.3726 eV and 3.3652 eV appear as shoulders on the transitions at 3.3731 eV and 3.3657 eV, respectively. The broad emission band between 3.3670 eV - 3.3710 eV is quenched and a transition at 3.3673 eV is observed, which remains visible even after 6.5 h of annealing. A line at 3.3608 eV, which was not visible in the as-grown material, is also observed after 1 h of annealing.

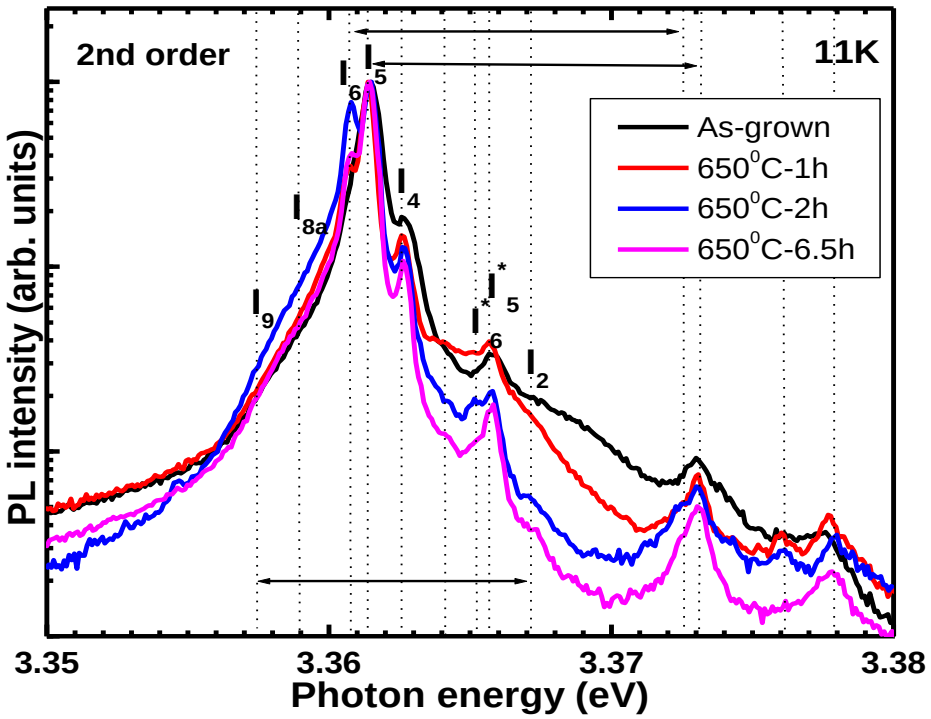

Figure 4.3: Normalized PL of ZnO isothermally annealed at 650°C in argon for different times.

Von Wenckstern *et al.* (132) investigated the defects in hydrothermally grown ZnO by means of PL, thermal admittance spectroscopy (TAS) and deep level transient spectroscopy (DLTS). One of three donor defects observed has a very shallow level of 13 meV and was correlated with the PL emission peak at 3.3730 eV. The PL intensity of this shallow donor increased upon annealing at temperatures of 600°C and above.

Moreover, a close analysis of the PL spectra presented in the work by Allen *et al.* (130) shows a correlation between the I_5 line and a transition at 3.3730 eV. The latter is always visible and even higher in intensity relative to the I_0 line when the I_5 line is dominant. Also, this line at 3.3730 eV is overshadowed by the I_0 line when the I_5 line is present with low intensity. A similar correlation between the line at 3.3731 eV and the I_5 line is found in the PL spectra of figure 4.3. Furthermore, Meyer *et al.* (119) reported on the correlation between different transitions in the NBE region. They found a correlation between the ionized donor bound exciton line I_0 and the neutral D^0X line I_{6a}. In other words, the I_0 appeared to involve the ionized donor responsible for

the I_{6a} transition. Therefore, in our investigation, the shoulder at 3.3726 eV could be related to the resolved I_6 transition at 3.3608 eV, which both appear after 2 h of isothermal annealing. Assuming that the 3.3726 eV transition results from excitons bound to the ionized donor giving rise to I_6, and using the empirical Haynes rules proposed by B.K. Meyer *et al.* (119), we calculated similar donor binding energies of 52.2 meV and 52.6 meV from the position of I_6 and from the transition at 3.3726 eV, respectively. These values are comparable to the donor binding energy of 51.55 meV found by Meyer *et al.* (19).

Similar calculations for the I_5 line and the transition at 3.3731 eV gives approximately the same donor binding energies of 50.55 meV and 51.6 meV, respectively. The line at 3.3731 eV is therefore related to the same donor responsible for the I_5 line, but the donor is in its ionized state.

The weak transition at 3.3673 eV, which is more visible after annealing for 2 h, is very close in energy to the I_2 line (19). The I_2 line has been assigned to the ionized donor bound exciton, while the corresponding neutral donor bound exciton is associated with the I_9 line (119). Therefore, the broad band on the lower energy side of I_{8a} may contain the I_9 line, with the corresponding ionized donor bound exciton line at 3.3673 eV. The presence of the I_9 line implies the presence of indium impurities in the ZnO material (19).

The doublet comprising the lines at 3.3657 eV (I_5^*) and 3.3652 eV (I_6^*) are separated by ~ 4.3 meV from the doublet formed by the I_5 and I_6 lines. This energy separation is very close to the ~ 5 meV splitting energy of the A-B valence bands. A similar energy separation was reported by Schrey *et al.* (133) and Meyer *et al*. (19) and the doublet was assigned to exciton states involving the B-valence band. These reports assigned the lines at 3.3657 eV and 3.3652 eV to excitons associated with the B-valence band, and bound to the same impurities/defects giving rise to I_5 and I_6, respectively.

The thermal stability of the I_4 is also remarkable. Many reports [(19), (56), (134)] have suggested that the I_4 line is quenched at 600°C, but surprisingly it is still visible even after 6.5 h of annealing. In order to further determine the thermal stability of the hydrogen-related I_4 line, 1 h isochronal annealing was performed from 650°C to 850°C, in 100°C increments. The results are described below.

4.3.2 Isochronal annealing

The effects of isochronal annealing on as-grown ZnO are presented in figure 4.4. The PL emission drastically changes with an increase in annealing temperature.

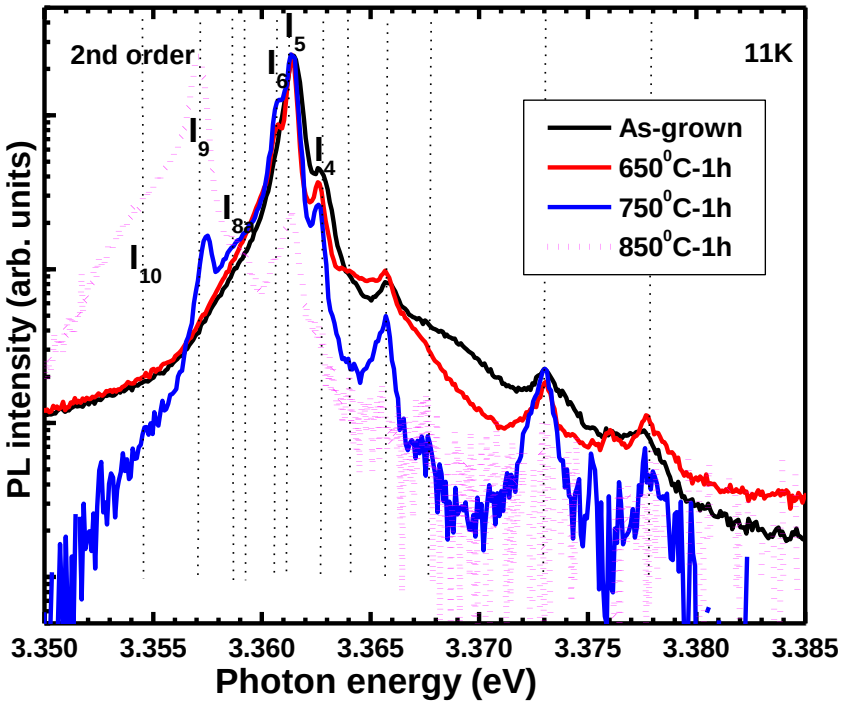

Figure 4.4: Normalized PL spectra of as-grown ZnO, and ZnO annealed for 1 h in argon at 650°C, 750°C and 850°C.

After annealing at 850°C, only a weak I_5 line and an additional emission line at 3.3571 eV are visible. The transition at 3.3571 eV initially appears after annealing at 750°C and increases in intensity until it dominates the PL spectra after annealing at 850°C. The I_4 line remains thermally stable up to an annealing temperature of 750°C and only disappears after annealing at 850°C. This is in contrast with many other thermal stability studies which have shown the disappearance of this transition after annealing at 600°C [(19), (63)]. Recently, Lavrov *et al.* found a correlation between the H_O defect and the I_4 line (63). The I_4 transition was readily enhanced

when the concentration of V_O in the sample was increased prior to hydrogenation. This defect (H_O) was reported to be stable only up to 500°C.

One possible explanation for the thermal stability of the I_4 line takes into account the contribution of the inactive hydrogen reservoir in ZnO. The creation of a high concentration of intrinsic defects (V_O, V_{Zn}), which occurs during high temperature annealing, could increase the concentration of the H_O defect. The formation of this defect could be enhanced by the thermal dissociation of the H_2 molecule (63) or the diatomic H_2^* complex (135) which will feed the V_O vacancy with hydrogen atoms and give rise to the shallow H_O defect. The trapping of hydrogen at V_O could therefore reduce the out-diffusion of hydrogen. Furthermore, the H_2^* complex has a large dissociation energy (~0.92 eV) and requires temperatures ≥ 400°C in order for dissociation to occur (64). This is in the range of the annealing temperatures used in this work. Dissociation of this complex will also promote the subsequent generation of H_O shallow donor impurities. Reynolds *et al.* (136), studied the changes in luminescence of ZnO crystals upon annealing at 800°C. They reported the disappearance of all the excitonic lines above 3.358 eV (including a strong bound exciton line at 3.36139 eV), in favour of a line at 3.3564 eV. They claimed that the donors that bind the excitons in as-grown crystals consist of defect pairs, which rearrange upon annealing to form more closely spaced pairs. The more distant pairs break up first upon annealing and then form more closely spaced pairs, which are responsible for localizing the excitons in samples annealed at 800°C, and which give rise to the new emission line at 3.3564 eV. Such a rearrangement implies a conservation of the total integrated intensity of the NBE emission and a broadening of the new line, as was observed by this group. This broadening which appeared for the new transition at 3.3571 eV is not observed in the present work and the total integrated intensity of the NBE emission is not conserved. The partial quenching of the $I_{5/6}$ line and the emergence of lower energy excitonic lines upon annealing in this work could be due the out-diffusion of the impurities responsible for the appearance of the $I_{5/6}$ lines. In addition, the NBE emission of as-grown ZnO could also have many unresolved transitions in the broad feature seen on the lower energy side of the spectrum of the as-grown ZnO sample (figure 4.1).The disappearance of the dominant lines ($I_{5/6}$) after annealing will then emphasize these unresolved lines.

4.4 Effect of annealing on deep level emission

The presence of deep impurities and intrinsic defects in this material may be deduced from figure 4.5. Three bands are inferred. The as-grown sample shows a band (marked A on the spectrum) centered at ~2.15 eV. Upon annealing at 650°C, the DLE becomes dominated by a band at ~2.07 eV, and a further increase in temperature, up to 850°C shows a fine-structured green luminescence. Intrinsic defects have been assigned to the band centered at ~2.15 eV, for example the V_{Zn} (137) and the O_i (138).

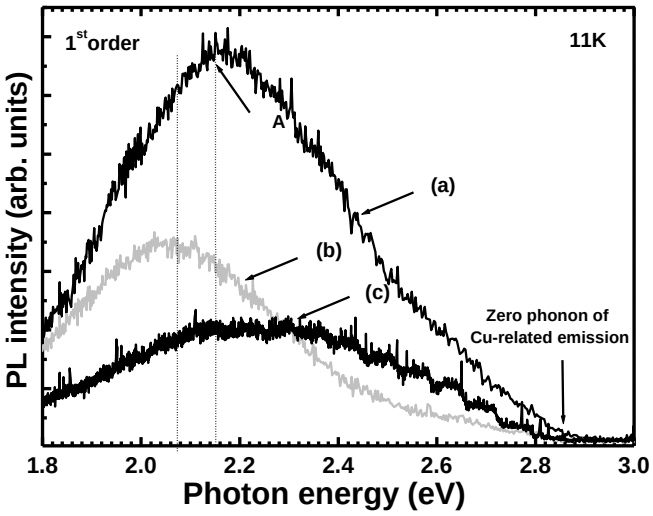

Figure 4.5: DLE of (a) as-grown ZnO, (b) ZnO annealed at 650°C in Ar for 2 h and (c) ZnO annealed at 850°C in Ar for 1 h.

However, impurities have also been deemed responsible for this band. Meyer *et al.* (139), for example, reported two bands at 2.17 eV and 2.1 eV, related to Na and Li respectively. The band at 2.1 eV is close to the band at ~2.07 eV reported in this work. Furthermore, Børseth *et al.* (140) described a Li-related band at 2.17 eV, which is very close to the band at ~2.15 eV observed in this work. Both Meyer *et al.* and Børseth *et al.* reported on hydrothermally grown ZnO. The Li_{Zn} impurity is known as a shallow acceptor and cannot be responsible for the DLE involving Li (76). Li probably forms complexes with other defects in the material to give rise to the DLE. Based on the reports of Meyer *et al.,* (139) and Børseth *et al.,* (140), one can then assume the

involvement of Li in both bands at ~2.15 eV and ~2.07 eV. Annealing at 650°C could induce a rearrangement of the Li-complex and cause the DLE at ~2.15 eV.

This rearrangement upon annealing may give rise to a new complex involving Li and responsible for the band at ~2.07 eV. McCabe *et al.* (141) reported on hydrothermally grown ZnO coated with a Li solution and annealed at a temperature of 700°C. They observed two zero phonon lines at 1.884 eV and 1.879 eV, and linked them both to Li. Although the energy separation between these two bands is much smaller than the two energy bands shown in figure 4.5, their report indicates a possible involvement of Li in more than one band in the DLE for ZnO containing Li. Wardle *et al.* (76) studied the different possible configurations of Li in ZnO and many complexes between Li and native defects were postulated for the DLE. A complex between Li_{Zn} and O_i has a calculated acceptor energy level of about 800-900 meV, which should give the DLE at ~2.53 eV (assuming an energy band gap of 3.43 eV at 11 K). Given the uncertainty in calculated defect energy levels, possible Stokes shifts when the charge state of a deep defect changes, and the possibility that these DLE bands result from donor-acceptor recombination, the energy position of the band observed in figure 4.5 at ~2.15 eV is compatible with recombination involving the complex mentioned above. Upon annealing at 650°C, the Li_{Zn}-O_i complex can dissociate and the O_i native defects can diffuse out, since they are more mobile than V_{Zn} and V_O native defects. Li_{Zn} can then form another complex with the less mobile native defects. For example, the (+/-) level associated with the Li_{Zn}-V_o complex was reported at around E_v+1.3 eV by the same group (76) and could also be responsible for the DLE at ~ 2.07 eV.

Fine-structured green luminescence has been reported by Dingle (142) in a ZnO crystal, which showed the involvement of substitutional Cu^{2+} in this band. Moreover, conversion of the stable Cu impurity from Cu^+ to Cu^{2+} upon high temperature annealing has been demonstrated in ZnO [(143), (144)]. Therefore, Cu^+ has to be present in the as-grown ZnO in order to generate the fine-structured green luminescence after annealing. Reynolds *et al.* (145) attempted to fit this band with each individual emission line modeled by a Gaussian function. They fitted the band assuming two shallow donors separated by 30 meV, and a deep acceptor ascribed to Cu^{2+}.

Figure 4.6 shows the fine-structured green luminescence of our ZnO sample annealed at 850 °C. The PL band obtained was fitted with a multi-Gaussian function. Our fitting gives a zero phonon

Cu-related emission at 2.829 eV. Two sets of phonon replicas were used with phonon energies of 66 meV and 74.9 meV respectively, comparable to the 64 meV local phonon energy and the 72 meV LO phonon energy reported by Reynolds *et al.*, (145). Two Huang-Rhys factors, S_1=4.32 and S_2=7.05 were found from our fitting. S_2 is very close to the Huang-Rhys factor for coupling with the local phonon, whereas S_1, which describes coupling with the LO phonon, is significantly higher than the value of 0.9 reported by Reynolds *et al.*, (145). The fitted in their work converged only up to the dominant 6th fine-structured green emission peak. A large divergence appears in their fitting for the rest of the band below this peak. Such a divergence could introduce a large error to the parameters used for the fitting, and could explain the discrepancy between the Huang-Rhys factor for coupling with the LO phonon reported in their work and our report. Furthermore, the fine-structured green luminescence reported here shows a maximum at the 7-phonon replica, whereas their spectrum peaked at the 6-phonon replica. These differences will give rise to different S-parameters. Our simulation also shows that the contribution of the band at ~ 2.07 eV to the structured green band is negligible, since the simulated spectrum fits the entire green band reasonably well.

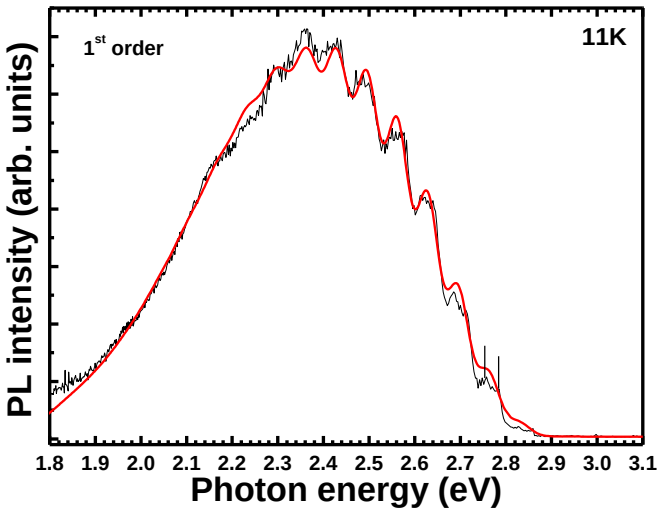

Figure 4.6: Multi-Gaussian fit to fit the fine-structured green band measured for the ZnO sample annealed at 850^{0}C in Ar for 1 h.

4.5 Effect of hydrogen plasma treatment on the near-band-edge PL

In order to determine the effect of hydrogen in ZnO, particularly on certain emission lines between 3.3615 eV and 3.3729 eV, the samples were subjected to a hydrogen plasma treatment at 200°C for different times. At this temperature, a diffusion coefficient D≈ 8.10^{-10} $cm^2.s^{-1}$ (146) is calculated and for a plasma exposure time varying between 15 min and 300 min, the diffusion length L (147) varies between ~8.5 µm and ~38 µm. The PL results obtained are presented in figure 4.7(A). As a reference, the PL of an as-grown sample has been included in the figure. The near-band-edge luminescence is clearly enhanced after plasma treatment for 45 minutes, due to the passivation of non-radiative defects and deep radiative defects (see next section, figure 4.8). The spectrum broadens drastically and an increase in intensity is observed for a new transition at ~3.361 eV.

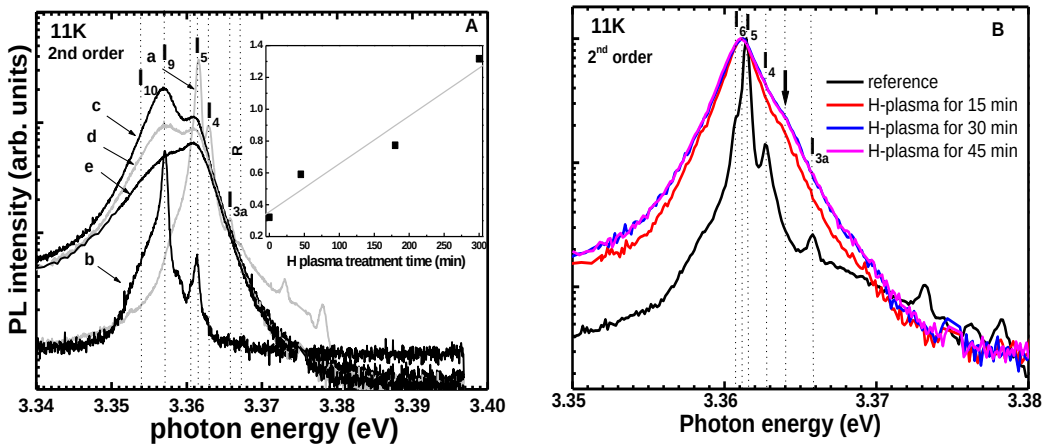

Figure 4.7: (A) NBE emission of (a) as-grown ZnO, (b) ZnO annealed at 850°C for 1 h in Ar. Spectra (c) to (e) are for material exposed to an H-plasma for 45 min, 180 min and 300 min, respectively, after first annealing the samples at 850°C for 1 h in Ar. The insert shows the ratio (R) of the intensity of the 3.361 eV line to that of the 3.357 eV line as a function of the hydrogen plasma treatment time before annealing. (B) Normalized NBE emission of as-grown ZnO and samples exposed to a H-plasma for 15 min, 30 min and 45 min.

The insert to figure 4.7(A) shows a plot of the ratio R of the intensity of the line at 3.361 eV to the intensity of the line at 3.357 eV. The line at ~3.361 eV increases in intensity faster than the

line at 3.357 eV, with the former becoming dominant after 5 h of plasma exposure. The slow quenching of the line at 3.361 eV could be explained by the involvement of hydrogen in this line. It is well-known that implantation generates high concentrations of non-radiative defects which quench the NBE luminescence (148). Therefore, the hydrogen plasma treatment would generate both hydrogen-related and non-radiative defects. The latter would quench the luminescence while the former would enhance the luminescence related to hydrogen. These effects work together to slow down the quenching of the line related to hydrogen. This is in good agreement with the slow quenching of the line at ~3.361 eV. The same increase in intensity of the transition at ~3.361 eV was noticed when as-grown ZnO was exposed to H plasma, as seen in figure 4.7(B). The transition at ~3.361 eV dominates the NBE emission after 15 min of H plasma treatment with an additional transition at ~3.364 eV (arrow in figure 4.7(B)). Using the Haynes formulation in Meyer *et al.* work's (119), donor binding energies of 51.62 and 43.5 meV, respectively, were calculated for these two transitions. The 51.62 meV donor binding energy is very close to the value (53 meV) of that of hydrogen at the bond-centered site (H_{BC}), deduced from a PL line at 3.3601 eV (63). It is tempting, therefore, to ascribe the transition at ~3.361 eV to H_{BC}. However, Lee *et al.* (148), found that the dominant line at 3.364 eV in the as-grown ZnO single crystal was surpassed in intensity by a new transition at ~3.361 eV when the ZnO sample was implanted with hydrogen. They suggested that the new transition at ~3.361 eV was a complex involving H and V_{Zn}, which were introduced during implantation. Subsequent annealing at 300^0C in vacuum was sufficient to restore the transition at 3.364 eV as the dominant line. In the work of Lavrov *et al.* (63), only a line at 3.3601 eV and the I_4 line were visible after the ZnO sample was annealed in hydrogen gas at 750°C. According to the work of Lee *et al.* (148), the high annealing temperature used in the work of Lavrov *et al.* (63) would make the transition at 3.361 eV unlikely to appear. Therefore, the line at ~3.361 eV in the present work is probably different from the H_{BC} related transition at 3.3601 eV.

It is not unusual to observe several shallow H-related donor transitions in ZnO. Karazhanov *et al.* (64) suggested in their theoretical work the possibility of four hydrogen complexes in Zn-deficient ZnO. In these configurations, the hydrogen atoms move towards their nearest O neighbors and saturate their dangling bonds, leading to the formation of O–H complexes. Since there are four dangling bonds, one can expect four different complexes, namely 1(O-H)-V_{Zn},

2(O-H)-V_{Zn}, 3(O-H)-V_{Zn} and 4(O-H)-V_{Zn}. Among these complexes, only the 3(O-H)-V_{Zn} and 4(O-H)-V_{Zn} configurations have shallow donor levels. The dissociation energy required to release one H atom from each of these two configurations was 1.1 eV and 0.8 eV, respectively. Karazhanov *et al.* also found that the 4(O-H)-V_{Zn} configuration was energetically the most favorable. Hydrogen plasma treatments can generate high concentrations of V_{Zn} and consequently the energetically favorable 4(O-H)-V_{Zn} might dominate, which could be responsible for the dominant transition at ~3.361 eV after hydrogen plasma treatment. Since it is thermally less stable than the 3(O-H)-V_{Zn} complex, it seems possible that it readily loses one hydrogen atom to convert to the 3(O-H)-V_{Zn} complex during thermal treatment. The 3(O-H)-V_{Zn} complex could then be responsible for the transition at 3.364 eV. This would explain the work by Lee *at al*. (148), where the dominant line at 3.361 eV is overshadowed by the transition at ~3.364 eV after annealing of the hydrogen-implanted ZnO sample. Since hydrothermally grown ZnO has been shown to be zinc-rich, the V_{Zn} likely has a low concentration in the as-grown material, preventing the appearance of the lines at ~3.364 eV and ~3.361 eV. It also appears that the hydrogen lines are strongly influenced by native defects or impurities. High concentrations of V_O would generate the I_4 line whereas high concentrations of V_{Zn} may generate the lines at ~3.361 eV and 3.364 eV.

Comparing the effect of hydrogen plasma treatment on annealed and as-grown ZnO samples in figure 4.7, it appears that the line at 3.364 eV is only visible after hydrogen plasma treatment on the as-grown sample. The presence of Cu^+ and H in the as-grown sample could allow the formation of Cu-H complex which is stable up to 650°C (149). Other complexes such as Cu_{Zn}-Cu_{Zn}-H_i and Cu_{Zn}-Cu_i-H_i [(149), (150)] could also be initially present in the as-grown sample. Thus, subsequent incorporation of H atoms by H plasma treatment can fill other optically active sites, giving rise to the transitions at ~3.361 eV and 3.364 eV. Furthermore, annealing at 850°C will dissociate the Cu-H complex, and possibly the Cu_{Zn}-Cu_{Zn}-H_i and Cu_{Zn}-Cu_i-H_i complexes. The H generated by the dissociation of these complexes will diffuse out, activating ionized Cu species such as Cu^+ and Cu^{2+}. The involvement of the latter in the fine-structured green luminescence after annealing at 850°C was showed in section 4.4. Therefore, subsequent H plasma treatment on the ZnO sample previously annealed at 850°C could form the Cu-H complexes, preventing the formation of other optically active hydrogen-related defects. Only the

energetically favorable 4(O-H)-V_{Zn} complex, related to the line at ~3.361 eV could form, in addition to the Cu-H complexes. This is consistent with the emergence of the solitary line at ~3.361 eV after hydrogen plasma treatment, as observed in figure 4.7(A).

4.6 Effect of hydrogen plasma treatment on deep level emission

Figure 4.8 shows the effect of hydrogen plasma treatment on the DLE of as-grown and annealed (at 650^0C and 850^0C) ZnO. For comparison the DLE of an as-grown sample, and a sample annealed at 850°C with no subsequent hydrogen exposure, were also included.

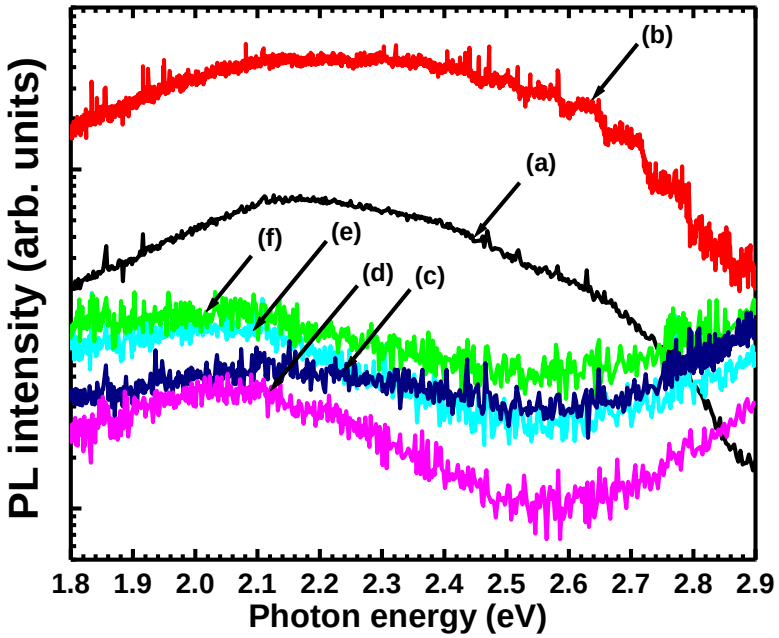

Figure 4.8: DLE of (a) as-grown ZnO, (b) ZnO annealed at 850°C for 1 h in Ar, (c) as-grown ZnO exposed to H-plasma for 3 h, (d) ZnO annealed at 650°C for 1 h in Ar and exposed to H-plasma for 3 h, (e) ZnO annealed at 850°C for 1 h in Ar and exposed to H-plasma for 1 h, (f) ZnO annealed at 850°C for 1 h in Ar and exposed to H-plasma for 3 h.

Interestingly, a weak DLE band at ~2.08 eV is still visible after hydrogen plasma treatment. This band is unaffected by the pre-annealing of the ZnO sample. This suggests that the defect could only be generated by the incorporation of hydrogen into the ZnO sample. There have been

reports on the possible involvement of hydrogen in the creation of deep levels. Karazhanov *et al.* (135) theoretically investigated a H_2^* complex, which involves a H atom tightly bound to the nearest O, forming the O-H complex, and a second H atom bound to the nearest Zn. Such a complex was suggested to have a deep level in the band gap and may be responsible for the emission at ~2.08 eV observed here. Indeed, Polyakov *et al.* (151) using deep level transient spectroscopy (DLTS), reported a deep hole trap located at 0.9 eV after hydrogen plasma treatment of n-type ZnO, which could give rise to PL at around 2.08 eV.

4.7 Conclusions

In conclusion, the effect of high temperature annealing on the PL of hydrothermally grown bulk ZnO shows an anomalous stability of the I_4 line related to hydrogen. This apparent stability is explained by the thermal dissociation of hidden H_2 molecules or complexes, which can feed the shallow hydrogen donor responsible for the I_4 line.

Efficient out-diffusion of hydrogen is observed after annealing at 850°C. This annealing temperature can also be used for out-diffusion of hydrogen in the ZnO:N samples (see chapter 6 and 7). Furthermore, the high temperature annealing can activate some deep level impurities such as Cu^{2+}, which are responsible for the fine-structured green luminescence.

The hydrogen plasma study shows the appearance of different hydrogen-related transitions in the NBE emission. In addition to the I_4 transition at 3.3628 eV, two other transitions appear at 3.364 eV and ~3.361 eV. Complexes such as 3(O-H)-V_{Zn} and 4(O-H)-V_{Zn} are suggested to be responsible for these transitions, due to the possible generation of V_{Zn} defect during plasma treatment.

5 Optical properties of ZnO/GaAs

5.1 Introduction

Based on first-principles calculations, it was predicted that ZnO doped with arsenic under oxygen-rich conditions would introduce a relatively shallow acceptor complex between As_{Zn} and $2V_{Zn}$. This complex, with a low formation energy and a shallow acceptor level at ~150 meV, is more likely to form than As_O, which violates the doping size principle (33). Moreover, theoretical calculations have shown that the As_O has a deep acceptor level at 1.15 eV (50) or 0.93 eV (152) above the valence band maximum (VBM), and thus the contribution to the hole density from the ionization of As_O should be negligible at room temperature compared to the contribution from the ionization of As_{Zn}-$2V_{Zn}$. Furthermore, the small size mismatch between As and Zn (see Table 2.1) could preferentially favour the formation of the As_{Zn} donor, which, when binding with $2V_{Zn}$ in significantly high concentrations under oxygen-rich growth conditions (52), can give rise to the shallow acceptor As_{Zn}-$2V_{Zn}$.

This defect can also be introduced into ZnO films grown on GaAs substrates and which are subsequently annealed. The As dopant will, in this case, diffuse from the substrate into the ZnO films during annealing. This process could, of course, be hampered by the diffusion of Ga into the ZnO films which can compensate the acceptor activity of arsenic in the ZnO films [(153), (107)]. Therefore, the choice of the optimum annealing temperature and the annealing ambient are crucial to minimize the diffusion of Ga, and for the optimization of the diffusion of As into the ZnO films.

In this chapter, a comparative study of the annealing ambient on the properties of ZnO films on semi-insulating GaAs substrate is presented. The films were annealed in either an oxygen or a nitrogen ambient. The effect of the annealing temperature on the optical properties of the ZnO/GaAs material is also studied. The ZnO samples were grown at 380°C for a $\frac{VI}{II}$ of 60. TBOH and DEZn were used as oxygen and Zn sources, respectively. The thickness of the films was ~ 1μm.

It is interesting to mention results from Hall effect measurements on as-grown and annealed samples here. Hall measurements were performed on as-grown and annealed samples, both

before and after etching away the ZnO films. Before removing the film, Hall measurements at room temperature on the as-grown ZnO/GaAs indicated *n*-type conductivity (carrier concentration = 5.10^{18} cm^{-3} and mobility = 50 $cm^2/V.s$, which are typical for ZnO/GaAs films grown in this laboratory using DEZn and TBOH as sources (129)). After removing the film by etching, no reliable measurements were possible due to the semi-insulating nature of the GaAs substrate. After annealing ZnO/GaAs samples (at 500°C and higher), *p*-type conductivity was typically observed with a similar hole concentration (~10^{18} cm^{-3}) and mobility (27 $cm^2/V.s$). Interestingly, after removing the annealed films by etching, *p*-type conductivity was still observed. It seems plausible that the *p*-type conductivity observed for annealed ZnO/GaAs arises from the diffusion of Zn from the ZnO films into the GaAs substrate, converting the near-surface region of the semi-insulating GaAs to *p*-type. Therefore, one should be cautious when interpreting electrical measurements on ZnO/GaAs. For example, Sun *et al.* (34), reported *p*-type conductivity for ZnO grown on semi-insulating GaAs by MOCVD, showing that *n*-type as-grown ZnO/GaAs converted to p-type when after annealing at temperatures between 520 and 560°C. This *p*-type conductivity could be due to the diffusion of Zn in the GaAs substrate.

5.2 Effect of annealing temperature and ambient

Figure 5.1 shows photoluminescence (PL) spectra of ZnO/GaAs annealed for 1 h at different temperatures in N_2 or O_2. The NBE emission of the as-grown samples is dominated by the $I_{6/6a}$ lines. Also visible are stacking fault related DAP and FA transitions at 3.301 eV and 3.315 eV (92), respectively and a transition at 3.332 eV, which can be assigned to the Y-line (19) related to a structural defect. A weak line at 3.338 eV is also visible after annealing in oxygen and is comparable in energy to an A°X line reported by Meyer *et al.* (19). After annealing at 500°C in either ambient, a transition at ~3.31 eV appears (see arrow). This transition is also visible in ZnO grown on sapphire (see figure 5.1-C). Its origin is as yet unknown and further investigation is needed to clarify its origin. Interestingly, after annealing in oxygen at 550°C, a transition at ~3.35 eV is visible. This transition is not visible for the sample annealed in N_2 at the same temperature. A further increase in the annealing temperature (600°C) has little effect on the PL spectrum of the sample annealed in N_2. However, the transition at 3.35 eV disappears when the sample is annealed in O_2 at this higher temperature. Furthermore, annealing in O_2 generates more

structural defects in the ZnO sample. This is illustrated by the increase in intensity of the Y-line

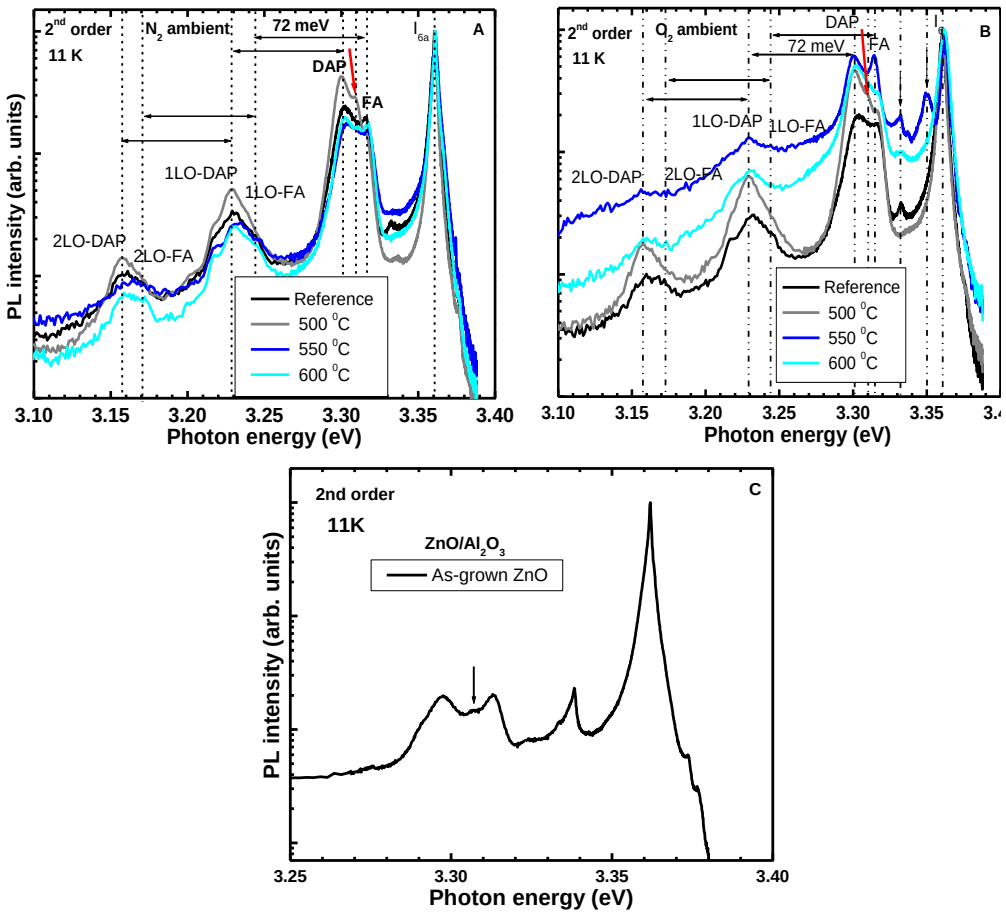

Figure 5.1: The NBE emission at 11 K of ZnO/GaAs annealed for 1 h at 500°C, 550°C and 600°C in A) nitrogen and B) oxygen. The respective PL spectra are normalized at the position of the $I_{6/6a}$ lines. For comparison, the NBE emission of ZnO grown on *c*-plane sapphire is shown in C.

at 3.332 eV and the stacking fault related transitions at 3.301 eV and 3.315 eV. A series of LO replicas of the FA and the DAP transitions appear on the lower energy sides of the spectra. The transition at ~3.35 eV has been assigned to an acceptor bound exciton (A°X) in ZnO:As [(154), (155), (156), (157)]. More evidence on the origin of this transition will be presented later in this chapter. It is interesting to mention that DAP and FA transitions at the energy positions of the stacking fault related lines have often been ascribed in literature to the As acceptor [(154), (158), (159)].

5.3 Effect of annealing time in nitrogen and oxygen ambient

The effect of annealing time on ZnO/GaAs was also studied at 550°C in nitrogen and oxygen. Figure 5.2 shows the normalized NBE emission of the ZnO films grown on GaAs substrate and subsequently annealed (after growth) for different times at 550°C in nitrogen and oxygen. It can be seen that a longer annealing time has a slightly quenches the DAP and FA related to the stacking fault, suggesting a reduction of stacking fault in the ZnO films then the annealing is performed in nitrogen. In the oxygen ambient, the transition at 3.35 eV increases in intensity for increased annealing times (from 1 h to 2 h). This increase in concentration of the defect responsible for the 3.35 eV transition is followed by a drastic increase in the PL from structural defects, as mentioned in section 5.2. A further increase in the annealing time decreases the PL line at 3.35 eV, which is accompanied by a decrease in the transitions related to the structural defects.

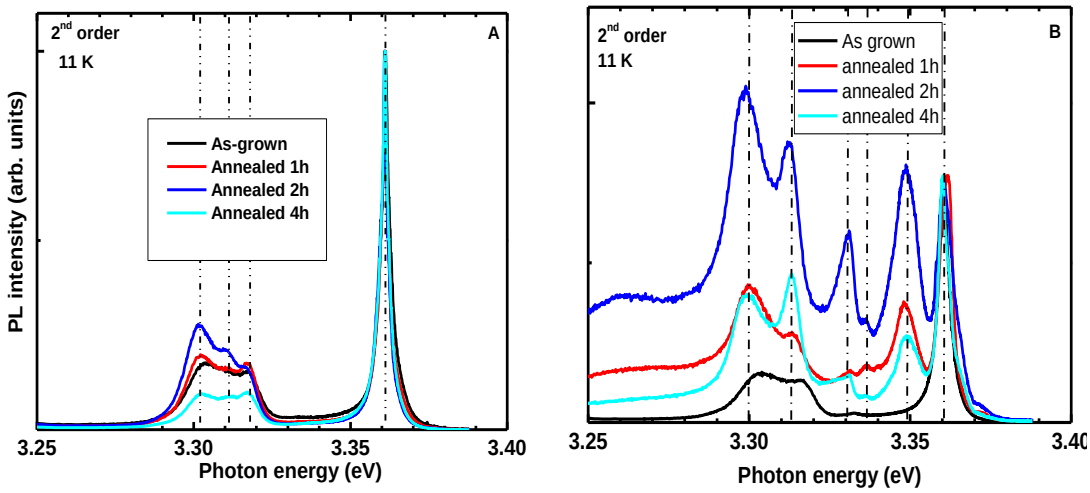

Figure 5.2: The NBE emission at 11K of ZnO/GaAs annealed at 550°C for 1h, 2h and 4h, respectively in A) nitrogen and B) oxygen. The PL spectra are normalized at the position of the $I_{6/6a}$ lines.

The appearance of the PL line at 3.35 eV is obviously strongly dependent on the annealing ambient. In fact, annealing in oxygen can promote high concentrations of V_{Zn}, but should also decrease the concentration of oxygen vacancies (V_O) in the ZnO sample. Therefore, it is more

likely that the As_{Zn}-$2V_{Zn}$ acceptor defect is created, instead of the As_O deep acceptor, when the annealing is performed in oxygen. The transition at 3.35 eV is thus tentatively suggested to be related to the As_{Zn}-$2V_{Zn}$ acceptor. Furthermore, the reduction of the stacking fault in the ZnO films annealed in the nitrogen ambient could be due to the low diffusion of As or Ga into the ZnO films during the annealing process. Returning to figure 5.1, the disappearance of this transition after annealing at 600°C is in excellent agreement with the work of Choi *et al.* (157), where x-ray photoelectron spectroscopy (XPS) showed a significant decrease in the intensity of the 43.9 eV peak related to the As_{Zn}-$2V_{Zn}$ defect in their As-doped, p-type ZnO thin films grown using sputter deposition.

5.4 Temperature dependent photoluminescence

To establish the nature of the transition at 3.35 eV, temperature dependent PL was performed on the ZnO/GaAs sample annealed at 550°C in oxygen for 2 h. Figure 5.3 shows the PL spectra obtained at different temperatures (11 K - 91 K). The $I_{6/6a}$ and the 3.35 eV emissions quench, while a transition at 3.373 eV becomes dominant with increasing temperature. This transition at 3.373 eV could be the A free exciton (FE), and its dominance with increasing temperature may be attributed to the thermal dissociation of the bound excitons. Furthermore, the 3.373 eV peak position is very close to the FE energy position reported by Meyer *et al*. (19) in bulk ZnO grown by different methods. By fitting the PL peak positions with Eq's. 3.3 and 3.15, and using $\beta = 920$ K (Debye temperature), it can be seen that the FE, $I_{6/6a}$ and 3.35 eV transitions depict the same trend with increasing temperature - they follow the shrinkage of the band gap with increasing temperature. Therefore, it appears reasonable to assume an excitonic nature for the 3.35 eV transition. Since it appears in the spectral region where acceptor bound excitons has been reported for ZnO [(19), (63)], this line is assigned to A°X.

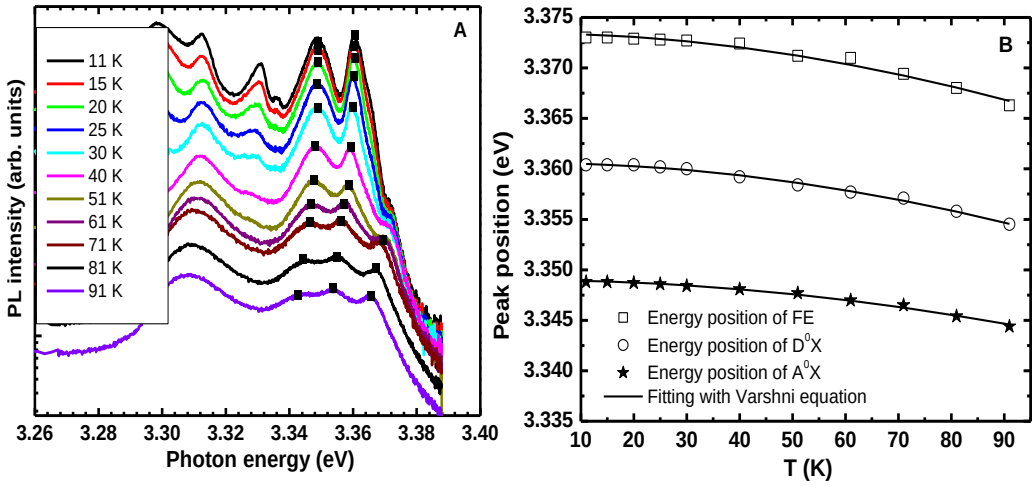

Figure 5.3: A) Temperature dependence (11 K-91 K) of the PL of ZnO/GaAs, annealed for 2 h at 550°C in O_2. B) Energy position of the three lines indicated by squares in (A), fitted to the Varshni equation.

Using Eq. (3.17), the decays of the integrated intensities of the $I_{6/6a}$ and 3.35 eV transitions with increasing temperature were fitted and the results are shown in figure 5.4. Surprisingly, both fits give the same quenching activation energy, E_i = 14.7 ± 1 meV. This value is very close to the localization energy, E_{loc}, of the $I_{6/6a}$ line (deduced from its position relative to that of the FE line) , which are the dominant transitions in the excitonic region of the NBE emission. However, for the (A°X) transition, the localization energy E_{loc} is underestimated by the thermal activation energy of the PL quenching E_i, since the position of the A°X line relative to the FE line implies $E_{loc} \approx 24\,meV$. The E_i value deduced from the fitting of the intensity of the A°X line could describe the thermal activation of some non-radiative process.

From a comprehensive study of acceptors in ZnO, Gutowski *et al.* (160) reported the following equation

$$E_{loc} = 0.24E_x^{(A^\circ X)} - 0.02\ (\text{meV})$$

which gives $E_x^{(A°X)}$= 100 meV. This value is in good agreement with the theoretical and experimental values reported for the acceptor binding energy of the As_{Zn}-$2V_{Zn}$ complex. In fact,

first-principle calculations reported a value of $E_x^{(A°X)}$= 150 meV for the As_{Zn}-$2V_{Zn}$ complex (33). Also from PL and Hall measurements, an acceptor binding energy of (120±10) meV was deduced by Ryu *et al.* (154) in arsenic-doped *p*-type ZnO grown by hybrid beam deposition.

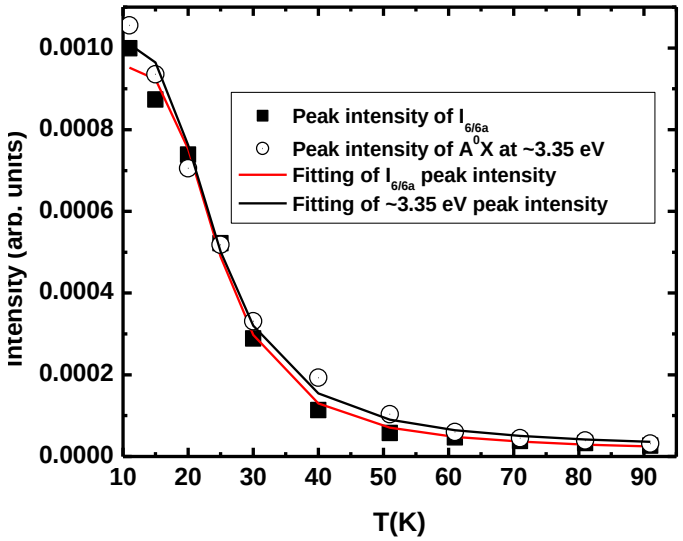

Figure 5.4: Intensity decay with increasing temperature of the $I_{6/6a}$ and A°X (~3.35 eV) lines. The data is fitted to Eq. (3.18).

5.5 Conclusions

The optical properties of ZnO/GaAs annealed at different temperatures in nitrogen or oxygen ambients revealed that As acceptors can diffuse into the ZnO films to form (possibly) the As_{Zn}-$2V_{Zn}$ shallow acceptor when annealing is performed in an oxygen ambient. In this ambient, high concentrations of V_{Zn} may be formed, as well as the reduction of the native point defects (V_O, Zn_i) due to the incorporation of oxygen into the ZnO sample during annealing. The generation of the shallow As_{Zn}-$2V_{Zn}$ acceptor is optimal after annealing at 550°C for 2 h. A further increase in the annealing temperature can result in the incorporation of more donor defects as illustrated by the increase in relative intensity of the D°X for longer annealing times.

6 Nitrogen solubility and optical properties of ZnO:N

6.1 Introduction

In order to grow p-type ZnO, a reproducible nitrogen doping process needs to be developed. The MOCVD growth technique allows one to vary the different growth parameters in a systematic way to achieve high quality undoped ZnO [(161), (162), (163), (164)]. This technique is suitable for in-situ doping of ZnO. Nitric oxide (NO) is used as both the nitrogen and oxygen precursors for the in-situ doping studies presented in this thesis.

As mentioned in section 2.4, the valence band maximum in ZnO lies close to the *p*-type pinning energy, $\varepsilon_F^{(P)}$, thus making the introduction of shallow acceptors into this material very difficult. As also mentioned in chapter 2, nitrogen doping of ZnO by MOCVD is hampered by many issues, such as the formation of self-compensating defects, the low solubility of nitrogen, and the passivation by hydrogen, which is present in high concentrations in ZnO films grown by MOCVD. Also, it seems as if the high growth temperatures required for high crystalline quality material is not favourable for the activation of the nitrogen acceptor dopant during deposition [(165), (166), (167)]. Furthermore, the concentration of carbon in ZnO doped with nitrogen using MOCVD increases at high growth temperatures (168). In view of these issues, good control of the growth parameters used during the synthesis of ZnO doped with nitrogen is imperative in order to optimize the efficiency of doping.

In this work, the effect of the oxygen to zinc ratio (30 to 120) and the growth temperature (270°C to 370°C) on the incorporation of nitrogen into the ZnO thin films is studied. Activation of nitrogen acceptors by post-growth annealing is also investigated. The thickness of the films ranged between 0.7 μm and 1.6 μm.

The influence of the growth parameters on the concentration of nitrogen (N), as well as the concentration of unwanted impurities such as hydrogen (H) and carbon (C), was studied by secondary ions mass spectroscopy (SIMS). The effect of post-growth annealing of the concentration of N, H and C was also studied.

Post-growth annealing in oxygen gives more information on the composition of the samples. While the nitrogen and hydrogen concentrations decrease for lower growth temperatures, no

significant decrease in the carbon and hydrogen concentrations are observed for higher growth temperatures. Different forms of complexes containing the different elements (N, H, C) are proposed to explain this behaviour with growth temperature.

The crystalline and morphological properties of as-grown and annealed samples have been studied using XRD and SEM. Improved crystallinity is observed for higher growth temperatures. A correlation between the out-diffusion of the H and C and the crystalline quality of the films is observed.

6.2 Solubility of nitrogen in ZnO grown on *c*-plane sapphire substrate

6.2.1 Effect of VI/II ratio

6.2.1.1 As-grown ZnO grown with NO

In order to confirm the presence of nitrogen and other unwanted impurities in the ZnO films grown with NO, SIMS measurements were carried out. A mass resolution of m/dm=1400 (medium high resolution) have been employed to resolve some of the possible interferences with the N-signal. Since the ionization probability of N is extremely small, the molecule $^{14}N^{16}O$ has been monitored instead, having a mass of 30 amu. At this mass unit, several interferences may occur. For example $^{12}C^{18}O$ is a possible interference that is not possible to resolve using high mass resolution, but most of the interferences are negligible in the present measurements. Furthermore, the first 150 nm of the sample is more or less correlated with a decrease in the matrix signal (specifically the zinc signal), indicating that the stoichiometry, impurity concentration or morphology induces a large change in the ionization efficiency and the concentrations up to this depth are thus not reliable. Therefore, the different plots do not include the erroneous concentrations of the different impurities in the first 150 nm. Also the difference in thickness observed for the samples results from the severe growth rate non-uniformity in the reactor.

Figure. 6.1 shows the concentration of H, C and N in ZnO grown at 310°C with different VI/II ratios. SIMS clearly shows high concentrations of nitrogen in the ZnO films. Also present are H and C. The concentration of H is higher than the concentration of N and C for all VI/II ratios. The sample grown with the highest VI/II ratio (=120) shows an increase in the concentration of

N compared to the values for samples grown with VI/II ≤60. This increase is in contrast with previous work (29), which predicts a decrease in nitrogen concentration with an increase in VI/II ratio. This report showed that for a sample grown at 400°C, using NO as both oxygen and nitrogen sources, an increase in the VI/II ratio yielded more atomic oxygen in the reactor chamber, and this possibly prevented the incorporation of nitrogen atoms into the ZnO films. Furthermore, it was suggested that at such a high growth temperature, the concentration of N decreases, because Zn prefers to bind with O due to the larger binding energy of the Zn-O bond (27). It seems very likely that the dependence of the incorporation efficiency on VI/II ratio will vary for different growth temperatures. The relatively low growth temperature (310 °C) used in this work could indeed cause an increase in N concentration with increasing VI/II ratio, especially taking into account that an increase in VI/II ratio is accompanied by an increase in the concentration of nitrogen as well as oxygen in the reactor. This behaviour will possibly be inverted for higher growth temperatures, where the preferential formation of Zn-O bonds with increasing oxygen concentration in the reactor will reduce the incorporation efficiency of nitrogen. Furthermore, at low growth temperature, high concentrations of native point defect such as Zn_i and V_O are expected (164) even for high VI/II ratio. These native defects have low formation energies in both Zn- and O-rich conditions (22). The presence of V_O in our samples grown at relatively low temperature could ease the substitution of N acceptor in this vacancy, giving rise to high concentration of N_O. The formation of H, C and N complexes can also be enhanced in ZnO:N films. Various complexes involving these impurities have been reported [(31), (32), (168), (169)]. The alkyl group CH_n (n = 1, 2, 3) has been found in high concentrations in undoped ZnO grown by MOCVD (170), using DEZn and O_2, and it is found to be the main source of carbon in this material. However, contrasting results have been reported on the presence of the alkyl group in ZnO:N. Zhang *et al.* (171) reported a FTIR signal related to the alkyl group in ZnO:N, prepared by rf reactive magnetron sputtering and using NH_3 as nitrogen source in. This FTIR signal was comparable in intensity to the N_O-H and O-H signals. The alkyl signal decreased in intensity when the sample was annealed at 500°C, suggesting a partial dissociation of the group or simply its out-diffusion from the films. On the other hand, comparing the FTIR signal related to the alkyl group in undoped ZnO and ZnO:N, both grown by MOCVD using DEZn and NO for nitrogen doping, Li *et al.* [(31), (170)] found a drastic reduction of the alkyl FTIR signal in the as-grown ZnO:N.

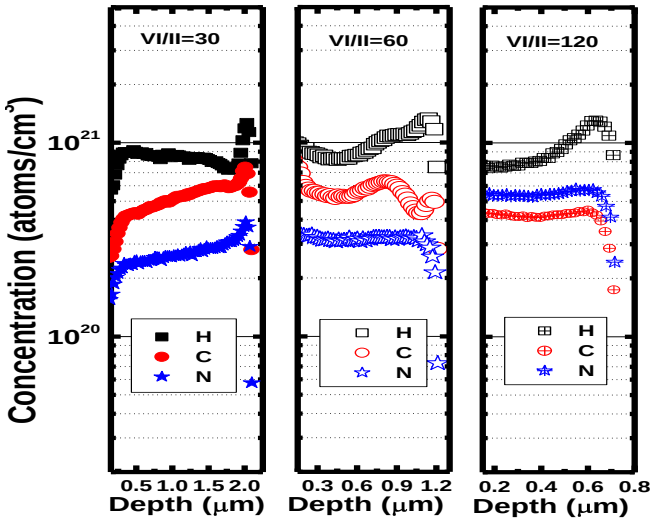

Figure 6.1: The concentration of H, C and N determined by SIMS for samples grown at 310 ^{0}C and using different VI/II ratios (VI/II=30, 60, 120).

More significantly, Nickel *et al.* (169) found no CH_n vibrational modes in ZnO:N grown by MOCVD, using dimethylzinc, tertiarybutanol and diallylamine as Zn, oxygen and nitrogen sources, respectively. These latter results indicate that the high incorporation of C in ZnO:N grown by MOCVD is not preferentially in the alkyl form This could be due to the higher formation energy of these complexes relative to that of other complexes involving carbon, such as $(CO)_O$ and $(NC)_O$ [(32), (170), (172)]. Moreover, the probable presence of the N_O acceptor could render the $(CO)_O$ complex unstable (32), resulting in a high incorporation of carbon in the form of $(NC)_O$. Furthermore, among the different charge states of the $(NC)_O$ complex, the +1 charge state exhibits the lowest formation energy (32) and could be one of the main sources of compensation of the N_O acceptor. Moreover, Volintiru *et al.* (173) reported an electrically inactive (-CN) which acts as impurity scattering centres. This complex was a source of incorporation of nitrogen in the ZnO grown by MOCVD.

The N_O-H complex is also stable in ZnO:N and is electrically inactive [(31), (174)]. This complex also has a small formation energy, suggesting that it will have a high concentration in ZnO:N. Another possible source of annihilation of the N_O acceptor activity in ZnO:N is the N_2 molecule, which can occupy different sites in the ZnO lattice. In the oxygen vacancy site, it

forms the $(N_2)_O$ defect which is more stable in the +2 charge state (32). The strong N-N bond combined with the weak interaction of N with the surrounding Zn atom, suggests that this complex can easily be removed by annealing [(23), (32)]. Recent work by Nickel *et al.* (175) found that the previously believed inert molecule, N_2, could have two energetically favourable localized states in the band gap. The formation energies of these N_2 configurations were even lower than that of $(N_2)_O$. In both cases, the Zn-O bond was broken to allow the insertion of the N_2 molecule either in the N_2O molecule form, or simply in its natural N_2 form, without any chemical bonding with the host lattice (175). The contribution of some of these complexes to the high concentration of non-radiative centres should also not be ruled out (see chapter 8).

All these possible complexes can only complicate the interpretation of the SIMS results, since this characterization technique does not give any information on the location of the impurities. However, post-growth annealing could dissociate the weakly bound complexes and should give more insight into the strongly bound complexes. In fact, annealing at high temperatures is commonly used to out-diffuse unwanted impurities and consequently activate the dopants in the grown samples. The samples grown in this study were therefore annealed in oxygen and the results are presented below.

6.2.1.2 Effect of post-growth annealing in oxygen

Figure 6.2 shows the concentration of H, C and N in ZnO grown using various VI/II ratios and subsequently annealed at 850°C in oxygen for 2 h. Annealing results in an overall slight decrease in the nitrogen content relative to that in the as-grown samples (see figure 6.1). At a VI/II ratio = 120, a strong accumulation of C, N and H is observed near the surface. Similar effects are evident near the interface with the substrate. The drastic decrease in H concentration in the bulk of all these samples reflects the efficient dissociation of the complexes involving H impurities and the subsequent out-diffusion of hydrogen. CH_n, N_O-H and H-CN can dissociate or out-diffuse in their initial forms during high temperature annealing. A previous report by Jokela et *al.* (176) showed that the N_O-H complexes dissociate at temperatures above 700°C. The IR signal related to this complex disappeared when the ZnO:N sample was annealed at 800°C.

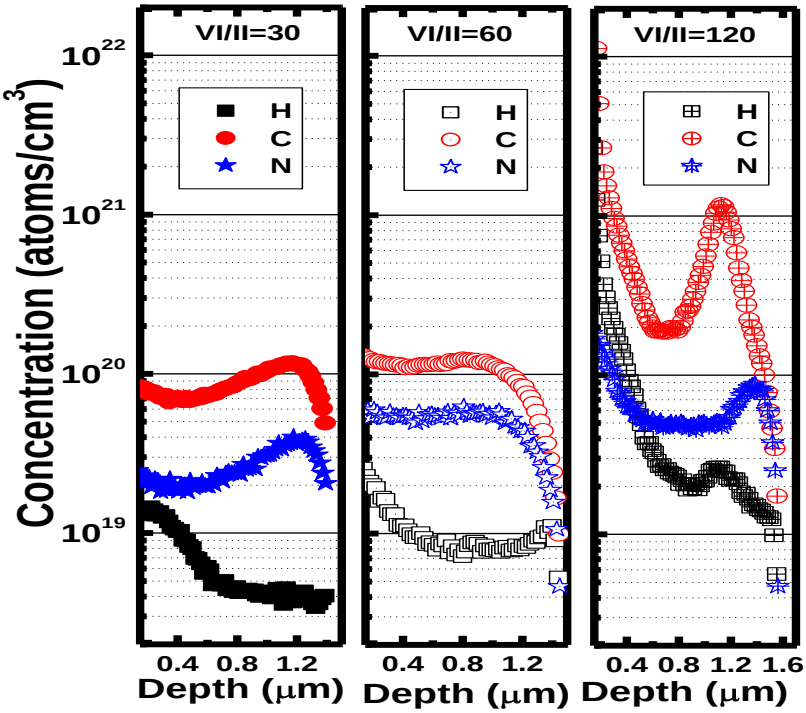

Figure 6.2: The concentration of H, C and N determined by SIMS for samples grown at 310 ^{0}C at different VI/II ratios. The samples were annealed at 850°C in oxygen for 2 h after growth.

Thus, for annealing temperatures higher than 800°C, such as that used in the present work, the total dissociation of the N_O-H complex can be assumed. Furthermore, in chapter 4 (section 4.3.2), it was shown that hydrogen can efficiently diffuse out of bulk ZnO at 850°C. Thus, the H liberated from N_O-H will out-diffuse from the sample. Furthermore, as-mentioned in section 6.2.1.1, due to the weak interaction between nitrogen (in the form of N_2) and the surrounding Zn atoms, N_2 molecules will easily out-diffuse from the samples. This out-diffusion of the N_2 molecule can also be responsible for the decrease in N concentration after annealing.

Interestingly, the depth profiles of C and N are very similar to each other for all the samples after annealing. This suggests the formation of complexes between C and N, such as the $(CN)_O$ complex, which are still present in these samples after annealing. In fact, the stability of this complex upon annealing was studied by Wang *et al.* (177). Their work showed that $(CN)_O$ was still present in ZnO:N sample after annealing at 800°C in oxygen. However, the higher

concentration of C compared to that of N in our work suggests that, in addition to the $(CN)_O$ complex, C could also be found in other forms. Upon annealing at high temperatures, these forms of carbon could be drawn near to the surface or the interface. Graphite, originally at the grain boundaries (178), is a possible candidate for the additional carbon at the surface. Furthermore, for the sample grown at VI/II=120, the accumulation of H, N and C near the interface indicates the possible formation of CH_n and $(CN)_O$ near the interface of this sample during annealing.

High temperature post-growth annealing treatment is expected to generate high concentrations of the N_O acceptor by dissociation of self-compensating defects such as N_O-H. However, the thermal energy supplied during the annealing process could also facilitate the formation of N_2 molecules [(179), (180)] which will subsequently diffuse out. Also, the high concentration of native point defects (V_O, V_{Zn}, Zn_i) [(181), (182)] could hinder the activity of nitrogen as an acceoptor. For example, the thermally excited N_O defect, in the metastable state, could form stable donor complexes with native point defects in the as-grown samples [(23), (56), (183)]. Due to the generally small binding energies of these complexes (23), they will completely dissociate at high annealing temperatures. The choice of oxygen as the annealing ambient is therefore important since one can reduce the concentration of these native defects and thus prevent their recombination with the N_O acceptor.

6.2.2 Effect of growth temperature

An important parameter for MOCVD is the growth temperature. Its effect on the incorporation of nitrogen in ZnO was investigated, and the results are presented below. The high cracking temperatures of the precursors used during the growth of ZnO leads to the assumption that at low growth temperatures, NO and DEZn arrive intact at the surface, where they decompose via the formation of an intermediate product. For growth temperatures higher than ~360°C, DEZn should be completely dissociated into Zn and alkyl groups (see chapter 4). A different reaction mechanism would therefore occur at growth temperatures above this value, which will influence the stoichiometry of the ZnO films as well as the incorporation of impurities into the ZnO films.

6.2.2.1 As-grown ZnO

6.2.2.1.1 Concentration of carbon

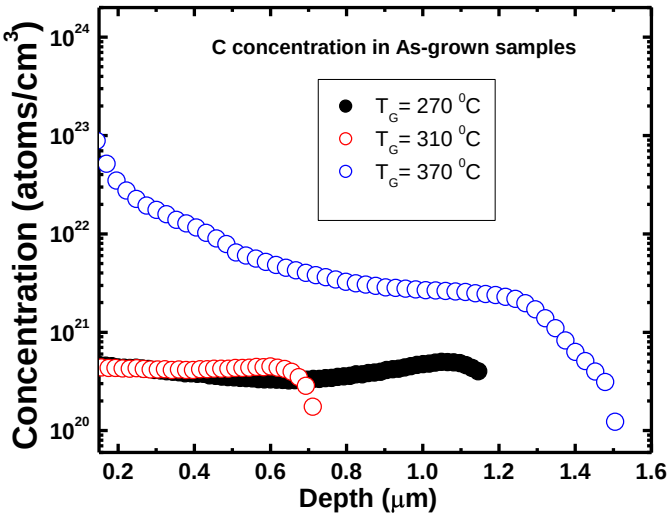

Figure 6.3: The concentration of carbon in as-grown ZnO grown with NO at different temperatures and a VI/II = 120.

Figure 6.3 shows the change in concentration of C when the growth temperature is varied from 270°C to 370°C. At low growth temperatures ($T_G \leq 310$°C), the concentration of C stays constant throughout the layer while for the highest growth temperature (T_G= 370°C), its concentration increases by up to 1 order of magnitude relative to that of the samples grown at low temperature. The drastic increase in carbon when the temperature is raised above the cracking temperature of DEZn, i.e. T=360°C (184), implies that its incorporation into the film results from the individual products formed during the dissociation of the DEZn.

At high temperatures there will be an increased concentration of reactive C and H containing species in the reaction chamber, facilitating the incorporation of these respective impurities into the ZnO films. In contrast, the constant concentration of C at low growth temperatures (below the cracking temperature of DEZn) indicates a different pathway for the incorporation of this impurity. The formation of an intermediate product, which dissociates at the surface of the

substrate, could be a possible explanation. Such a product would introduce the same types of impurities, in approximately the same concentration, as long as the dissociation mechanism stays the same.

6.2.2.1.2 Concentration of hydrogen

Figure 6.4 shows the concentration of hydrogen in ZnO films grown at different temperatures and a constant VI/II ratio of 120. Comparable concentrations (~10^{21} atoms/cm^3) of H and C (compare figure 6.3) are observed at low growth temperatures, which strongly support the notion that H and C are incorporated simultaneously at low growth temperatures. At the highest growth temperature (370°C), H accumulates in high concentrations near the surface and decreases in the bulk of the ZnO sample, eventually reaching the same concentration as in the samples grown at lower temperatures.

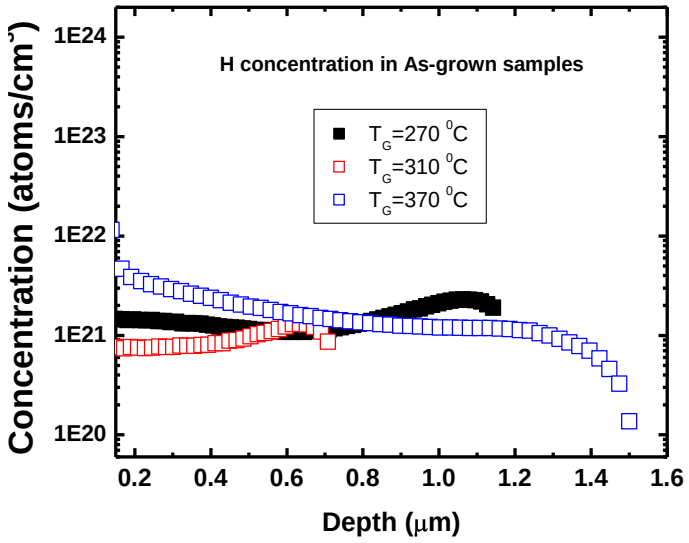

Figure 6.4: The concentration of hydrogen in as-grown ZnO grown with NO at different temperatures and a VI/II=120.

The decrease in the concentration of H in the bulk of this sample may be due to behaviour of H related defect during growth at higher temperatures. In fact, it has been shown that the O-H defect can anneal out at 150°C to give rise to inactive H_2 species which can dissociate at temperatures near 400°C (185). Moreover, it was demonstrated that H_2 effusion at ~200°C was

governed by mono-atomic diffusion from the bulk to the surface [(186), (187), (188)]. Therefore, the excess hydrogen generated by the cracking of the DEZn source at high temperatures can promote the formation of H_2 molecules in the ZnO sample. These molecules can dissociate into atomic hydrogen during growth at temperature 400°C (here 370°C), which will diffuse to the surface where they can interact with C atoms to form alkyls.

6.2.2.1.3 Concentration of nitrogen

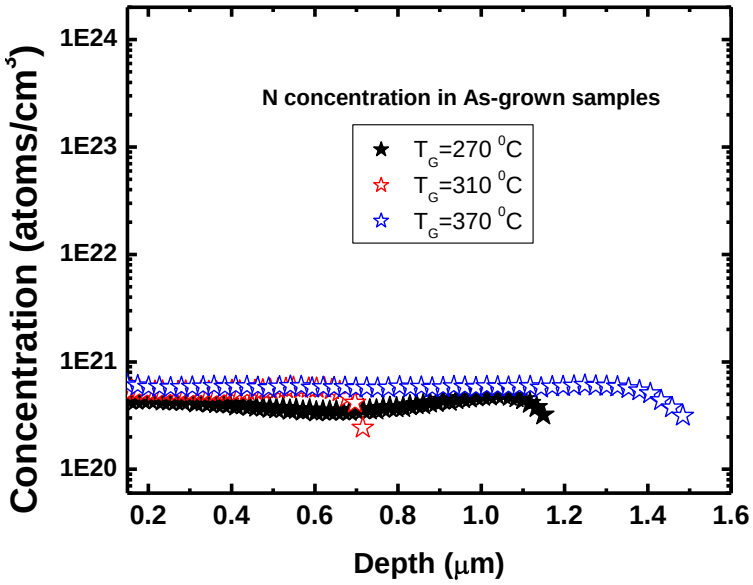

Figure 6.5: Concentration of nitrogen in as-grown ZnO grown with NO at different temperatures and a constant VI/II of 120

The concentration of nitrogen for samples grown at different temperatures and a constant VI/II ratio of 120 is shown in figure 6.5. The amount of nitrogen seems insensitive to the growth temperature. For the samples grown at lower temperatures (≤ 310°C), the nitrogen concentration is similar to that of carbon and hydrogen. This observation could indicate that the different impurities (H, C, N) can be introduced in the ZnO films as the HCN complex reported in ref. (173). Therefore, other defects involving nitrogen are negligible in the sample grown at low temperature. At growth temperatures above the cracking temperature of the DEZn, the increase in C and H concentrations (see figure 6.3 and figure 6.4) does not influence the concentration of N in the sample, supporting the incorporation of additional C and H in other forms when the

growth temperature is increased. Alkyl groups and graphite could be these principal sources of C and H for the highest growth temperature.

6.2.2.2 Post-growth annealing in oxygen

SIMS measurements carried out on the ZnO samples annealed at different temperatures are discussed in this section, since it provides some insight into the diffusion efficiency of the common impurities (H, C and N) and their possible chemistry in the ZnO samples grown at different temperatures.

6.2.2.2.1 Concentration of carbon

Figure 6.6 shows the evolution of the carbon concentration in ZnO grown at different temperatures and subsequently annealed for 2 h at 700°C and 850°C in oxygen. The concentration of C decreases significantly with the annealing temperature when the sample is grown at 270°C. For higher growth temperatures, no decrease in C concentration after annealing is evident; rather, the carbon seems to redistribute in the samples upon annealing. Furthermore, in figure 6.3, it was shown that the concentration of carbon was relatively similar for samples grown at 270°C and 310°C. Thus, one would expect the carbon in the samples grown at 270°C and 310°C to behave similarly. It is evident that the carbon distribution in the sample grown at the lowest temperature is far more uniform than in those grown at higher temperatures and a significant reduction in concentration is also observed after annealing for this layer. It seems therefore plausible that the diffusion of carbon is influenced by other properties of the ZnO films. The crystallinity of the films, for example, can play a major role in the diffusivity of the impurities. In fact, with increasing temperature, the crystalline quality of the ZnO films improve, resulting in denser films (this will be illustrated in section 6.3).

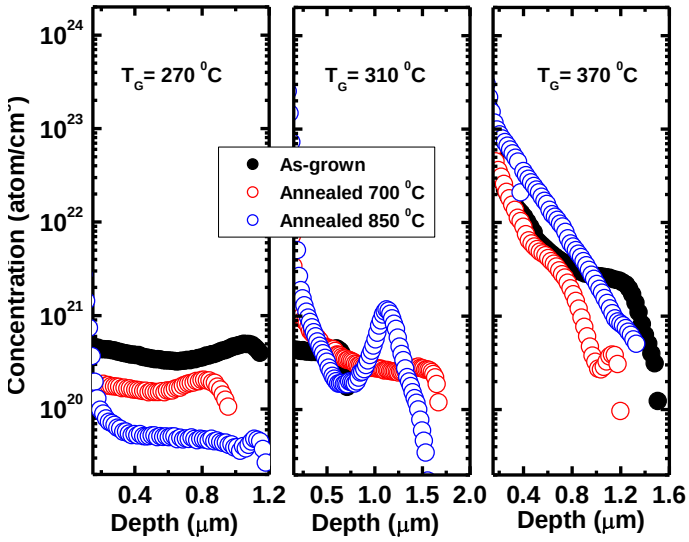

Figure 6.6: The concentration of carbon in ZnO grown with NO at different temperatures and subsequently annealed for 2 h at 700°C and 850°C in oxygen.

Consequently, the diffusivity of the different constituents of the ZnO films will decrease with increasing growth temperature. The improved crystallinity for higher growth temperatures can therefore explain the resistance to out-diffusion of C in these films.

6.2.2.2.2 Concentration of hydrogen

In figure 6.7, the concentration of hydrogen in the ZnO films grown at different temperatures and subsequently annealed at 750°C or 850°C in oxygen is shown. The similarity between the changes in hydrogen and carbon concentrations (figure 6.6) is striking. As was the case for C, a drastic drop in H concentration is also observed for the sample grown at 270°C and the decrease in H concentration is attenuated with increasing growth temperature. In the case of higher growth temperatures, the hydrogen concentration drops near the interface after annealing at 700°C and remains unaffected by a further increase in post-growth annealing temperature to 850°C.

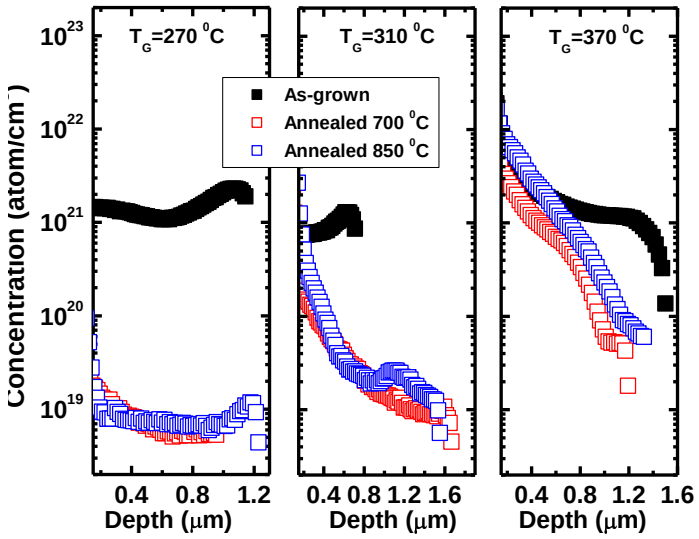

Figure 6.7: The concentration of hydrogen in ZnO grown with NO at different temperatures and subsequently annealed for 2 h at 700°C and 850°C in oxygen.

The similarity in the trends observed for C and H upon annealing the samples grown at different temperatures, supports the suggestion that the high concentrations of H and C in samples grown at temperatures above the cracking temperature of DEZn, results from the direct incorporation of alkyl groups. At lower temperatures, this complex will be reduced in the bulk of the ZnO film, and will also readily diffuse out during annealing, because of the high porosity of the films (see section 6.3) This assumption is in excellent agreement with the progressive increase in the concentration of H remaining in the sample after annealing at 850°C, with an increase in T_G.

6.2.2.2.3 Concentration of nitrogen

Figure 6.8 shows the concentration of nitrogen in ZnO grown with NO at different temperatures and subsequently annealed for 2 h at 700°C and 850°C in oxygen. The concentration of N decreases with the annealing temperatures. In particular, for the sample grown at higher temperature (T_G=370°C), significant decrease in N concentration is also observed, unlike for C and H concentrations. Furthermore, for samples

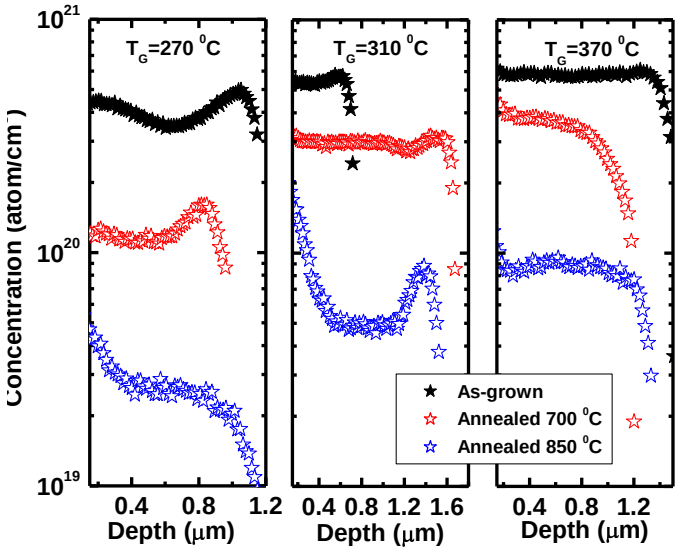

Figure 6.8: The concentration of nitrogen in ZnO grown with NO at different temperatures and subsequently annealed at 700°C and 850°C in oxygen for 2 h.

annealed at 850°C, the accumulation of nitrogen near the surface decreases with the increase in growth temperature. This accumulation is comparable to that of C for the samples grown at lower temperatures (TG≤310°C). The dissociation of HCN complexes is possible at high temperature. The by-products can easily move in the porous structure deduced for low growth temperatures (see section 6.3) and accumulate near the surface or diffuse out of the samples.

6.3 Crystalline and morphological properties

6.3.1 Morphology

Figure 6.9 compares SEM micrographs of the surfaces of the films grown at 270°C, 310°C and 370°C (VI/II = 120), before and after annealing for 2 h at 850°C in oxygen. After annealing, blisters (marked A) and craters (marked B) are visible at the surfaces of the sample grown at 310°C and 370°C. These defects are not observed for the lowest growth temperature.

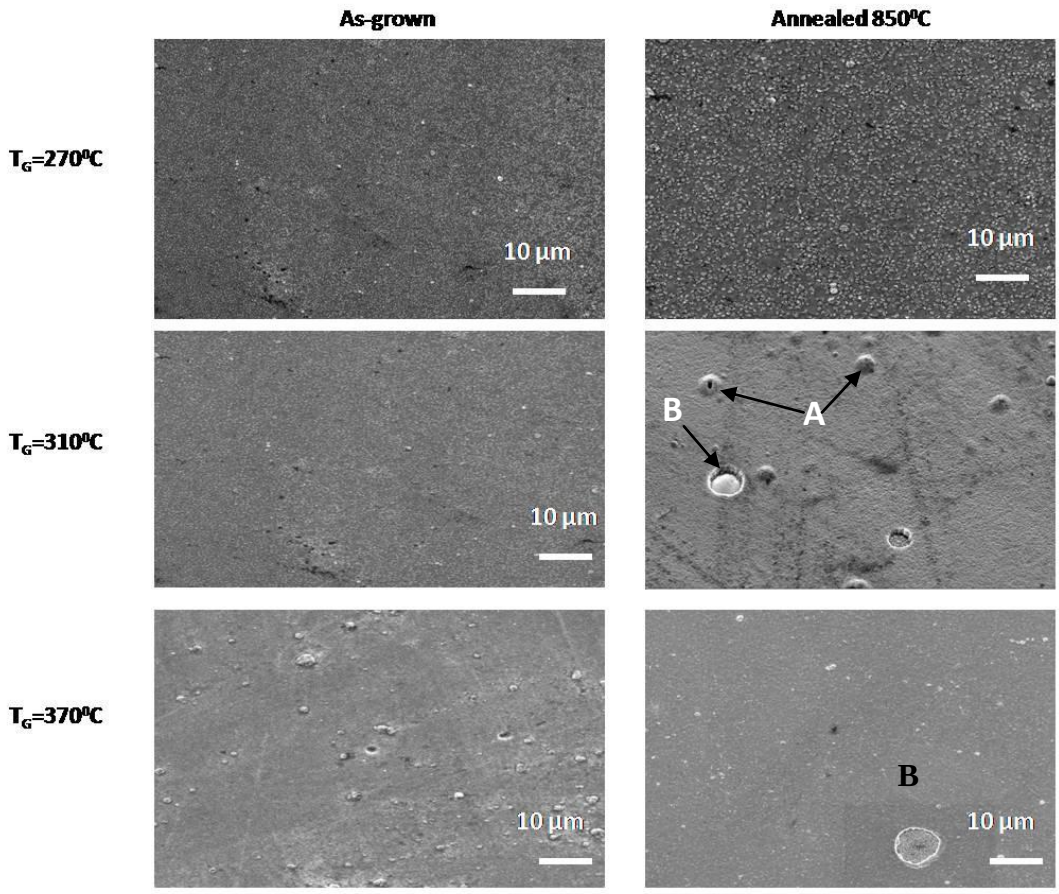

Figure 6.9: SEM top view of as-grown ZnO with NO at 270°C, 310°C and 370°C and subsequently annealed at 850°C in oxygen for 2 h.

The formation of blisters with increasing temperature supports the suggestion given in section 6.2.2.2.1, namely that the mobility of impurities is strongly influenced by the crystalline quality of the films. In fact, the sample grown at 270°C could have a high porosity, allowing the impurities to escape through pores. At an intermediate temperature (T_G=310°C), the porosity of the films will decrease, making it more difficult for impurities to diffuse out, but they will still be mobile. This may cause their accumulation near the interface, resulting in the formation of blisters, and even craters where these blisters had burst under high pressure. At higher growth temperature, the films will be denser, making the impurities less mobile. Consequently, fewer blisters and craters are expected on the surface of these samples. This is in excellent agreement with the SEM image of the sample grown at 370°C, where only one crater is visible.

6.3.2 Microstructure

The crystalline quality of the ZnO films could also strongly influence the impurity chemistry in the sample and the efficiency of out-diffusion. High crystalline quality will result in fewer broken bonds and potential sites for impurities incorporated in the lattice. These impurities could therefore migrate towards other sites in the lattice where they can be accommodated in different electronic states. The growth temperature is the main parameter which determines the crystallinity of the ZnO samples. Generally, the deposition of the thin film begins with the decomposition of the precursors followed by the nucleation at the surface of the substrate, where collisions between atoms occur and coalescence of small nuclei occurs. The temperature of the substrate strongly influences these two steps. High growth temperatures cause an improvement in the coalescence of nuclei, but may also influence the way the films evolve. The transition from 3D to 2D and 1D growth, governed by preferential lateral or vertical growth, is also influenced by the substrate temperature. High substrate temperatures could lead to structures such as rods [(189), (190), (191)] and needles [(192), (193), (194)]. It is also important to mention that a low reactor pressure, such as that used in the present study, results in a high arrival rate of the precursor at the growing surface. This high arrival rate will increase the growth rate, which could then have an impact on the nucleation. Figure 6.10shows the morphology of ZnO grown at 270°C, 310°C and 370°C. For the lower growth temperatures ($T_G \leq 310$°C), the films are dominated by plate-like structures which are inclined to the substrate. When the substrate temperature is increased to 370 ^{0}C, a radical change in the morphology of the ZnO sample is observed. Flat terraces with steps at their hexagonally shaped ends appear. This could suggest layer-by-layer growth on a pyramidal column [(13), (190)]. Each column is perpendicular to the substrate. The hexagonal shape of each layer also suggests higher crystalline properties of this sample compared to the ZnO grown at lower temperatures.

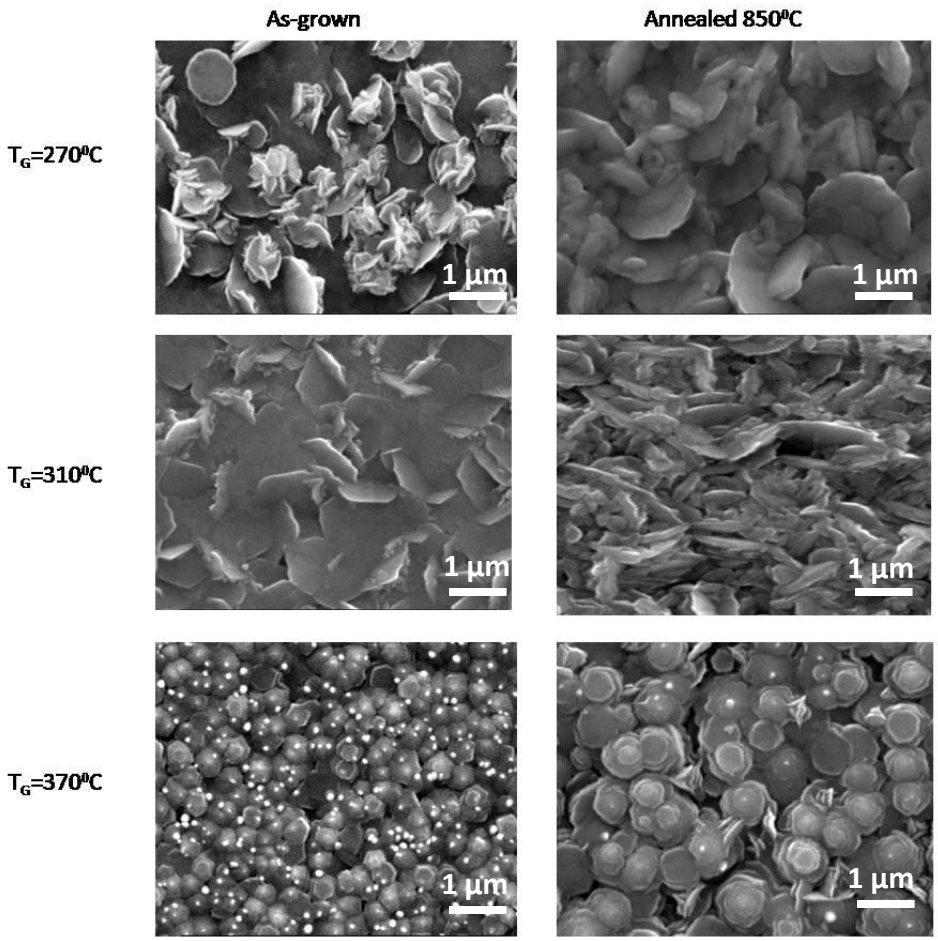

Figure 6.10: SEM images of ZnO grown at 270°C, 310°C and 370°C. The morphologies of both the as-grown samples and those of samples annealed for 2 h at 850°C in oxygen are shown.

Furthermore, it is clear that the diffusion efficiency of the different impurities studied is principally linked to the porosity of the ZnO film. At low growth temperatures, porous structures are observed, whereas at high growth temperatures, the structure becomes denser.

6.3.3 Crystallinity

To investigate the crystallinity of the samples, XRD was performed and the results are shown in figure 6.11. Here only XRD of the samples annealed at 850°C are shown. The (0002) ZnO peak is dominant for all the ZnO samples. They are thus preferentially orientated with the *c*-axis perpendicular to the substrate. This is in good agreement with the results of figure 6.10. Moreover, this peak increases considerably in intensity as the growth temperature increases. This increase in intensity suggests an improvement in the crystalline quality of the sample at higher growth temperatures. This correlates with the hexagonally shaped columns shown in figure 6.10 when the ZnO films are grown at 370°C.

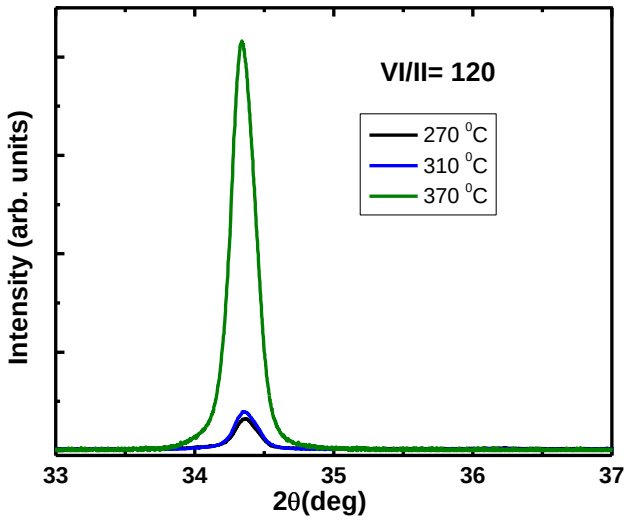

Figure 6.11: XRD of ZnO grown with NO at different temperatures and a VI/II of 120. All samples were annealed for 2 h at 850°C in O_2.

ZnO Furthermore, the presence of NO during growth could lower the cracking temperature of DEZn. Thiandoume et *al.* (184) studied the decomposition kinetics of TBOH and DEZn precursor sources used to grow ZnO. They found that, in the presence of TBOH, the total decomposition of DEZn occurs 50°C lower than without TBOH. Similarly, a mixture of DEZn and NO is expected to decrease the decomposition temperature of DEZn.

6.4 Conclusions

SIMS measurements on films grown at various VI/II ratios and temperatures were performed to investigate the nitrogen, carbon and hydrogen contents in the films. The effect of annealing on these concentrations is also investigated. The concentrations of all three of these impurities increase with an increase in the VI/II ratio. Post-growth annealing at 850°C in oxygen leads to the out-diffusion of H, whereas the presence of complexes between nitrogen and carbon (such as $(CN)_O$) is likely even after annealing.

The growth temperature also plays a major role in the incorporation of N, C and H. At high growth temperatures, above the cracking temperature of DEZn, high concentrations of C and H are observed, and even the highest annealing temperature used here (850°C) could not decrease these concentrations. The C- and H-rich environment in the reactor, which occurs due to the dissociation of DEZn, could be the reason for the efficient incorporation of these impurities. Also, the improved crystalline quality of the sample grown at the highest temperature (370°C) could prevent the out-diffusion of these impurities due to a reduction in the porosity of these polycrystalline films.

Therefore, low growth temperatures seem favourable for the out-diffusion of impurities incorporated into ZnO films. In particular, post-growth annealing shows the efficient out-diffusion of C and H, which could subsequently activate the nitrogen acceptor in the ZnO grown at low temperatures. However, a low growth temperature results in highly porous ZnO films, with poor crystalline quality. The high diffusivity seems to be linked to the porosity of the films. Therefore, it seems that the improved solubility of nitrogen in films grown at lower temperatures is offset by a deterioration in crystalline quality of the films deposited.

7 Optical properties of ZnO grown with NO

7.1 Introduction

In chapter 6, the solubility of nitrogen in ZnO films was studied. High temperature post-growth annealing was found to dissociate the some complexes involving the nitrogen dopant. In this chapter, the effect of post-growth annealing on the optical properties of the ZnO films will be studied.

Using low temperature PL, different DAP transitions previously reported to be related to the nitrogen acceptor, were found after annealing. The effects of excitation power and temperature on these PL lines are investigated to confirm the nature of these transitions. Time-delayed PL was also used to give more insight into these lines. These investigations have allowed us to deduce three acceptors with binding energies of ~192, ~250 and ~350 meV. The nature of these acceptors is also discussed with respect to previous results obtained by other authors.

7.2 Effect of IV/II ratio

It is important to mention that the as-grown ZnO samples showed no optical activity, probably due to the high concentration of non-radiative defects in these samples. These non-radiative defects were possibly generated by the incorporation of nitrogen into the ZnO layers. Indeed, doping ZnO with nitrogen could promote the formation of optically inactive defects such as N_2 molecules, which results in broken bonds in the sub-lattice (179). In general, these broken bonds are non-radiative centers. Moreover, high concentrations of carbon and hydrogen are expected in ZnO thin films grown by MOCVD [(168), (170)]. These impurities could also form non-radiative complexes in ZnO films. Such a high concentration of non-radiative defects would dominate the radiative centers and would result in an optically inactive sample. A reduction of these non-radiative centers is therefore vital. Post-growth annealing is a commonly used method to reduce the concentration of non-radiative defects. Indeed, the thermal energy supplied during annealing at high temperatures could be the driving force for the out-diffusion of impurities incorporated unintentionally into the ZnO films during growth. In addition, single-crystal ZnO has always been observed to contain excess metal (i.e oxygen deficient) under experimentally attainable zinc and oxygen partial pressures (195). It is quite possible that ZnO thin films grown

by MOCVD are also oxygen deficient, even under typically O-rich growth conditions. Annealing in oxygen ambient therefore allows for the reparation of dangling bonds in oxygen deficient ZnO samples (see section 7.8.1). Because of the excess zinc in ZnO thin films, it is reasonable to assume more dangling bonds in the vicinity of the zinc metal. These dangling bonds are most likely caused by the lack of oxygen in the ZnO films. Therefore, annealing in an oxygen environment could lead to the passivation of these dangling bonds with oxygen, improving the optical quality of the ZnO sample.

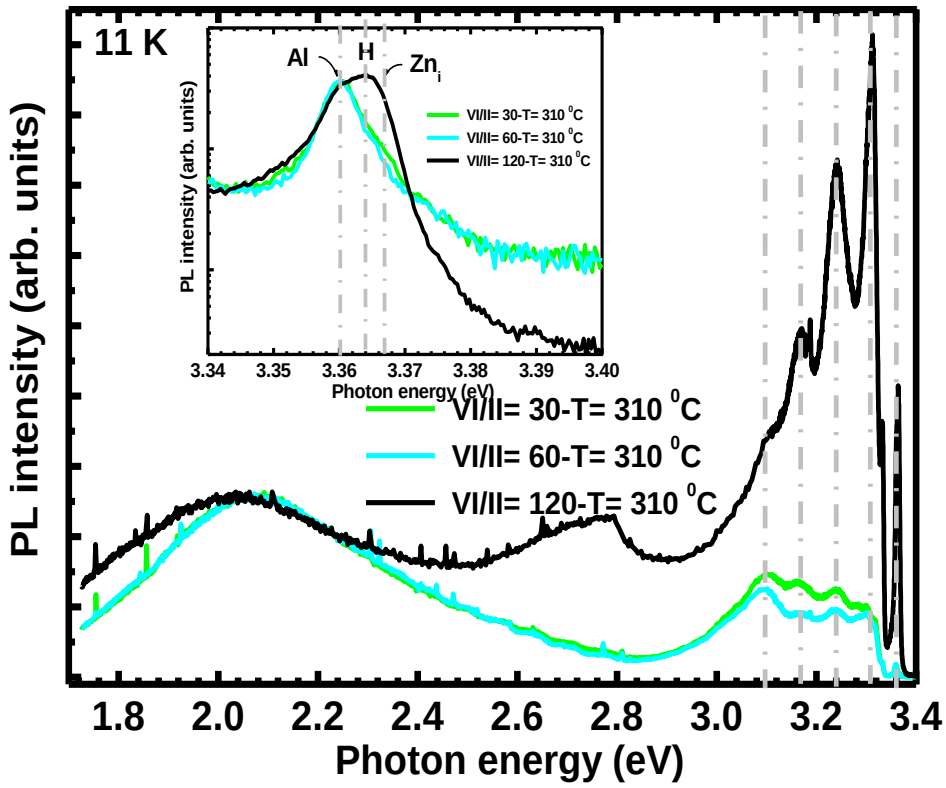

Figure 7.1: Low temperature PL spectra of ZnO grown with VI/II = 30, 60, 120 at 310°C, and subsequently annealed at 850°C for 2 h in oxygen. The insert shows the NBE emission at ~3.366 eV related to Zn_i.

Figure 7.1 shows low temperature PL spectra of ZnO grown with various VI/II ratios at 310°C and subsequently annealed in oxygen. At low VI/II ratios (30 and 60), it can be seen that the DLE at ~2.1 eV dominates the spectra. The emission in the 3.0 eV – 3.34 eV energy range contains four distinctive lines at about 3.31 eV, 3.24 eV, 3.17 eV and 3.10 eV. In this energy region, the spectra are dominated by the transition at ~3.10 eV. The transitions at ~3.10 eV (196), ~3.17 eV [(197), (198), (199)] and ~3.24 eV [(197), (200), (201)] have been assigned to recombination involving the N_O acceptor and will be studied in more detail later.

In the BE region, a weak Al-related D^0X transition at 3.3593 eV (I_{6a}) (19) with a shoulder at ~3.366 eV, is also visible (see insert of figure 7.1). This shoulder may be related to interstitial zinc (Zn_i) as reported by Sann *et al.* (55). This assignment is also supported by the relatively low VI/II ratio used to grow these samples. In such zinc-rich conditions, the Zn_i has a small formation energy (52) and can predominate in the ZnO films.

It is worthwhile to mention that the samples studied here are all highly resistive. No reliable Hall measurements were possible. It is possible that these samples are strongly compensated. Moreover, the absence of identifiable acceptor bound excitonic emission and the presence of donor bound excitons show the dominance of shallow donors in these samples. Thus, it is more likely that DAP transitions will be observed, rather than FA transitions as reported by Georgobiani *et al.* (196). This group assigned a peak at ~3.1 eV as a FA transition involving the N_O acceptor. It is more likely that the transition at ~3.1 eV is due to DAP emission involving the N_O acceptor in our samples. However, based on theoretical predictions, V_{Zn} has also been assigned to a transition at ~3.1 eV [(138), (202)]. A transition at ~3.1 eV was also observed in nominally undoped p-type ZnO (203) and in ZnO:Sb (204). In the nominally p-type ZnO grown by MOCVD (using O_2) (203), high concentration of the native defect, V_{Zn}, which is a relatively shallow acceptor, are possible because of the high oxygen partial pressure used to grow the material. The formation of V_{Zn} is also supported by the following defect reactions (138)

$$\frac{1}{2}O_2 + V_O = O_O \qquad (7.1)$$

$$\frac{1}{2}O_2 = V_{Zn} + O_O \qquad (7.2)$$

where O_O denotes oxygen on its normal lattice site. From these reactions, it was deduced that the V_{Zn} concentration depends on the O_2 partial pressure as $[V_{Zn}] \propto p_{O_2}^{1/2}$, while the V_O concentration obeys the relationship $[V_O] \propto p_{O_2}^{-1/2}$. It becomes clear then that the concentration of V_{Zn} will increase with the oxygen partial pressure and consequently will give rise to a transition which could cause the ~3.1 eV line. This is in good agreement with the increase in intensity of the transition at ~3.1 eV for the highest VI/II ratio (=120) used in this work. Indeed, in the present work, for significant increase in the VI/II ratio, the oxygen partial pressure may similarly increase in the reactor like when O_2 is used. Therefore high concentration of V_{Zn} defect may be possible in the ZnO films which will consequently increase the intensity of the possible V_{Zn}-related transition at ~3.1 eV. Furthermore, for ZnO:Sb (17), V_{Zn} can form the shallow acceptor complex Sb_{Zn}-$2V_{Zn}$. Therefore, the high concentration of V_{Zn} in the ZnO:Sb samples could also give rise to an additional V_{Zn}-related transition. Therefore, as suggested in (203) and (204), the involvement of V_{Zn} in the transition at ~3.1 eV appears reasonable.

At the highest VI/II ratio (i.e. 120), a band at ~2.8 eV appears in addition to the lines observed for lower VI/II ratios. For all the samples, a DLE at ~2.1 eV is visible. The band at 2.8 eV and the DLE will be discussed later.

7.3 Effect of growth temperature

The effect of growth temperature on the optical properties of the ZnO samples grown with NO was studied using PL. The samples were annealed at 850°C in oxygen to enhance their optical properties. The excitonic and NBE emissions between 2.9 eV and 3.38 eV and DLE regions will be discussed in this section.

7.3.1 Near-band-edge emission (≤3.34 eV)

Figure 7.2 shows the NBE emission of ZnO grown at different temperatures. Several PL lines can be observed in the spectra. Emission lines at 3.359, 3.363, 3.366 and 3.374 eV were extracted after fitting and these transitions have been labelled I_{6a}, I_4, I_{Zn} and FE, respectively. The transition at 3.359 eV is commonly assigned to aluminium (19), while that at 3.363 eV has been assigned to hydrogen (19). As already mentioned in section 7.2, the transition at 3.366 eV is

believed to be related to Zn_i. The transition at 3.374 eV could be the free exciton (FE) transition since it is very close in energy to the FE energy reported by many groups [(19), (114), (131)]. The NBE emission of the different samples can be divided according to growth temperature in two groups: low growth temperature (270°C - 310°C) and high growth temperature (330°C - 370°C). At low growth temperatures (270°C - 310°C), the NBE is dominated by the I_{6a} and I_4 emissions. A weak FE transition is also visible. Interestingly, for the sample grown at 270°C, I_{6a} dominates I_4 in intensity, whereas at the higher temperatures (290°C and 310°C) this is reversed. This is in good agreement with the SIMS measurements (chapter 6-section 6.2.2.2.2), where the concentration of hydrogen increased by an order of magnitude when the growth temperature was increased from 270°C to 310°C. An increase in the concentration of hydrogen in the ZnO sample will enhance the concentration of some radiative centres related to this impurity. Furthermore, the I_4 line was assigned to H_O (see chapter 4-section 4.3.2). Poor crystallinity of the ZnO sample was also observed for sample grown at low temperature (see chapter 6- section 6.3.2). High concentration of V_O could be generated in these samples grown at low temperature and consequently hydrogen can readily fill these V_O defects giving rise to high concentration of H_O. At higher growth temperatures (330 ^{0}C - 370 ^{0}C), the I_4 emission is overshadowed by the I_{6a} line. This decrease in the I_4 emission with the increase in growth temperature, suggests that H in these samples is mainly in a different configuration or chemical state than that responsible for the I_4 transition. As also mentioned in chapter 7, the increase in growth temperature improves the crystallinity of the ZnO sample and thus, significant decrease in concentration of of native defects, including V_O defects is expected. Consequently the I_4 line will decrease in intensity. This is in excellent agreement with the dropping in intensity of the I_4 line relative to I_{6a} for high growth temperature.

The increase in intensity of the FE emission observed for the samples grown at higher temperatures also confirms the enhancement of the crystallinity of the ZnO sample with increasing growth temperature. Fewer defect levels in the band gap are then expected in the sample grown at high temperature. Therefore, the C, H, and N impurities may give rise either to inactive complexes or to fewer deep native defects in the band gap, as well as to levels inside the conduction or valence bands. The H_2 molecules (20) could be in abundance in these specific samples. Furthermore, H species could passivate some native point defects (205). Some shallow

double donors $(N_2)_O$ and $(CN)_O$ could still be present in the ZnO films after annealing. The latter has its level inside the conduction band (32).

In fact, high growth temperature could generate the impurities in different forms, and for growth temperatures higher than the cracking temperature of DEZn, hydrogen could be found predominantly as alkyl or H_2 molecules.

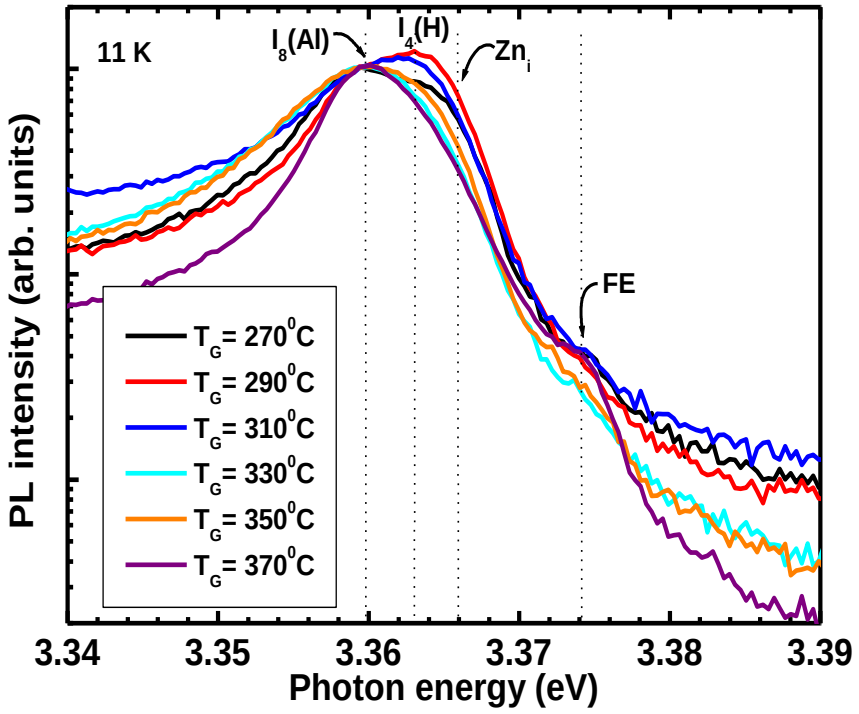

Figure 7.2: Low temperature PL spectra of the bound exciton region in ZnO grown at different temperatures with VI/II =120, and subsequently annealed in oxygen at 850°C for 2 h. The spectra have been normalised at the position of I_8. Line.

Therefore, the incorporation of hydrogen in the form of alkyl or H_2 molecules may occur at temperatures below 360°C. A similar mechanism for incorporating H into the samples grown at higher temperatures is therefore possible, in good agreement with the decrease in the I_4 emission in the samples grown at higher temperatures (330°C - 370°C).

7.3.2 Near band edge region (2.9 eV-3.35 eV)

Figure 7.3 shows the PL spectra in the 2.9 - 3.35 eV energy range. For comparison, sample grown with TBOH and subsequently annealed at 850°C in O_2 was also added to the spectra. Transitions at 3.314, 3.242 and 3.17 eV dominate the spectrum for all the samples. Furthermore, these lines are approximately separated by the longitudinal optical (LO) phonon energy (72 meV). An intuitive explanation would be that the transitions at 3.242 and 3.17 eV are the 1LO and 2LO replicas of the zero phonon line (ZPL) at 3.314 eV, like in the sample grown with TBOH. However, their relative intensities do not follow the Poisson distribution. For example, the sample grown at 350°C has a ~3.17 eV transition with a higher intensity than the line at ~3.242 eV, while for samples grown at 270°C, 290°C and 310°C, the ~3.242 eV transition dominates the ~3.17 eV transition.

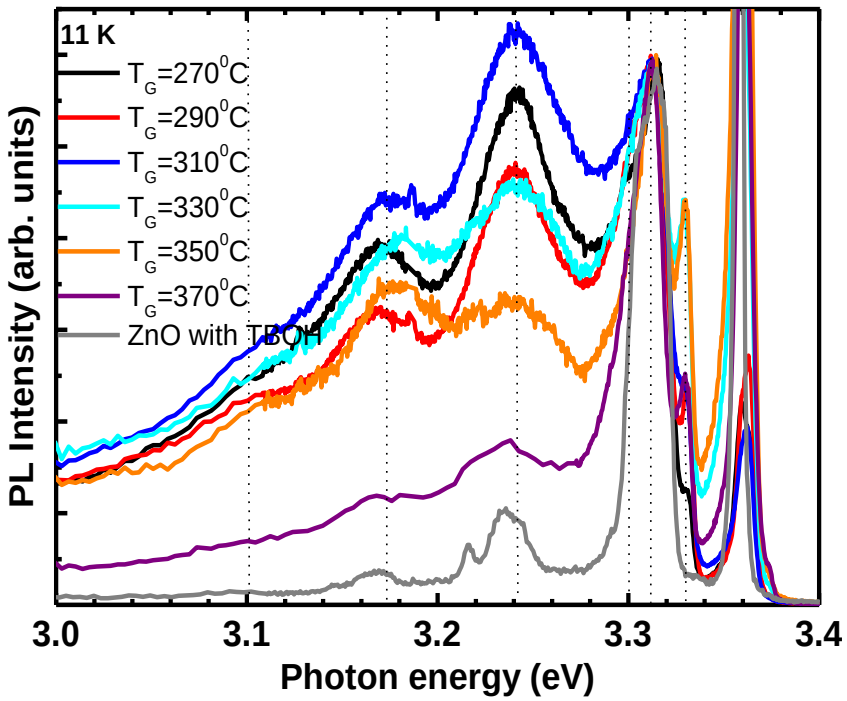

Figure 7.3: Low temperature PL spectra of the 2.9 eV - 3.35 eV region of ZnO grown at different temperatures with VI/II =120, and subsequently annealed in oxygen at 850 ^{0}C for 2 h. An undoped ZnO sample grown with TBOH (at 380^{0}C) and subsequently annealed at 850°C in O_2 is also added for comparison. The spectra have been normalized at the position of the FA at ~3.315 eV.

In fact, the Huang-Rhys factor, S, which can be deduced from the ratios between the LO replicas and zero phonon line (ZPL) intensities (see Eq 3.13), should be defect specific, and therefore the intensity distribution of the ZPL and its respective LO lines should be constant. Table 7.1 shows the different S factors for these different lines. The discrepancy in the S factor values is obvious and hints at the involvement of other transitions contributing to the spectra at about the same energies as the LO replicas of the ZPL at 3.314 eV. The suspected additional transitions cause the observed deviations from a Poisson distribution. These additional transitions at ~3.242 and ~3.17 eV could be the DAP recombination mentioned in section 7.2, and more evidence will be presented in sections 7.4 and 7.5 for these assignments. If the involvement of the N_O acceptor in the DAP is assumed, it is clear that the activation of this acceptor is more effective in samples grown at lower temperatures (270°C, 290°C, 310°C), since the lines at ~3.242 and ~3.17 eV are more intense in these PL spectra.

Table 7.1: Probable Huang-Rhys factors S for the defect giving rise to the line at 3.314 eV, assuming that the lines at 3.242 eV and 3.17 eV are phonon replicas. Eq. (3.14) was used to calculate the S-values.

Growth temperature	S(n=1)	S(n=2)
270°C	0.95	1.15
290°C	0.80	1.04
310°C	1.05	1.22
330°C	0.79	0.36
350°C	0.54	1.09
370°C	0.30	0.64
380°C undoped	**0.18**	**0.21**

A transition at 3.329 eV is also visible in figure 7.3, but its origin is unclear yet. It has been assigned to the two electron satellite (TES) of a bound exciton transition (206). However, the same transition was assigned to an A°X transition in undoped ZnO (207) and in ZnO:As where the acceptor was assumed to be arsenic (156). Furthermore, other reports assigned this transition to the 1LO replica of the free exciton transition in ZnO:N (208) and to grain boundary related transitions (209) in Bi_2O_3-doped ZnO grains.

7.3.3 Deep level emission

The PL spectra depicting the DLE of samples grown at various temperatures are presented in figure 7.4(A). Two main transitions at about 2.1 and 2.8 eV are visible. Interestingly, a correlation between the transition at ~3.242 eV and the DLE at ~2.8 eV is observed. An increase in intensity of the transition at ~3.242 eV is accompanied by an increase in intensity of the transition at ~2.8 eV. Furthermore, the transition at ~2.8 eV is not visible for the sample grown at 370°C where the transition at ~3.242 eV is overshadowed by the 1LO of the ZPL at ~3.314 eV. It is therefore reasonable to assume the involvement of the same defect in both transitions at approximately 2.8 and 3.242 eV. As mentioned in section 7.1, the participation of the N_O acceptor in a transition at ~3.24 eV has been reported [(197), (200), (201)] Moreover, it is likely that the increase in intensity of the transition at 3.242 eV is due to the activation of N_O. The similar increase in intensity of the DLE at ~2.8eV and the transition at ~3.242 eV could therefore suggest the involvement of N_O in the DLE at ~2.8 eV. It is not unusual during doping with a foreign atom of a different size from that of the host atom to form deep centres (AX centres - see section 2.4).

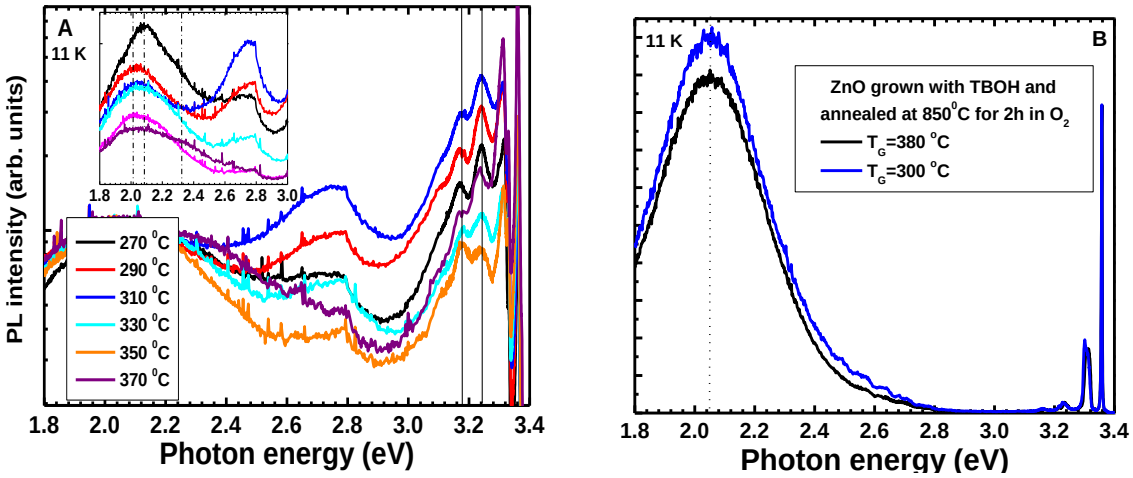

Figure 7.4: Low temperature PL spectra of A) the DLE region of ZnO grown at different temperatures with VI/II = 120. The insert shows the different bands involved in the DLE. B) Undoped ZnO grown with TBOH at a VI/II of 120. All samples were annealed at 850°C for 2 h in oxygen.

Due to the small size-mismatch between the ionic radii of nitrogen and oxygen (Table 2.1), nitrogen will not preferentially form the deep centre and this could explain the weak DLE of the ~2.8 eV transition compared to the intensity of the transition at 3.242 eV. In other words, the relaxation induced by the incorporation of nitrogen on the oxygen site will result in fewer broken bonds, Therefore, the DLE at ~2.8 eV is tentatively assigned to the deep AX centre. Furthermore, the disappearance of the band at ~2.8 eV for the sample grown at 370°C indicates few N_O related deep centers and subsequently fewer broken bonds in the host lattice which can influence the crystallinity of the sample.

Another N-related DLE could be the N_2 reported by Nickel et *al.* (175), the concentration of which may increase with an increase in growth temperature (see chapter 7). It is expected therefore, that if the N_2 defect were responsible for the ~2.8 eV band, the intensity of this band would have increased with an increase in growth temperature. However, the intensity of this band decreases with an increase in growth temperature, as already pointed out. The involvement of the N_2 defect in the ~2.8 eV DLE can therefore be ruled out.

To confirm the assignment of the 2.8 eV band, the PL spectra of undoped ZnO grown at 300°C and 380°C with TBOH and a VI/II ratio of 120 (and subsequently annealed in oxygen for 2 h), are presented in figure 7.4(B). The growth temperatures in this case were chosen according to the two ranges of growth temperature for which the band at ~2.8 eV was either visible or not. No transition at ~2.8 eV is visible in either sample, suggesting that the ~2.8 eV is strongly related to the incorporation of nitrogen in the ZnO sample. Additionally, the energy of the DLE at ~2.1 eV in these spectra is similar to that of the dominant DLE in samples grown with NO. This DLE is therefore probably generated by native point defects. Furthermore, for the samples grown with NO, this DLE band decreases in intensity with an increase in growth temperature to reach its minimum intensity for samples grown at 370°C (see insert to figure 7.4(A)). At higher growth temperatures, the more efficient decomposition of DEZn will make more reactive Zn available in the reactor chamber, which will make the vapour phase in the reactor less oxygen rich. This should result in a significant reduction in the concentrations of energetically favourable point defects generated in an oxygen-rich environment (O_i, O_{Zn} and V_{Zn}) [(22) (52), (210)]. However, the O-deficient nature of the ZnO films, even in the O-rich conditions, could suggest the low concentration of these native defects. Nonetheless, one of the essences of annealing in oxygen ambient is to balance the Zn and O concentration in the ZnO films. High annealing temperature could introduce oxygen in the ZnO films. Furthermore, due to the high porosity observed in the sample grown at low temperatures (see section 7.3.2), the oxygen atom from the annealing ambient could be introduced into the ZnO films more easily in the sample grown at low temperatures via these pores, in comparison to those grown at high temperatures. More O-rich native defects could therefore be generated after the high temperature annealing. Interstitial oxygen (O_i) related emission has been reported at ~2.1 eV [(211), (212)] and could be responsible for the transition at ~2.1 eV reported in this work. In addition, in chapter 7 (section 7.3.3), it was showed that the crystalline quality of the ZnO samples improves with an increase in growth temperature, reducing the native point defect concentrations in the initial ZnO films [(213), (164)].

7.4 Laser power dependence

To gain further insight into the recombination mechanisms at about 3.1, 3.17 and 3.24eV, the laser power dependence of the PL at low temperature (1.6 K) was studied for a sample at 350°C

with VI/II= 120. This sample exhibits these different transitions at relatively high intensities. The results are shown in figure 7.5. No shift was noticed for the transitions at 3.359 and 3.314 eV, proving their excitonic nature.

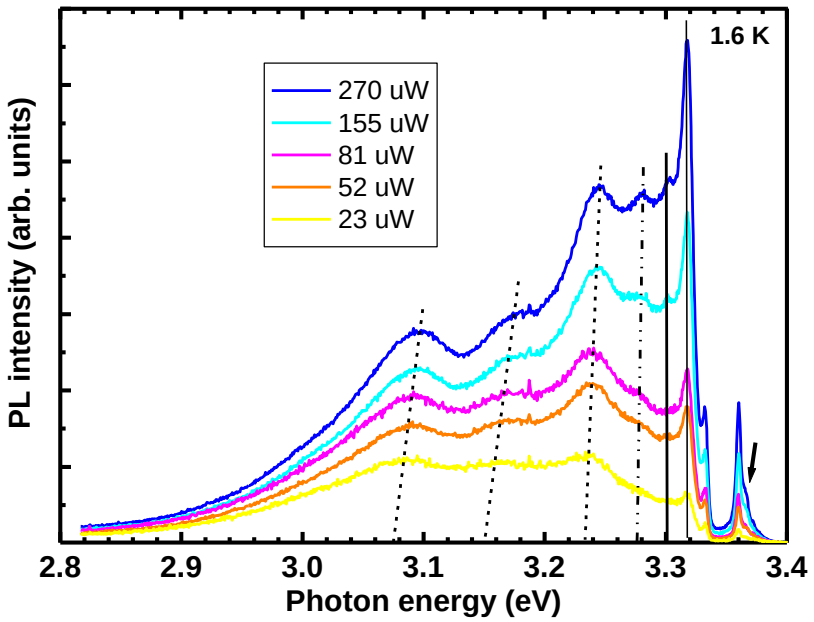

Figure 7.5: Laser power dependence of PL of ZnO grown with NO at 350 ^{0}C and VI/II=120, and subsequently annealed in O_2 for 2h.

For the transitions at approximately 3.1, 3.17 and 3.24 eV, a blue-shift is evident when the laser power is increased. This blue-shift is greater for the transitions at ~3.1 and ~3.17 eV (~17 meV) compared to the shift of the transition at ~3.242 eV (~10 meV). If the transition at ~3.17 eV was the 1LO of the ZPL at ~3.242 eV, one would expect the same blue-shift for both transitions, in contrast with the observed shift in figure 7.5.

As described for DAP transition in section 3.1.2, as the excitation intensity increases, PL from distant pairs saturates due to their longer lifetime and transitions between close pairs dominate. As a result of the strong coulombic interaction between the close pairs, the PL band blue-shifts with increasing excitation rate. The small blue-shift observed for the transitions at ~3.1 eV and ~3.17 eV with increasing excitation intensity suggests the involvement of shallow donor in these

DAP recombinations (89). Moreover, the even smaller shift observed for the transitions at ~3.24 eV and ~3.28 eV, compared to that of the transitions at ~3.17 and ~3.1 eV indicates the involvement of shallower donor in these DAP transitions, relative to those involved in the DAP at ~3.1 eV and ~3.17 eV. Due to the shallow nature of the donors involved in the pairs responsible to these DAP transitions, thermal ionization of these donors at low temperature is likely. Furthermore, the change of their intensities with the increase in laser power may also provide more information regarding the nature of these transitions. For DAP transition, with increasing excitation intensity, distant pairs emitting at lower energies due to weaker coulombic interaction contribute less due to their earlier saturation, since the PL lifetime for distant pairs is longer than for close ones. Implicitly, the close pairs emitting at higher energies will dominate the spectra with increasing excitation intensity due to their shorter lifetime. This is in good agreement with the abrupt increase in intensity of the higher energies transitions at ~3.24 eV and ~3.28 eV relative to the lower energies transitions at ~3.1 eV and ~3.17 eV in figure 7.5. The DAP transitions at ~3.24 and ~3.17 eV could involve the N_O-acceptor. Rogozin *et al*. (200) reported a DAP emission at 3.24 eV in their p-type ZnO grown with NO and the acceptor was assigned to N_O. Makino et *al*. (197) also assigned two transitions at 3.24 eV and 3.17 eV to DAP transitions which involve recombination between the same acceptor (N_O) and a shallow and deep donor, respectively.

7.5 Temperature dependence

Figure 7.6 presents the temperature dependence PL on the sample grown at 310 ^{0}C with a VI/II=120 and annealed at 850 ^{0}C in oxygen. The transition at ~3.30 eV is rapidly quenched and disappears at 41 K. The quenching of the line at ~3.311 eV is much slower and this transition remains visible up to 150 K. These two transitions have been assigned to acceptors associated with basal plane stacking faults in ZnO (92).

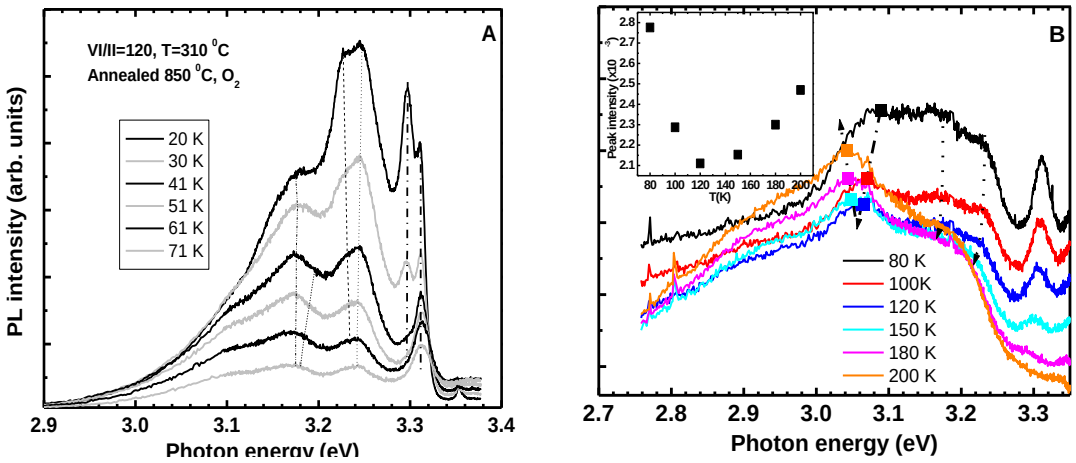

Figure 7.6: Temperature dependent PL of samples grown at 310°C, VI/II=120, and subsequently annealed at 850°C in oxygen for 2 h. A) 20 K to 71 K, and B) 80 K to 200 K. Insert: Intensity of transition at ~3.1 eV as a function of temperature.

More interestingly, two transitions at 3.226 and 3.245 eV are distinguishable. The former decreases in intensity with an increase in temperature and blue-shifts towards the latter. This behaviour is typical for DAP recombination. Upon an increase in sample temperature, the donor (presumably having the smaller binding energy) readily ionizes. These released electrons will then be captured by neutral acceptors to give rise to a free-to-bound transition (FA), which will appear on the high energy side of the DAP emission. Therefore, the transitions at 3.226 and 3.245 eV are assigned to DAP and FA, respectively. Furthermore, from the energy position of the FA transition at 20 K, an acceptor binding energy of 192 meV is calculated from the Eq. (3.11)

$$E_A = E_G - E_{FA} + \frac{kT}{2} \qquad (3.11)$$

where E_G is the band gap energy at 20 K (3.437 eV), E_{FA} is the energy position of the FA transition at 20 K, k is Boltzmann's constant and T is the temperature in Kelvin. Several investigations of DAP recombination in nitrogen-doped ZnO samples have been carried out, and activation energies of 266 (199), 209 ± 3 (214), 195 (215) and 120 meV (201) for the nitrogen

acceptor were reported. The activation energy of 192 meV reported in this study is consistent with the values reported in ref. (214) and (215). In contrast to the transition at ~3.24 eV, the one at ~3.17 eV shows a lower quenching rate between 20 K and 61 K and no significant shift is observed. Beyond 61 K, a hint of a shoulder appears on the high energy side of the 3.17 eV band, at ~3.185 eV. The appearance of this shoulder is accompanied by a faster thermal quenching rate of the transition at ~3.17 eV (between 61 K and 71 K), compared to the transition at ~3.24 eV. This is illustrated by the weaker intensity of this band compared to that at ~3.24 eV above 61 K. The sudden thermal quenching of the transition at ~3.17 eV, followed by the appearance of the transition at ~3.185 eV, suggests the thermal ionization of a donor involved in the transition at ~3.17 eV, which will give rise to a FA line at a higher energy. Thus, the transition at ~3.17 eV is also assigned to DAP recombination. From the position of this new FA transition at 61 K, a binding energy of ~250 meV is calculated, which is close to the binding energy for a nitrogen-related acceptor reported by Tamura *et al* (199). Positron annihilation spectroscopy (PAS) suggests the existence of N_O-V_{Zn} complexes in N^+-implanted ZnO crystals (183). This complex is also an acceptor and is likely to form when both N_O and V_{Zn} are present in ZnO:N films after annealing. This complex was shown to be stable even above 1000°C. Therefore, the N_O-acceptor and N_O-V_{Zn} complex seem to be involved in the DAP transitions at ~3.242 and ~3.17 eV, respectively. This is in good agreement with refs. (197) to (201) where the involvement of N_O in transitions at both ~3.24 eV and ~3.17 eV was suggested. Nevertheless, a correlation between the N_O-V_{Zn} complex and one of the two DAP transitions at ~3.24 and ~3.17 eV still needs to be established.

In addition, the transition at ~3.1 eV (11 K) is also visible at 80 K (at 3.07 eV), and it red-shifts upon a further increase in temperature. However, the behaviour of its intensity with an increase in temperature differs. It firstly decreases in intensity between 80 K and 120 K, and recovers when the annealing temperature is further increased from 120 K to 200 K (see insert of figure 7.6(B)). Interestingly, the recovery of this band occurs in the temperature range (180 K-200 K) where most of the transitions to higher energy are rapidly quenched. In particular, the FA emission related to stacking faults is completely quenched in this temperature range. The hole released from the ionization of the FA could be recaptured in this deeper level, which will increase the related emission band intensity Furthermore, the large capture cross section of the

deep level can facilitate the trapping of a large amount of carriers. As has already been mentioned in section 7.1, the V_{Zn} defect has been suggested to cause emission at ~3.1 eV [(138), (202),]. This point defect can predominate in the oxygen-rich growth conditions used to grow this sample.

7.6 Time delayed photoluminescence

To gain more insight into the different optical mechanisms involved in the sample grown at high temperature, time delayed photoluminescence (TDPL) was performed at 1.6 K. Figure 7.7 shows the TDPL of the sample grown at 370 ^{0}C and then annealed in oxygen at 850 ^{0}C. With a variation in the time delay after excitation, one can discriminate the different overlapped lines observed in this sample. The recombination with the shortest lifetimes will disappear with increasing time delay. The optical processes with longer lifetimes will therefore become dominant in the spectra with increasing time delay. It is clear from figure 7.7 that for delay time of 750 ns and longer, the NBE emissions (i.e excitonic and stacking fault-related) which have the shortest lifetimes, are drastically quenched. The disappearance of these lines, especially the LO phonon replicas of the stacking fault-related emission, leaves behind transitions at ~3.05 eV, ~3.17 eV, ~3.22 eV, ~3.26 eV and ~3.28 eV. The transitions at ~3.05 eV, ~3.17 eV and ~3.22 eV are very close in energy to the DAP transitions observed in the samples grown at low temperature. If one assumes that the transitions at ~3.05 eV, ~3.17 eV and ~3.22 eV observed with increasing time delay for the sample studied here, are in fact the DAP transitions found in the samples grown at $T_G \leq 310$°C, , these transitions, especially those involving deep donors, are expected to shift to lower energies (216). This effect is caused by the predominance of recombination between more distant pairs with increasing time delay. Therefore with the involvement of more distant pairs, the final state coulombic interaction becomes weaker and consequently, the band will red-shift with increasing delay time. In other words, the absence of noticeable shift may imply the involvement of shallow donors in the DAP recombination. Therefore, with the assumption that the transitions at ~3.05 eV, ~3.17 eV and ~3.28 eV are DAP transitions, they should all involve shallow donors since no significant red-shift was observed for any of these transitions.

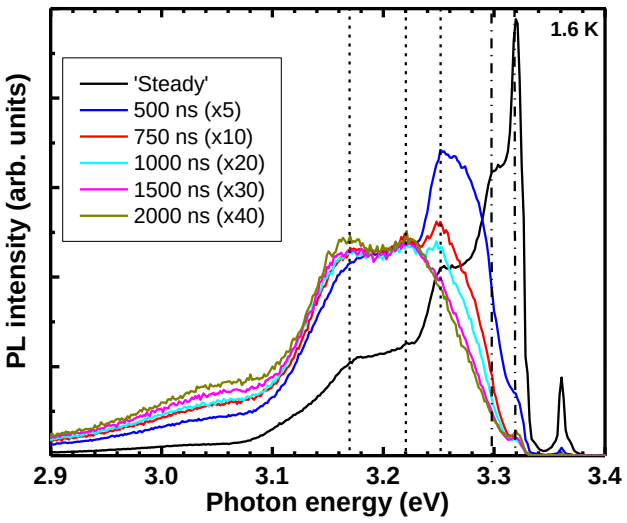

Figure 7.7: Low temperature TDPL spectra observed for different time delays on samples grown at 370 ^{0}C and annealed at 850 ^{0}C in oxygen ambient for 2 h. For delays of 500 ns and longer, the spectra were normalized at 3.22 eV.

More evidence regarding the mechanism governing these transitions will be presented in the following section.

7.7 Effect of temperature on time delayed PL

To confirm the mechanisms governing the transitions at ~3.22 and ~3.17 eV, the TDPL spectra taken at 1.6 K and 30 K for a time delay of 750 ns were compared and are presented in figure 7.8. At 30 K the transitions at ~3.22 and ~3.17 eV were not observed, but lines at ~3.24 eV and ~3.18, at their respective higher energy sides, are visible. These transitions could be the FA lines resulting from the ionization of the donors involved in the respective DAP transitions at ~3.22, and ~3.17 eV.

Using Eq. 3.11, binding energies of 198 and 257 meV were calculated for the acceptors taking part in the DAP transitions at ~3.22, and ~3.17 eV, respectively. These acceptor binding energies are in excellent agreement with the values obtained from the temperature dependent PL of the sample grown at 310°C.

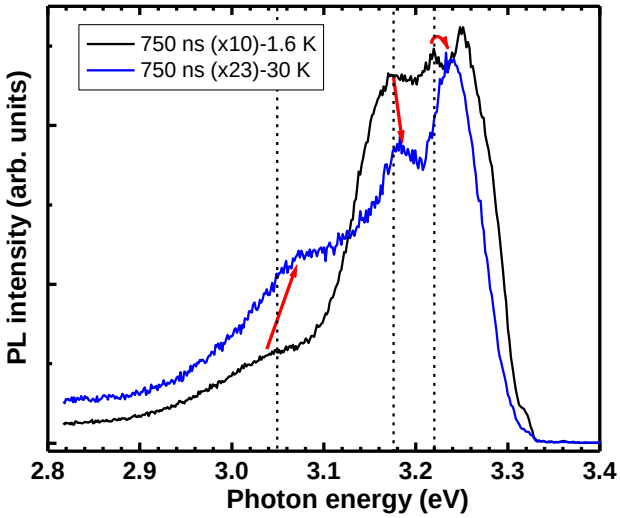

Figure 7.8: Temperature effects on TDPL spectra of samples grown at 370 ^{0}C and annealed at 850 ^{0}C in oxygen for 2 h.

This confirms that the nature of the acceptor, in samples grown at different temperatures, is the same. Interestingly, with the increase in temperature, a broad band at ~3.08 eV appears, which is on the higher energy side of the broad band at ~3.05 eV. Since an increase in temperature result in blue-shift, the new band could be the FA resulting from the ionization of the shallow donor in this DAP transition. The ionization of the shallow donor will give rise to FA with a V_{Zn} as the acceptor. From the FA energy position, the V_{Zn} activation energy of ~350 meV is calculated, in excellent agreement with the positron binding energy of V_{Zn} in a non-relaxed configuration reported by Brauer *et al.* (217), and confirmed by theoretical calculations (33).

7.8 Post-growth treatment

It is important to investigate the effect of the annealing ambient during post-growth treatment, since an efficient activation of the nitrogen acceptor depends on the concentration of other defect-types which can compensate the N_O acceptor. In the next section, a comparative study of annealing in an inert Ar ambient and an oxygen ambient is performed.

7.8.1 Choice of annealing ambient

Figure 7.9 shows the effect of the annealing ambient on the low temperature PL for two samples grown at 310 ^{0}C and 370 ^{0}C. The overall intensities are enhanced when the post-growth annealing is performed in oxygen. Furthermore, regardless of the annealing ambient, similar features appear for each sample grown at the same temperature. The differences appear only in the sharpness and the intensities of the lines. This indicates that the annealing ambient can enhance the radiative recombination centres to different degrees. An oxygen ambient seems to be more promising for improving the luminescent efficiency. In fact, as suggested previously, the as-grown ZnO samples may contain high concentrations of O-deficient native defects such as oxygen vacancies, which can be filled when annealing is performed in oxygen ambient. Consequently, the concentration of dangling bonds, which are mostly created by the absence of oxygen atoms (218), may be reduced.

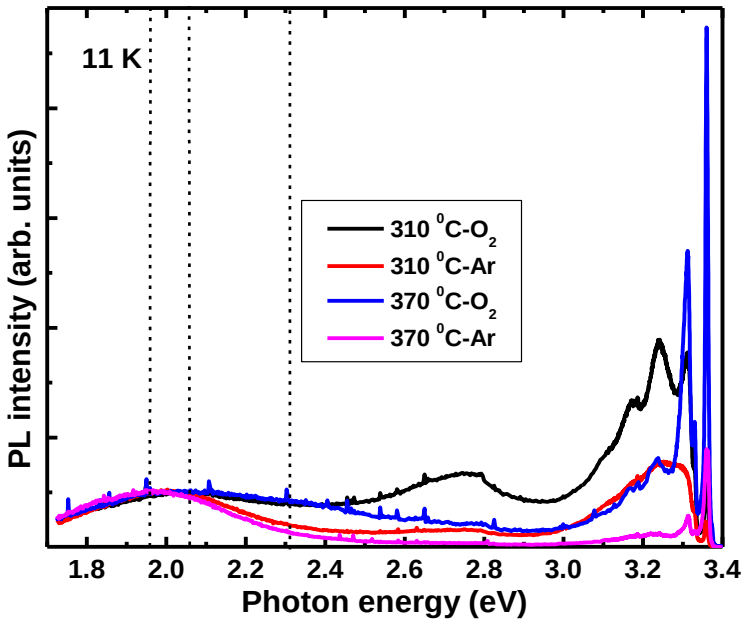

Figure 7.9: Low temperature PL spectra of samples grown at 310 ^{0}C and 370 ^{0}C (VI/II=120) and subsequently annealed in oxygen and argon at 850 ^{0}C for 2 h.

Furthermore, oxygen reacts efficiently at the surface of the ZnO films with some impurities which diffuse out from the bulk of the sample. Impurities such as carbon and hydrogen which are found predominantly in ZnO films grown by MOCVD, can react with oxygen to give CO, CO_2 and H_2O. Therefore, oxygen can be the driving force for the out-diffusion of impurities embedded in the film. A stronger reduction in the concentrations of non-radiative centres related to these impurities in the presence of oxygen is thus expected, which explains the enhancement in the luminescence when post-growth annealing is performed in oxygen gas.

Annealing in argon produces one red band at ~1.96 eV, whereas two bands at ~2.1 and ~2.3 eV appear after annealing in the oxygen ambient. These three bands appear to have different origins and the respective defect concentrations are evidently influenced by the annealing ambient. The bands at ~2.1 and ~2.3 eV, which are observed for annealing in an oxygen-rich environment, probably stem from native point defects such as O_i, V_{Zn} and O_{Zn}. The yellow band at ~2.1 eV is attributed to O_i (see section 7.1). Børseth *et al.* (140) attributed a PL band at 2.35 eV to V_{Zn}. This band appeared to be dominant when single crystal ZnO was annealed in oxygen at 1050 ^{0}C. It seems plausible that the band at ~2.3 eV, which appears after annealing in oxygen at 850 ^{0}C in the present study, has the same origin. The red luminescence which appears in the sample annealed in argon obviously has a different origin from those which are observed in the oxygen-rich annealing ambient. The high temperature anneal in the oxygen-poor ambient could generate native point defects such as V_O, which has been assigned to red luminescence (219).

7.8.2 Effect of annealing temperature

The effect of annealing temperature on the low temperature PL spectra of the samples grown at different temperatures was also studied and the results are shown in figure 7.10. Annealing at 700°C and 800°C induces a dominant red DLE at ~1.96 eV also observed when the annealing was performed in Ar (see section 7.8.1). A further increase in the annealing temperature to 850°C reveals a prominent yellow band at ~2.1 eV, which is assigned to O_i. This blue shift is emphasized for the samples grown at low temperatures (270°C and 310°C) and the effect becomes less obvious for the samples grown at higher temperatures. The band at ~2.8 eV also appears after annealing at 700°C, and an increase in its intensity is generally accompanied by an increase in intensity of the lines at ~3.17 eV and ~3.24 eV. The disappearance of the band at

~1.96 eV at the highest annealing temperature is not surprising. Chao *et al.* (220) reported a similar blue shift of the dominant DLE band from 1.8 to 2.25 eV when their

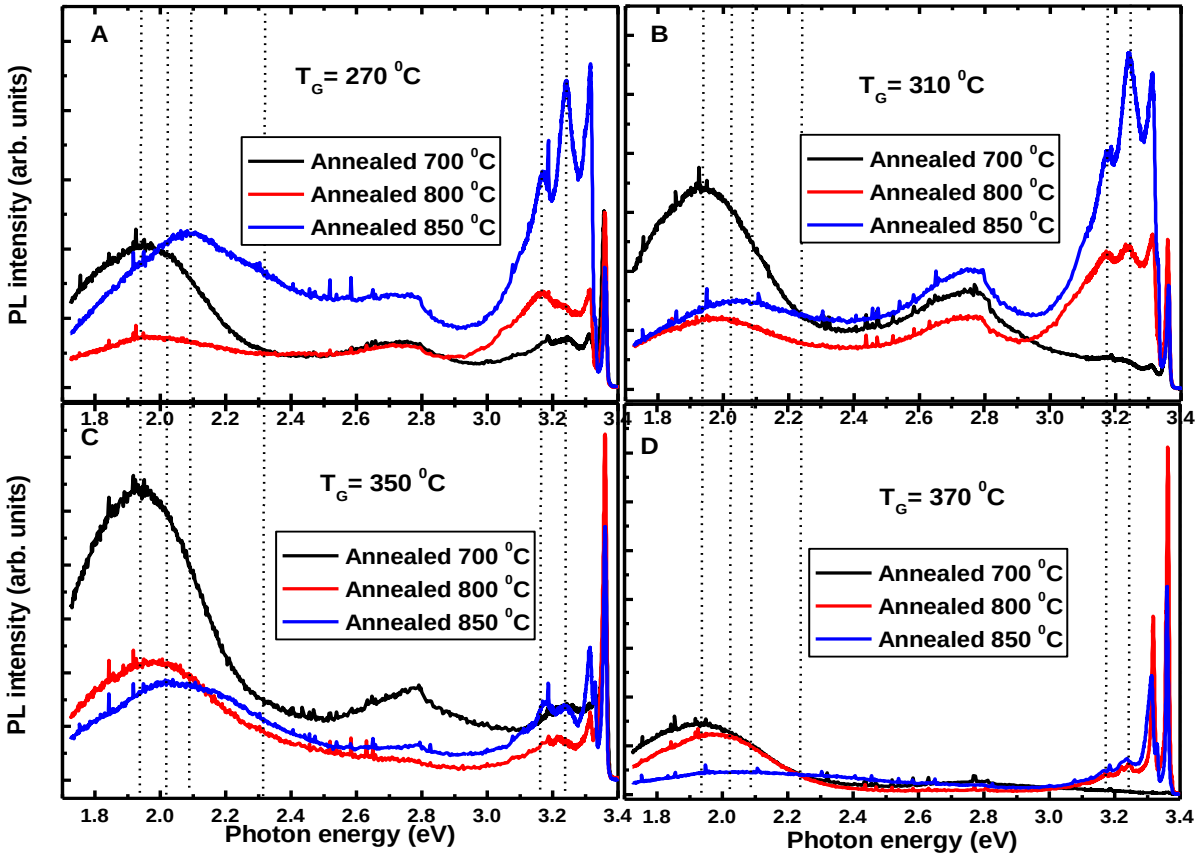

Figure 7.10: The effect of post-growth annealing temperature on low temperature PL spectra of ZnO samples grown with VI/II = 120 and at A) 270°C, B) 310°C, C) 350°C and D) 370°C, and subsequently annealed at 700°C, 800°C or 850°C for 2 h in oxygen.

ZnO films, prepared by chemical vapour deposition utilizing zinc acetate dehydrate, were annealed at 750°C and 1000°C, respectively. They assigned this shift to a change from an excess of oxygen or zinc interstitials to point defects located at the surface resulting from the decomposition of ZnO. Wang *et al.* (221) reported on the evolution of visible luminescence in

ZnO produced by thermal oxidation of zinc films at temperatures varying from 400°C to 950°C. A green luminescence band at 2.4 eV was observed for thermal oxidation temperatures up to 750°C. Further increases in the oxidation temperature to 800°C yielded two distinct bands at 2.1 and ~1.9 eV. The latter disappeared for higher oxidation temperatures. The blue-shift from 1.96 eV to 2.1 eV is also observed in this work when the annealing temperature is increased from 800°C to 850°C. In addition, the simultaneous enhancement of both transitions at ~3.24 and ~3.17 eV, related to the N_O acceptor, and the disappearance of the red band at ~1.96 eV, can be explained as follows: at annealing temperatures of 700°C and 800°C, the V_O defect is generated in films annealed even in the oxygen ambient. At the highest annealing temperature, the enhanced cracking of oxygen molecules into single atoms and their diffusion into the sample, may annihilate the V_O, resulting in the quenching of the red band at ~1.96 eV. Moreover, at this high annealing temperature, oxygen interstitials and zinc vacancies can form, giving rise to the transitions at ~2.1 and ~2.3 eV, respectively. For higher growth temperatures (T_G= 370 ^{0}C), the dominance of the excitonic emission suggests that the sample is relatively free from defects. At high annealing temperatures, the highly mobile O_i (222) can recombine with V_O, resulting in an oxygen atom in its lattice position (223). This type of substitution will also quench the red luminescence at ~1.96 eV. This result is further supported by theoretical and experimental work (219). Although V_O has been identified as a negative U defect, i.e. the (+2/+1) level lies above the (+/0) level (52), the metastable (+/0) level is observable in transitions involving optical excitation. As concluded by EPR measurements [(224), (225)], transitions at ~2.0 eV can be assigned to V_O^+. This assignment is also consistent with first-principles calculations which indicate a zero phonon line transition involving $V_O^{0/+}$ at ~2.0 eV (219).

Back to figure 7.9, the V_O-related transition at ~1.96 eV is also observed when annealing is performed at 850°C in Ar. In this O-poor ambient, the high temperature could help the out-diffusion of oxygen from the films, increasing the concentration of V_O.

Figure 7.11 presents the results of a comparison of the intensities of the 3.24 eV PL line and the DLE as a function of annealing temperature and growth temperature. The transition at 3.24 eV gains in intensity relative to the DLE intensity with an increase in annealing temperature. This effect is more pronounced for samples grown at lower temperatures (T_G= 270°C and 310°C).

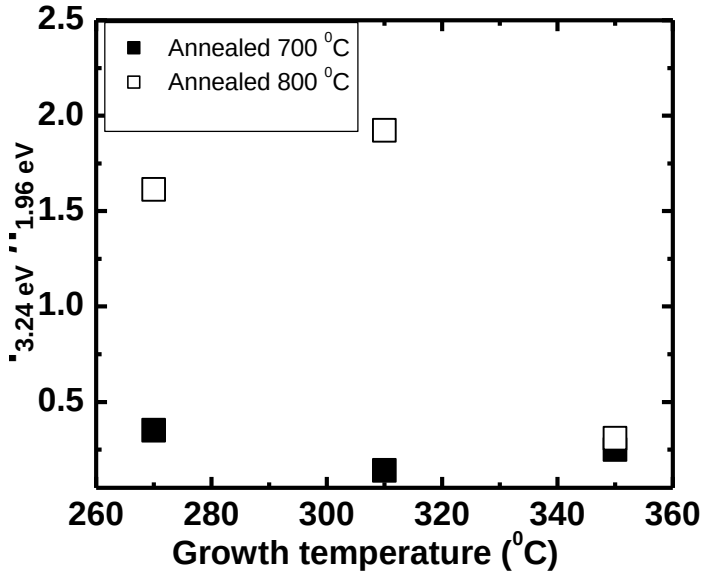

Figure 7.11: A comparison of the intensities of the 3.24 eV PL line and the DLE as a function of annealing temperature.

Although the DLE remains more intense for these samples, probably due to the low growth temperature, the activation of the nitrogen acceptor seems more efficient. The intensity ratio of these PL transitions is strongest for the sample grown at 310°C after annealing at 800°C. At this low growth temperature, the generation of V_O defect will assist optimal activation of nitrogen substitution at the oxygen site. Increase in N_O concentration will therefore be followed by a decrease in the V_O concentration. Therefore, T_G = 310°C was determined to be the optimum growth temperature for our ZnO:N samples, illustrating by the high ratio shows for the sample grown at 310°C.

At higher growth temperatures, the small increase in the ratio indicates that few nitrogen acceptors are activated. This could be due to the low concentration of V_O in this sample as proven by the good crystalline quality of this sample (see chapter 7- section 7.3.3).

7.9 Conclusions

Three DAPs transitions at 3.24, 3.17 and 3.1 eV were found in ZnO grown with NO using MOCVD. These were observed using low temperature steady state PL and TRPL. Activation energies of approximately 192, 250 and 350 meV for the respective acceptors involved in these DAP transitions were calculated. The acceptor with a binding energy of 350 meV was tentatively assigned to the V_{Zn} defect. Although the exact nature of the acceptors with binding energies of 192 and 250 meV are not yet known, the formation of N_O-acceptors and N_O-V_{Zn} complexes in ZnO:N can be related to these.

Strong DAPs at about 3.24 and 3.17 eV are visible for samples grown at low temperatures. This could indicate the efficient incorporation of nitrogen acceptors into ZnO films grown at low temperatures. Thus, the optimum growth temperature for the incorporation of nitrogen acceptors in our MOCVD system seems to be $T_G = 310°C$.

Annealing in oxygen ambient seems favourable for activation of N_O acceptor. The high generation of V_O in the sample grown at low temperature could be the cause of the activation of the N_O acceptor. Also, annealing in oxygen at higher temperature (850°C) generates only O-rich defects that could not annihilate the activity of the N_O acceptor.

8 Conclusion

In this thesis, the optical properties of bulk ZnO and MOCVD grown ZnO films were studied. From studies of the PL spectra of bulk ZnO annealed and/or treated in a hydrogen plasma, the following conclusions have been drawn: Besides the well-known I_4 line at 3.3628eV, hydrogen can give rise to other lines. In the case of hydrogen plasma treated samples, two H-related lines at 3.361 eV and 3.364 eV were deduced. These lines have been ascribed to two complexes between hydrogen and V_{Zn}. An annealing temperature of 850°C is suitable for reducing the shallow donor-related PL lines, included hydrogen, as demonstrated by the quenching of the NBE emission after annealing at this temperature. This temperature was therefore used for the out-diffusion of shallow hydrogen donors in the ZnO films in subsequent studies.

Annealing of undoped ZnO films grown on GaAs generates a shallow arsenic-related acceptor level in the band gap which is deduced form the PL measurements. A shallow As related-acceptor, namely the As_{Zn}-$2V_{Zn}$ complex, is suggested to be involved in the A°X transition at ~3.35 eV. Furthermore, the incorporation of As into the ZnO films is only possible in a narrow range of annealing temperatures (around 550°C) in an oxygen ambient. Annealing times of longer than 2 h at ~550°C as well as higher annealing temperatures rather enhance the formation of shallow donors instead of the As-related acceptor line. The incorporation of the As into the ZnO films also generate structural defects, inlcuding stacking faults, in the films since similar annealing studies in a nitrogen ambient shows no PL line at ~3.35 eV. Also, no Y-line is visible and a quenching of the PL lines related stacking faults is observed for annealing in nitrogen. Therefore, the simultaneous appearance of the ~3.35 eV transition and the Y-line, as well as the increase in intensity of the stacking fault related emission for the samples annealed in oxygen at 550°C constitute strong evidence for an increase in the concentration of structural defects during diffusion of As in the film.

SIMS results on ZnO:N grown with NO show the presence of nitrogen in the ZnO films. The solubility of nitrogen may be enhanced by the formation of complexes with hydrogen and carbon, which are present in high concentrations in the ZnO films. The effect of annealing temperature on these complexes shows that the out-diffusion of these impurities is primarily dependent of the crystallinity of the ZnO films. In poor crystalline quality films, with high

porosity, the impurities diffuse out efficiently, whereas in films with higher crystalline quality, the diffusion is ineffective. The dissociation and out-diffusion of these complexes are necessary for the activation of the nitrogen as an acceptor. Therefore, high crystalline quality films, which are essential for optoelectronic devices, seem to be unfavourable for efficient nitrogen doping, in particular for the activation of the nitrogen acceptor in these MOCVD-grown ZnO films.

The investigation of the optical properties of ZnO:N by low temperature PL, confirms this conclusion. For samples grown at lower temperatures (≤310°C), which have poor crystallinity, the activation of the nitrogen acceptor, which may take part in the DAP transitions at ~3.24 eV and ~3.17 eV is observed. In addition to these two transitions, another DAP transition at ~3.1 eV, previously assigned to the nitrogen acceptor, is suggested to be related to V_{Zn} instead. Also present is the A-center which may give rise to the band at ~2.8 eV, suggesting the deterioration of the crystalline quality of the samples upon nitrogen incorporation, since this center induces broken bonds in the material. Furthermore, the appearance of the luminescence after annealing at 700°C and above indicates a high concentration of non-radiative center in the as-grown material. Moreover, the activation of the nitrogen acceptor in the samples grown at low temperatures is more effective due to the high concentration of native point defects and V_O in particular. The presence of V_O in these samples could ease the formation of the N_O-acceptor. The increase in relative intensity of the DAP transitions at ~3.24 eV and ~3.17 eV after annealing at 850°C, the temperature where most of the hydrogen-related donors are expected to anneal out, confirms that the presence of hydrogen effectively hampers the activation of the nitrogen acceptor and needs to be remove from the sample for better activity of the acceptor.

At high growth temperatures (370°C), where the crystalline quality of the films is improved, in addition to the weak out-diffusion of the impurities present in the films, the lower concentration of V_O in the films could be a contributing factor to the inefficient activation of N_O.

In summary, higher crystalline quality of ZnO:N films results in less efficient activation of the nitrogen acceptor. Also knowing that MOCVD-grown ZnO:N is prone to a high incorporation of carbon and hydrogen, which need to be removed, and that the removal of these impurities seems to be more effective in material with poor crystalline quality, the question whether MOCVD (using DEZn and NO as was the case in this study) for nitrogen doping, remains open. Other

ways need to be implemented to prevent the incorporation of carbon and hydrogen in ZnO grown at higher temperatures, where the requirement of high crystalline quality films is met, but to still achieve a high activity of nitrogen as an acceptor. The addition of oxygen in the reactor during growth could be a possible solution. The presence of oxygen should prevent the incorporation of carbon and hydrogen impurities by forming CO_2 and H_2O either in the vapour phase or at the evolving film surface, which can then be transported away from the surface of the sample. Also, using a nitrogen plasma to generate elemental nitrogen, in conjunction with the addition of oxygen in the reaction chamber, could be favorable to increase the nitrogen acceptor concentrations in films grown at higher temperature. These suggestions could form the basis of meaningful future research in this laboratory.

9 References

1. **U.S. Department of Energy.** *The promise of solid state lighting for general illumination, Conclusions and recommendations from OIDA technology roadmaps.* 2001.

2.**, M. W. Hodapp.** Applications for high-brightness light-emitting diodes. *Semiconductor and semimetals.* London : Academic Press, 1997, Vol. 48, p. 228.

3. **Global Information Inc.** *UV LED '09.* s.l. : Yole Developpement, 2009.

4. *SiC blue LED's by liquid-phase epitaxy.* **H. Matsunami, M. Ikeda, A. Suzuki, and T. Tanaka.** 1977 , Electron Devices, IEEE Transactions on, Vol. 24, pp. 958 - 961.

5. *High-power GaN p-n junction blue light emitting diodes.* **S. Nakamura, T. Mukai, and M. Senoh.** 1991, Jpn. J. Appl. Phys. , Vol. 30, p. L1998.

6. **H. E. Ruda.** *Narrow Gap II-VI Widegap II-VI compounds for opto-electronic applications.* Electronic Materials. London : Chapman and Hall, 1992. Vol. 1.

7. *InGaN-Based Near-Ultraviolet and Blue-Light-Emitting Diodes with High External Quantum Efficiency Using a Patterned Sapphire Substrate and a Mesh Electrode.* **M. Yamada, T. Mitani, Y. Narukawa, S. Shioji, I. Niki, S. Sonobe, K. Deguchi, M. Sano, and T. Mukai.** 2002, Jpn. J. Appl. Phys., Vol. 41, pp. L1431-L1433.

8. *Blue LEDs, UV photodiodes and high-temperature rectifiers in 6H-SiC* . **J. A. Edmond, H. -S. Kong, and C. H. Carter Jr.** 1993, Physica B: Condensed Matter, Vol. 185, pp. 453-460 .

9. *Growth of low resistivity p-type GaN by metal organic chemicalvapour deposition.* **C. J. Eiting, P. A. Grudowski, and R. D. Dupuis.** 1997, Electronics Letters, Vol. 33, pp. 1987 - 1989.

10. *Interband Magnetoreflection of ZnO.* **K. Hümmer.** 1973, Phys. Stat. Sol. B , Vol. 56, p. 249.

11. *Fundamental energy gap of GaN from photoluminescence excitation spectra.* **B. Monemar.** 1974, Phys. Rev. B, Vol. 10, p. 676.

12. *Optically pumped lasing of ZnO at room temperature.* **D. M. Bagnall, Y. F. Chen, Z. Zhu, T. Yao, S. Koyama, M. Y. Shen, and T. Goto.** 1997, Appl. Phys. Lett. , Vol. 70, p. 2230.

13. *Room-temperature ultraviolet laser emission from self-assembled ZnO microcrystallite thin films.* **Z. K. Tang, G. K. L. Wong, P. Yu, M. Kawasaki, A. Ohtomo, H. Koinuma, and Y. Segawa.** 1998, Appl. Phys. Lett., Vol. 72, p. 3270.

14. *Effects of an extremely thin buffer on heteroepitaxy with large lattice mismatch.* **Y. F. Chen, S. K. Hong, H. J. Ko, V. Kirshner, H. Wenisch, T. Yao, K. Inaba, and Y. Segawa.** 2001, Appl. Phys. Lett., Vol. 78, p. 3352.

15. *Stimulated emission induced by exciton–exciton scattering in ZnO/ZnMgO multiquantum wells up to room temperature.* **H. D. Sun, T. Makino, N. T. Tuan, Y. Segawa, Z. K. Tang, G. K. L. Wong, M. Kawasaki, A. Ohtomo, and K. Tamura.** 2000, Appl. Phys. Lett., Vol. 77, p. 4250.

16. *Thermal stability of supersaturated MgxZn1–xO alloy films and MgxZn1–xO/ZnO heterointerfaces.* **A. Ohtomo, R. Shiroki, I. Ohkubo, H. Koinuma, and M. Kawasaki.** 1999, Appl. Phys. Lett. , Vol. 75, p. 4088.

17. *Optical and structural analysis of ZnCdO layers grown by metalorganic vapor-phase epitaxy.* **T. Gruber, C. Kirchner, R. Kling, F. Reuss, A. Waag, F. Bertram, D. Forster, J. Christen, and M. Schreck.** 2003, Appl. Phys. Lett. , Vol. 83, p. 3290.

18. *First-principles study of native point defects in ZnO.* **A. F. Kohan, G. Ceder, D. Morgan, and C. G. Van de Walle.** 22, 2000, Phys. Rev. B, Vol. 61, p. 15 019.

19. *Bound exciton and donor–acceptor pair recombinations in ZnO.* **B. K. Meyer, H. Alves, D. M. Hofmann, W. Kriegseis, D. Forster, F. Bertram, J. Christen, A. Hoffmann, M. Straßburg, M. Dworzak, U. Haboeck, and A. V. Rodina.** 2, 2004, phys. stat. sol. (b), Vol. 241, pp. 231– 260.

20. *"Hidden hydrogen" in as-grown ZnO.* **G. A. Shi, M. Saboktakin, M. Stavola, and S. J. Pearton.** 2004, Appl. Phys. Lett., Vol. 85, p. 5601.

21. *First-principles calculations of solubilities and doping limits: Li, Na, and N in ZnSe.* **C. G. Van de Walle, D. B. Laks, G.F. Neumark, and S. T. Pantelides.** 1993, Phys. Rev. B, Vol. 47, p. 9425.

22. *Intrinsic n-type versus p-type doping asymmetry and the defect physics of ZnO.* **S. B. Zhang, S.-H. Wei, and A. Zunger.** 2001, Phys. Rev. B , Vol. 63, p. 075205.

23. *Compensation mechanism for N acceptors in ZnO.* **E.-C. Lee, Y.-S. Kim, Y.-G. Jin, and K. J. Chang.** 2001, Phys. Rev. B, Vol. 64, p. 085120.

24. *Optical and electrical properties of radical beam gettering epitaxy grown n- and p-type ZnO single crystals.* **T. V. Butkhuzi, A. V. Bureyev, A. N. Georgobiani, N. P. Kekelidze, and T. G. Khulordava.** 1992, J. Cryst. Growth , Vol. 117, p. 366.

25. *Fabrication of the low-resistive p-type ZnO by codoping method.* **M. Joseph, H. Tabata, H. Saeki, K. Ueda, and T. Kawai.** 2001, Physica B, Vol. 140, pp. 302–303.

26. *Characterization of homoepitaxial p-type ZnO grown by molecular beam epitaxy.* **D. C. Look, D. C. Reynolds, C. W. Litton, R. L. Jones, D. B. Eason, and G. Cantwell.** 10, SEPTEMBER 2002, App. Phys. Lett., Vol. 81.

27. *Influence of substrate temperature on N-doped ZnO films deposited by RF magnetron sputtering.* **J. Wang, V. Sallet, F. Jomard , A. M. B. do Rego , E. Elamurugu, R. Martins, and E. Fortunato.** 2007, Thin Solid Films, Vol. 515, pp. 8785–8788.

28. *Growth of p-type Zinc Oxide Films by Chemical Vapor Deposition.* **K. Minegishi, Y. Koiwai. Y. Kikuchi, K. Yano, M. Kasuga, and A. Shimizu.** 1997, Jpn. J. Appl. Phys. , Vol. 36, p. L1453.

29. *Chemical vapor deposition-formed p-type ZnO thin films.* **X. Li, Y. Yan, T. A. Gessert, C. L. Perkins, D. Young, C. DeHart, M. Young, and T. J. Coutts.** 4, 2003, J. Vac. Sci. Technol. A, Vol. 21, p. 1342.

30. *Atmospheric pressure MOCVD growth of high-quality ZnO films on GaN/Al2O3 templates.* **J. Dai, H. Liu, W. Fang, L. Wang, Y. Pu, Y. Chen, and F. Jiang.** 2005, J. Cryst. Growth , Vol. 283, pp. 93–99.

31. *Hydrogen passivation effect in nitrogen-doped ZnO thin films.* **X. Li, B. Keyes, S. Asher, S. B. Zhang, S.-H. Wei, T. J. Coutts, S. Limpijumnong, and C. G. Van de Walle.** 2005, Appl. Phys. Lett., Vol. 86, p. 122107.

32. *Substitutional diatomic molecules NO, NC, CO, N2, and O2:Their vibrational frequencies and effects on p doping of ZnO.* **S. Limpijumnong, X. Li, S.-H. Wei, and S. B. Zhang.** 2005, Appl. Phys. Lett., Vol. 86, p. 211910.

33. *Doping by Large-Size-Mismatched Impurities: The Microscopic Origin of Arsenic or Antimony-Doped p-Type Zinc Oxide.* **S. Limpijumnong, S. B. Zhang, S.-H. Wei, and C. H. Park.** 2004, Phys. Rev. Lett., Vol. 92, p. 155504.

34. *Annealing effects on electrical and optical properties of ZnO films deposited on GaAs by metal organic chemical vapor deposition.* **J. Sun, H. Liang, J. Zhao, Q. Feng, J. Bian, Z. Zhao, H. Zhang, Y. Luo, L. Hu, and G. Du.** 2008, Applied Surface Science, Vol. 254, pp. 7482–7485.

35. *A comprehensive review of ZnO materials and devices.* **Ü. Özgür, Ya. I. Alivov, C. Liu, A. Teke, M. A. Reshchikov, S. Doğan,V. Avrutin, S.-J. Cho, and H. Morkoç.** 2005, J. Appl. Phys., Vol. 98, p. 041301.

36. *Orientation relationships of zinc oxide on sapphire in heteroepitaxial chemical vapor deposition* . **M. Kasuga, and M. Mochizuki.** 1981, J. Cryst. Growth , Vol. 54, pp. 185-194.

37. *Angle-resolved photoemission from polar and nonpolar zinc oxide surfaces.* **W. Göpel, J. Pollmann, I. Ivanov, and B. Reihl.** 1982, Phys. Rev. B , Vol. 26, p. 3144.

38. *Electronic structure of ideal and relaxed surfaces of ZnO: A prototype ionic wurtzite semiconductro and its surface properties.* **I. Ivanov, and J. Pollmann.** 1981, Phys. Rev. B, Vol. 24, p. 7275.

39. **Kaldis, E., [ed.].** *Zinc Oxide, Properties and Behaviour of the Bulk, the Solid / Vacuum and Solid/Gas Interface,* . s.l. : Current Topics in Materials Science, North-Holland publishing Company, 1981. Vol. 7.

40. **N. Riehl.** *Physik und Technische Anwendungen der Lumineszenz,.* Berlin : Julius-Springer- Verlag, 1941.

41. *Wide band-gap II–VI compounds—can efficient doping be achieved?* **Desnica, U. V.** 3-4, 1998, Vacuum, Vol. 50, pp. 463-471.

42. *Native defects in gallium nitride.* **P. Boguslawski, E. L. Briggs, and J. Bernholc.** 23, 1995, Phys. Rev. B, Vol. 51, p. 17255.

43. *Deep energy levels of defects in the wurtzite semiconductor AlN, CdS, CdSe, ZnS, and ZnO.* **A. Kobayashi, O. F. Sankey, and J. D. Dow.** 2, 1993, Phys. Rev. B, Vol. 28, p. 946.

44. *Activation of shallow dopants in II-VI compounds.* **Walukiewicz, W.** 1996, J. Cryst. Growth, Vol. 159, pp. 244-247.

45. *Intrinsic electron mobilities in CdSe, CdS, ZnO, and ZnS and their use in analysis of temperature-dependent Hall measurements.* **X. Yang, C. Xu, and N. C. Giles.** 2008, J. Appl. phys., Vol. 104, p. 073727.

46. *A comparative electron paramagnetic resonance study of vanadium in n-type, semi-insulating and p-type CdTe.* **H. J. von Bardeleben, V. Mazoyer, X. Launay and J. C. Launay.** 1995, Vol. 10, pp. 162-166.

47. *Practical Doping Principles.* **A. Zunger.** Denver, Colorado : NREL, March 24-26, 2003. National Center for Photovoltaics and Solar Program Review Meeting. p. 831.

48. *Carrier Mobility and Shallow Impurity States in Znse and ZnTe.* **M. Aven, and B. segall.** 1, 1963, Phys. Rev., Vol. 130, p. 81.

49. *Atomic geometry and electronic structure of native defects in GaN.* **J. Neugebauer, and C. G. Van de Walle.** 11, 1994, Phys. rev. B, Vol. 58, p. 8067.

50. *Origin of p-type doping difficulty in ZnO: The impurity perspective.* **C. H. Park, S. B. Zhang, and S.-H. Wei.** 2002, Phys. Rev. B , Vol. 66, p. 073202.

51. *Hydrogen diffusion behavior in N doped ZnO: First-principles study.* **J. Hu, H. Y. He, and B. C. Pan.** 2008, J. Appl. Phys., Vol. 103, p. 113706.

52. *Native point defects in ZnO.* **A. Janotti, and C. G. Van de Walle.** 2007, Phys. Rev. B , Vol. 76, p. 165202.

53. *Residual Native Shallow Donor in ZnO.* **D. C. Look, J. W. Hemsky, and J. R. Sizelove.** 12, 1999, Phys. Rev. Lett., Vol. 82.

54. *Conductivity and Hall Effect of ZnO at Low Temperatures.* **Harrison, S. E.** 1954, Phys. Rev. , Vol. 93, p. 52.

55. *Zn interstitial related donors in ammonia-treated ZnO powders.* **J. Sann, J. Stehr, A. Hofstaetter, D. M. Hofmann, A. Neumann, M. Lerch, U. Haboeck, A. Hoffmann, and C. Thomsen.** 2007, Phys. Rev B , Vol. 76, p. 195203.

56. *Evidence for Native-Defect Donors in n-Type ZnO.* **D. C. Look, G. C. Farlow, P. Reunchan, S. Limpijumnong, S. B. Zhang, and K. Nordlund.** 2005, Phys. Rev. Lett., Vol. 95, p. 225502.

57. *Energetics of native defects in ZnO.* **F. Oba, S. R. Nishitani, S. Isotani, H. Adachi, and I. Tanaka.** 2, 2001, J. Appl. Phys., Vol. 90, p. 824.

58. *A FP–LMTO study on the native shallow donor in ZnO.* **S. Yuming, X. Pengshou, S. Chaoshu, X. Faqiang, P. Haibin, and L. Erdong.** 2001, J. Electron Spectrosco. Relat. Phenom. , Vols. 114-116, p. 1123.

59. *Effect of different dopant elements on the properties of ZnO thin films.* **P. Nunesa, E. Fortunato, P. Tonello, F. B. Fernandes, P. Vilarinho, and R. Martins.** 2002, Vacuum , Vol. 64, pp. 281-285.

60. *Electrical properties of transparent and conducting Ga doped ZnO.* **V. Bhosle, A. Tiwari, and J. Narayan.** 2006, J. Appl. Phys., Vol. 100, p. 033713.

61. *Universal alignment of hydrogen levels in semiconductors, insulators and solutions.* **C. G. Van de Walle, and J. Neugebauer.** 2003, Nature, Vol. 423, pp. 626–628.

62. *Hydrogen as a Cause of Doping in Zinc Oxide.* **Walle, C. G. Van de.** 5, 2000, Phys. Rev. Lett., Vol. 85, p. 1012.

63. *Identification of two hydrogen donors in ZnO.* **E. V. Lavrov, F. Herklotz, and J. Weber.** 2009, Phys. Rev. B , Vol. 79, p. 165210.

64. *Hydrogen complexes in Zn deficient ZnO.* **S. Zh. Karazhanov, E. S. Marstein, and A. Holt.** 2009, J. Appl. Phys., Vol. 105, p. 033712.

65. *On the theory of superlattice structures in alloys.* **W. Hume- Rothery, and H. M. Powell.** 1935, Z. Krist., Vol. 91, p. 23.

66. *Effective ionic radii in oxides and fluorides.* **R. D. Shannon, and C. T. Prewitt.** 1969, Acta. Cryst. B , Vol. 25, p. 925.

67. **Kroger, F.A.** *The Chemistry of lmperfect Crystals,.* Amsterdam : Nort-Holland, 1964.

68. *Mechanism of Fermi-level stabilization in semiconductors.* **Walukiewicz, W.** 9, 1988, Phys. Rev. B, Vol. 37, p. 4760.

69. *A phenomenological model for systematization and prediction of doping limits in II-VI and I-III-VI.* **S. B. Zhang, S.-H. Wei, and A. Zunger.** 1998, J. Appl.Phys., Vol. 83, p. 3192.

70. *Chemical Potential Dependence of Defect Formation Energies in GaAs: Application to Ga Self-Diffusion.* **S.B Zhang, and J.E. Northrup.** 1991, Phys. Rev. Lett., Vol. 67, p. 2339.

71. *Calculated natural band offsets of all II–VI and III–V semiconductors: Chemical trends and the role of cation d orbitals.* **S.-H. Wei, and A. Zunger.** 16, 1998, Appl. Phys. Lett., Vol. 72, p. 2011.

72. *Origins of the doping asymmetry in oxides: Hole doping in NiO versus electron doping in ZnO.* **S. Lany, J. Osorio-Guillén, and A. Zunger.** 2007, Phys. Rev. B, Vol. 75, p. 241203(R).

73. *The phosphorus acceptor in ZnSe.* **G. Neu, C. Morhain, E. Tournie, and J. P. Faurie.** 1998, J. Cryst. Growth, Vol. 184/185, pp. 515-519.

74. *Doping limits in ZnSe* . **D. B. Laks, and C. G. Van de Walle.** 1-4, 1993, Physica B: Condensed Matter, Vol. 185, pp. 118-127 .

75. *First-principles study of the compensation mechanism for nitrogen acceptors in ZnSe.* **B.-H. Cheong, C. H. Park, and K. J. Chang.** 1995, Phys. Rev. B, Vol. 51, p. 10610.

76. *Theory of Li in ZnO: A limitation for Li-based p-type doping.* **M. G. Wardle, J. P. Goss, and P. R. Briddon.** 2005, Phys. Rev. B , Vol. 71, p. 155205.

77. *Solution using a codoping method to unipolarity for the fabrication of p-type ZnO.* **T. Yamamoto, and H. Katayama-Yoshida.** 1999, Jpn. J. Appl. Phys., Vol. 38, p. L166.

78. *Compensation of p-type Doping in ZnSe: The Role of Impurity-Native defect Complexes.* **A. Garcia, and J. E. Northrup.** 1995, Phys. Rev. Lett., Vol. 74, p. 1131.

79. *Self-compensation through a large lattice relaxation in p-type ZnSe.* **D. J. Chadi, and K. J. Chang.** 6, 1989, Appl. Phys. Lett., Vol. 55, p. 575.

80. *Column V acceptors in ZnSe: Theory and experiment.* **D. J. Chadi.** 27, 1991, Appl. Phys. Lett., Vol. 59, p. 3589.

81. *Bulk Lattice Instability in II-VI Semiconductors and Its Effect on Impurity Compensation.* **C. H. Park, and D. J. Chadi.** 1995, Phys. Rev. Lett., Vol. 75, p. 1134.

82. *Predictor of p-type doping in II-VI semiconductors.* **D. J. Chadi.** 23, 1999, Phys. Rev. B , Vol. 59, p. 15181.

83. *Energy of formation of Li defects in ZnSe deposited by molecular beam epitaxy.* **Krasnov, A. N.** 1-2, 1994, J. Cryst. Growth, Vol. 141, pp. 89-92.

84. *Pair Spectra and the Shallow Acceptors in ZnSe.* **J. L. Merz, K. Nassau, and J. W. Shiever.** 1973, Phys. Rev. B, Vol. 8, p. 1444.

85. *Evidence of N-related compensating donors in lightly doped ZnSe:N.* **E. Tournie, P. Brunet, and J.-P. Faurie.** 15, 1999, Appl. Phys. Lett., Vol. 74, p. 2200.

86. *Cathodoluminescence and transmission electron microscopy study of the influence of crystal defects the influence of crystal defects on optical transitions in GaN",.* **G. Salviati, M. Albrecht, C. Zanotti-Fregonara, N. Armani, M. Mayer, Y. Shreter, M. Guzzi, Y. V. Melnik, K. Vassilevski, V. A. Dmitriev, and H. P. Strunk.** 1999, Phys. Stat. Sol. A, Vol. 171, p. 325.

87. *Unusual luminescence lines in GaN.* **M. A. Reshchikov, D. Huang, F. Yun, P. Visconti, L. He, H. Morkoç, J. Jasinski, Z. Liliental-Weber, R. J. Molnar, S. S. Park, and K. Y. Lee.** 2003, J. Appl. Phys. , Vol. 94, p. 5623.

88. *Dislocation luminescence in wurtzite GaN.* **Y. G. Shreter, Y. T. Rebane, T. J. Davis, J. Barnard, M. Darbyshire, J. W. Steeds, W. G. Perry, M. D. Bremser, and R. F. Davis.** 1997, Mater. Res. Soc. Symp. Proc. , Vol. 449, p. 683.

89. *Luminescence properties of defects in GaN.* **M. A. Reshchikov, and H. Morkoç.** 2005, J. Appl. Phys., Vol. 97, p. 061301.

90. *Comparison of MOCVD-grown with conventional II-VI materials parameters for EL thin film.* **Dean, P. J.** 1984, Phys. Stat. Sol. A, Vol. 81, p. 625.

91. *Luminescence due to lattice-mismatch defects in ZnTe layers grown by metalorganic vapor phase epitaxv .* **A. Naumov, K. Walf, T. Reisinger, H. Stanzl, and W. Gebhardt.** 1998, J. Appl. Phys. , Vol. 73, p. 2581.

92. *Stacking fault related 3.31-eV luminescence at 130-meV acceptors in zinc oxide.* **M. Schirra, R. Schneider, A. Reiser, G. M. Prinz, M. Feneberg, J. Biskupek, U. Kaiser, C. E. Krill, K. Thonke, and R. Sauer.** 2008, Phys. Rev. B, Vol. 77, p. 125215.

93. *Optical investigations on excitons bound to impurities and dislocations in ZnO.* **H. Alves, D. Pfisterer , A. Zeuner , T. Riemann , J. Christen, D. M. Hofmann, and B. K. Meyer.** 2003, Optical Materials , Vol. 23, pp. 33–37.

94. *Effects of dislocation density on the properties of liquid phase epitaxial GaAs.* **Ettenberg, M.** 1974, J. Appl. Phys. , Vol. 45, p. 901.

95. *Degradation of II-VI based blue green light emitters.* **S. Guha, J. M. Depuydt, M. A. Haase, J. Qiu, and H. Cheng.** 1993, Appl. Phys. Lett. , Vol. 63, p. 3107.

96. *Status of hydrothermal growth of bulk ZnO:Latest issues and advantages.* **L. N. Dem'yanets, and V. I. Lyutin.** 2008, J. Cryst. Growth, Vol. 310, pp. 993–999.

97. *ZnO single crystals: Synthesis and characterization.* **L. Yin, L. Zhang, F. Li, M. Yu.** 2005, Materials Research Bulletin , Vol. 40, pp. 2219–2224.

98. *Growth of the 2-in-size bulk ZnOsingle crystals by the hydrothermal method.* **E. Ohshima, H. Ogino, I. Niikura, K. Maeda,M. Sato, M. Ito, and T. Fukuda.** 2004, J. Cryst. Growth, Vol. 260, pp. 166–170.

99. *Growth of ZnO single crystals by chemical vapour transport.* **M. Shiloh, and J. Gutman.** 2, 1971, J. Cryst. Growth, Vol. 11, pp. 105-109.

100. *Growth of ZnO crystals by vapour transport: Some ways to act on physical properties.* **R. Tena-Zaera, C. Martínez-Tomás, C. J. Gómez- García, and V. Muñoz-Sanjosé.** 8, 2006, Cryst. Res. Technol., Vol. 41, pp. 742 – 747.

101. *Crystal growth of ZnO by chemical transport using HgCl2 as a transport agent.* **K. Matsumoto, and K. Noda.** 1-2, 1990, J. Cryst. Growth, Vol. 102, pp. 137-140.

102. *ZnO broadens the spectrum.* **J.E. Nause.** 4, 1999, Ill-Vs Review , Vol. 12, p. 28.

103. *High-quality, melt-grown ZnO single crystals.* **D. C. Reynolds, C. W. Litton, D. C. Look, J. E. Hoelscher, B. Claflin, T. C. Collins, J. Nause, and B. Nemeth.** 2004, J. Appl. Phys., Vol. 95, p. 4802.

104. *Effects of oxygen plasma condition on MBE growth of ZnO.* **K. Sakurai, M. Kanehiro, K. Nakahara, T. Tanabe, Sh. Fujita, S. Fujita.** 2000, J. Cryst. Growth, Vol. 209, pp. 522-525.

105. *Post deposition annealing behavior of rf sputtering ZnO films.* **R. J. Lad, P. D. Funkenbusch, and C. R. Aita.** 1980, J. Vac. Sci. Technol., Vol. 17, p. 808.

106. **J. A. Venables, and G. L. Price.** Nucleation of thin films. [book auth.] J.W. Matthews. *Epitaxial Growth, part B.* s.l. : Academic Press, Inc, 1957, pp. 381-436.

107. *ZnO films grown by MOCVD on GaAs substrates: Effects of a Zn buffer deposition on interface, structural and morphological properties.* **S. Agouram, M. C. Martınez-Tomas, and V. Munoz-Sanjose.** 2009, J. Cryst. Growth, Vol. 311, pp. 2564–2571.

108. *Observation of interfacial reactions and recrystallization of extrinsic phases in epitaxial grown ZnO/GaAs heterostructures* . **H. F. Liu, A. S. W. Wong, G. X. Hu, and H. Gong.** 2008, J. Cryst. Growth, Vol. 310, pp. 4305-4308 .

109. *Single crystal ZnO films grown on lattice-matched ScAlMgO4(0001) substrates.* **A. Ohtomo, K. Tamura, K. Saikusa, K. Takahashi, T. Makino, Y. Segawa,H. Koinuma, and M. Kawasaki.** 1999, Appl. Phys. Lett., Vol. 75, p. 2635.

110. *Photoluminescence of AlxGa1-xAs alloys.* **L. Pavesi, and M. Guzzi.** 10, 1994, J. appl. Phys., Vol. 75, p. 4779.

111. **Sze, S. M.** *Physics of Semiconductor Devices.* New York : Wiley, 1981.

112. *Recombination in semiconductors.* **Landsberg, P. T.** 1991, Cambridge University Press.

113. **Cho, K.** *Excitons* . Berlin : Springer, Topics in Current Physics, 1979. Vol. 14.

114. *The exciton spectrum of zinc oxide* . **Thomas, D.G.** 1-2, 1960, J. Phys. Chem.Solids, Vol. 15, p. 86.

115. **Landoldt-Börnstein.** *Numerical data and functional relationships in science and technology.* [ed.] O. Madelung. Berlin : Springer-Verlag, 1982. Vol. III/17b .

116. *Properties of Excitons Bound to Ionized Donors.* **T. Skettrup, M. Suffczynski, and W. Gorzkowski.** 1971, Phys. Rev. B, Vol. 4, p. 512.

117. *Exciton-Donor Complexes in Semiconductors.* **R. R. Scharma, and S. Rodriguez.** 1967, Phys. Rev., Vol. 159, p. 649.

118. *Experimental proof of the existence of a new electronic complex in silicon.* **Haynes, J. R.** 1960, Phys. Rev. Lett., Vol. 4, p. 361.

119. *Ionized and neutral donor-bound excitons in ZnO.* **B. K. Meyer, J. Sann, S. Lautenschläger, M. R. Wagner, and A. Hoffmann.** 2007, Phys. Rev. B, Vol. 76, p. 184120.

120. *Pair spectra in GaP.* **J. J. Hopfield, D. G. Thomas, and M. Gershenzon.** 1963, Phys. Rev. Lett. , Vol. 10, p. 162.

121. *Excitation-power dependence of the near-band-edge photoluminescence of semiconductors.* **T. Schmidt, K. Lischla, and W. Zulehner.** 1992, Phys. Rev. B, Vol. 45, p. 8989.

122. *Theory of light absorption and non radiative transitions in F centres.* **K. Huang, and A. Rhys.** 1950, Proc. R. Soc. Lond. A, Vol. 204, pp. 406-423.

123. *Temperature dependence of the energy gap in semiconductors* . **Y. P. Varshni.** 1967, Physica, Vol. 34, pp. 149-154.

124. *Luminescence of bound excitons in epitaxial ZnO thin films grown by plasma-assisted molecular beam epitaxy.* **Y. S. Jung, W. K. Choi, O. V. Kononenko, and G. N. Panin.** 2006, J. Appl. Phys. , Vol. 99, p. 013502.

125. *Use of Metal-Oganics-Semiconductor Material.* **Simpson, H. M. Manasevit and W. I.** 1969, J. Electrochem. Soc., Vol. 116, pp. 1725-1732.

126. **Catalogue, Alfa.** Organometallics for Electronic. s.l., USA : Ventron Corporation, 1978.

127. **R.C. Reid, J.M. Prausnitz, and T.K. Sherwood.** *The Properties of Gases and Liquids.* New york : McGraw-Hill, 1977.

128. *Use of Nitrogen as the Ambient in the LP-MOVPE of III/V's.* **Hardtdegen, H.** [ed.] Electrochemical Society Proceedings. 1996. Vols. 96-2, p. 49 .

129. **Roro, K. T.** *MOCVD growth and characterization of ZnO thin films.* Physics, Nelson Mandela Metropolitan University. 2008.

130. *Influence of spontaneous polarization on the electrical and optical properties of bulk, single crystal ZnO.* **M. W. Allen, P. Miller, R. J. Reeves, and S. M. Durbin.** 2007, Appl. Phys. Lett., Vol. 90, p. 062104.

131. **Adachi, Sadao.** *Group-IV, III-V and II-IV Semiconductors.* West Sussex : John Wiley & Sons Ltd, 2005. p. 121. 0-470-09032-4.

132. *Defects in hydrothermally grown bulk ZnO.* **H. von Wenckstern, H. Schmidt, M. Grundmann, M. W. Allen, P. Miller, R. J. Reeves, and S. M. Durbin.** 2007, Appl. Phys. Lett., Vol. 91, p. 022913.

133. *Excited states of bound excitons in ZnO.* **H. Schrey, and C. Klingshrin.** 1980, Solid State Commun., Vol. 33, pp. 485-488.

134. *Remote hydrogen plasma doping of single crystal ZnO.* **Y. M. Strzhemechny, H.L. Mosbacker, D.C. Look, D.C. Reynolds, C.W. Litton, N.Y. Garces, N.C. Giles, and L.E. Halliburton.** 14, 2004, Appl. Phys. Lett., Vol. 84, p. 2545.

135. *Role of diatomic hydrogen in the electronic structure of ZnO.* **S. Zh. Karazhanov, and A.G. Ulyashin.** 2008, Phys. Rev. B, Vol. 78, p. 085213.

136. *Neutral-donor–bound-exciton complexes in ZnO crystals.* **D. C. Reynolds, D. C. Look, B. Jogai, C. W. Litton, T. C. Collins, W. Harsch and G. Cantwell.** 15, 1998, Phys. Rev. B, Vol. 57, p. 12151.

137. *Effect of Hydrogenation on ZnO Luminescence.* **T. Sekiguchi, N. Ohashi and Y. Terada.** 1997, Jpn. J. Appl. Phys. , Vol. 36, pp. L289-L291.

138. *Green luminescent center in undoped zinc oxide films deposited on silicon substrates.* **B. Lin, Z. Fu, and Y. Jia.** 7, 2001, Appl. Phys. Lett., Vol. 79, p. 943.

139. *Lithium and sodium acceptors in ZnO.* **B. K. Meyer, J. Sann, and A. Zeuner.** 2005, Superlattices and Microstructures , Vol. 38, pp. 344–348.

140. *Identification of oxygen and zinc vacancy optical signals in ZnO.* **T. M. Børseth, B. G. Svensson, A. Yu. Kuznetsov, P. Klason, Q. X. Zhao, and M. Willander.** 2006, Appl. Phys. Lett., Vol. 89, p. 262112.

141. *Optical absorption of a Li-related impurity in ZnO.* **D. Mc Cabe, K. Johnston, M. O. Henry, E. Mc Glynn, E. Alves,and J. J. Davies.** 2003, Physica B , Vols. 340–342, pp. 225–229.

142. *Luminescent transitions associated with divalent copper impurities and the green emission from semiconducting zinc oxide.* **Dingle, R.** 11, 1969, Phys. Rev. Lett., Vol. 23, p. 579.

143. *Role of copper in the green luminescence from ZnO crystals.* **N.Y. Garces, L. Wang, L. Bai, N.C. Giles, L.E. Halliburton, and G. Gantwell.** 4, 2002, Appl. Phys. Lett., Vol. 81, p. 622.

144. *Green Luminescence Band of Zinc Oxide Films Copper-Doped by Thermal Diffusion.* **Y. I. Alivov, M. V. Chukichev, and V. A. Nikitenko.** 1, 2004, Semiconductors, , Vol. 38, pp. 31–35.

145. *Fine structure on the green band in ZnO.* **D.C. Reynolds, D. C. Look, and B. Jogai.** 11, June 2001, J. Appl. Phys., Vol. 89, p. 6189.

146. *Hydrogen incorporation and diffusivity in plasma-exposed bulk ZnO.* **K. Ip, M. E. Overberg, Y. W. Heo, D. P. Nortgon, S. J. Pearton, C. E. Stutz, B. Luo, F. Ren, D. C. Look, and J. M. Zavada.** 2003, Appl. Phys. Lett. , Vol. 82, p. 385.

147. **Sze, S. M.** *Semiconductor Devices, Physics and Technology.* New York : Wiley, 1985.

148. *Optical observation of donor-bound excitons in hydrogen-implanted ZnO.* **J.-K. Lee, M. Nastasi, . W. Hamby and D. A. Lucca.** 2005, Appl. Phys. Lett., Vol. 86, p. 171102.

149. *Theory of Fe, Co, Ni, Cu, and their complexes with hydrogen in ZnO.* **M. G. Wardle, J. P. Goss, and P. R. Briddon.** 2005, Phys. Rev. B, Vol. 72, p. 155108.

150. *Optical and paramagnetic properties of ZnO-Crystals simultaneously doped with copper and hydrogen* . **E. Mollwo, G. Müller, and D. Zwingel.** 1974, Solid State Commun. , Vol. 15, p. 1475.

151. *Hydrogen plasma treatment effects on electrical and optical properties of n-ZnO.* **A. Y. Polyakov, N. B. Smirnov, A. V. Govorkov, K. Ip, M. E. Overberg, Y. W. Heo, D. P. Norton, S. J. Pearton, B. Luo, F. Ren, J. M. Zavada.** 1, 2003, J. Appl. Phys., Vol. 94, p. 400.

152. **B. D. Cullity, and S. R. Stock.** Elements of X-ray Diffraction. [book auth.] Englewood Cliffs. [ed.] 3. New Jersey : Prentice-Hall, 2001, p. 93.

153. *Annealing effects on electrical and optical properties of ZnO thin-film samples deposited by radio frequency-magnetron sputtering on GaAs (001) substrates.* **H. F. Liu, S. J. Chua, G. X. Hu, H. Gong, and N. Xiang.** 2007, J. Appl. Phys., Vol. 102, p. 063507.

154. *Properties of arsenic-doped p-type ZnO grown by hybrid beam deposition.* **Y. R. Ryu, T. S. Lee, and H. W. White.** 2003, Appl. Phys. Lett., Vol. , Vol. 83, p. 87.

155. *Investigation on the p-type formation mechanism of arsenic doped p-type ZnO thin film.* **H. S. Kang, G. H. Kim, D. L. Kim, and H. W. Chang,.** 2006, Appl. Phys. Lett., Vol. 89, p. 181103.

156. *Photoluminescence study and structural characterization of p-type ZnO doped by N and/or As acceptors.* **E. Przezdziecka, E. Kaminska, K. P. Korona, E. Dynowska, W. Dobrowolski, R. Jakieła, Ł. Kłopotowski, and J. Kossut.** 2007, Semicond. Sci. Technol. , Vol. 22, pp. 10-14.

157. *Realization of As-doped p-type ZnO thin films using sputter deposition.* **H. -K. Choi, J. -H. Park, S. -H. Jeong, and B. -T. Lee.** 2009, Semicond. Sci. Technol. , Vol. 24, p. 105003.

158. *Arsenic-related recombination in MOVPE-grown ZnO/GaAs films.* **J. R. Botha, K. T. Roro, C. Weichsel, A. W. R. Leitch, and J. Weber.** 2007, Superlattices and Microstructures , Vol. 42, pp. 26–32.

159. *Optical properties of ZnO fabricated on GaAs by molecular beam epitaxy.* **Z. Z. Zhang, D. Z. Shen, Y. M. Lu, J. Y. Zhang, B. H. Li, D. X. Zhao, B. Yao, and X. W. Fan.** 2007, Journal of Luminescence , Vols. 122–123 , pp. 202–204.

160. *Acceptor-exciton complexs in ZnO: A comprehensive analysis of their electronic states by high-resolution magnetooptics and excitation spectroscopy.* **J. Gutowski, N. Presser, and I. Broser.** Phys. Rev. B , Vol. 38, p. 9746.

161. *MOCVD layer growth of ZnO using DMZn and tertiary butanol.* **B Hahn, G Heindel, E Pschorr-Schoberer, and W Gebhardt.** 1998, Semicond. Sci. Technol. , Vol. 13, pp. 788–791.

162. *The growth and annealing of single crystalline ZnO films by low-pressure MOCVD.* **J. Ye, S. Gu, S. Zhu, T. Chen, L. Hu, F. Qin, R. Zhang, Y. Shi, and Y. Zheng.** 2002 , Journ. Cryst. Growth , Vol. 243, pp. 151–156.

163. *Temperature-dependent Hall effect studies of ZnO thin films grown by metalorganic chemical vapour deposition.* **K T Roro, G H Kassier, J K Dangbegnon, S Sivaraya, J E Westraadt, J H Neethling, AWR Leitch, and J R Botha.** 2008 , Semicond. Sci. Technol. , Vol. 23, p. 055021.

164. *Influence of metal organic chemical vapor deposition growth parameters on the luminescent properties of ZnO thin films deposited on glass substrates.* **K.T. Roro, J. K. Dangbegnon, S. Sivaraya, A.W.R. Leitch, and J.R. Botha.** 2008, J. Appl. Phys. , Vol. 103, p. 053516.

165. *Doping engineering of p-type ZnO.* **Y. Marfaing, and A. Lusson.** 2005, Superlattices and Microstructures , Vol. 38, pp. 385–396.

166. *Study on the Hall-effect and photoluminescence of N-doped p-type ZnO thin films.* **Y. J. Zeng, Z. Z. Ye, W. Z. Xu, B. Liu, Y. Che, L. P. Zhu, and B. H. Zhao,.** 2007, Mater. Lett. , Vol. 61, pp. 41–44.

167. *Repeated temperature modulation epitaxy for p-type doping and light-emitting diode based on ZnO.* **A. Tsukazaki, A. Ohtomo, T. Onuma, M. Ohtani, T. Makino, M. Sumiya, K. Ohtani, S.F. Chichibu, S. Fuke, Y. Segawa, H. Ohno,H. Koinuma, and M. Kawasaki.** 2005, nature materials , Vol. 5, p. 42.

168. *Correlation between nitrogen and carbon incorporation into MOVPE ZnO at various oxidizing conditions.* **J.J. Zhu, L.Vines,T.Aaltonen, and A.Yu.Kuznetsov.** 2009, Microelectronics Journal, Vol. 40, pp. 232–235.

169. *Vibrational spectroscopy of undoped and nitrogen-doped ZnO grown by metalorganic chemical vapor deposition.* **N. H. Nickel, F. Friedrich, J. F. Rommeluère, and P. Galtier.** 2005, Appl. Phys. Lett. , Vol. 87, p. 211905.

170. *Impurity effects in ZnO and nitrogen-doped ZnO thin films fabricated by MOCVD.* **X. Li, S. E. Asher, S. Limpijumnong, B. M. Keyes, C. L. Perkins,T. M. Barnes, H. R. Moutinho, J. M. Luther, S.B. Zhang,S.-H. Wei, and T. J. Coutts.** 2006, Journ. Cryst. Growth, Vol. 287, pp. 94–100.

171. *Properties of N-doped ZnO thin films in annealing process.* **Y. Zhang, J. Lu, L. Chen, and Z. Ye.** 2007, Solid State Communications , Vol. 143, pp. 562–565.

172. *Unintentional doping and compensation effects of carbon in metal-organic chemical-vapor deposition fabricated ZnO thin films.* **X. Li, S. E. Asher, S. Limpijumnong,S. B. Zhang, S.-H. Wei,Teresa M. Barnes, T. J. Coutts, and R. Noufi.** 4, 2006, J. Vac. Sci. Technol. A, Vol. 24, p. 1213.

173. *Nitrogen incorporation during metal organic chemical vapor deposition of ZnO films using a remote Ar/N2 plasma.* **I. Volintiru, M. Creatore, W. H. van Helvoort, J. L. Linden, and M. C. M. van de Sanden.** 2006, Appl. Phys. Lett., Vol. 89, p. 022110.

174. *Roles of hydrogen and nitrogen in p-type doping of ZnO.* **J.G. Lu, S. Fujita, T. Kawaharamura, and H. Nishinaka.** 2007, Chemical Physics Letters, Vol. 441, pp. 68–71.

175. *Defects in Compound Semiconductors Caused by Molecular Nitrogen.* **N.H. Nickel, and M A. Gluba.** 2009, Phys. Rev. Lett, Vol. 103, p. 145501.

176. *Unambiguous identification of nitrogen-hydrogen complexes in ZnO.* **S.J. Jokela, and M.D. McCluskey.** 2007, Phys. Rev. B , Vol. 76, p. 193201.

177. *Effect of annealing on the properties of N-doped ZnO films deposited by RF magnetron sputtering.* **J. Wang, E. Elamurugu, V. Sallet, F. Jomard, A. Lusson, A. M. B. do Rego, P. Barquinha,G. Gonçalves, R. Martins, E. Fortunato.** 2008, Applied Surface Science , Vol. 254, pp. 7178–7182.

178. *Carbon clusters in N-doped ZnO by metal-organic chemical vapor deposition.* **K. Tang, S. Gu, S. Zhu, W. Liu, J. Ye, J. Zhu, R. Zhang, Y. Zheng, and X. Sun.** 2008, Appl. Phys. Lett., Vol. 93, p. 132107.

179. *Study of a nitrogen-doped ZnO film with synchrotron radiation.* **C. W. Zou, X. D. Yan, J. Han, R. Q. Chen, W. Gao, and J. Metson.** 2009, Appl. Phys. lett., Vol. 94, p. 171903.

180. *Direct Observation of Nitrogen Location in Molecular Beam Epitaxy Grown Nitrogen-Doped ZnO.* **P. Fons, H. Tampo,A. V. Kolobov, M. Ohkubo, S. Niki, J. Tominaga, R. Carboni, F. Boscherini and S. Friedrich.** 2006, Phys. Rev. Lett. , Vol. 96, p. 045504.

181. *Production of native donors in ZnO by annealing at high temperature in Zn vapor.* **L. E. Halliburton, N. C. Giles, N. Y. Garces, M. Luo, C. Xu, L. Bai, and L. A. Boatner.** 2005, Appl. Phys. Lett. , Vol. 87, p. 172108.

182. *Annealing Effect on the Luminescent Properties and Native Defects of ZnO.* **A. N. Gruzintsev, and E. E. Yakimov.** 7, 2005, Inorganic Materials, Vol. 41, pp. 725–729.

183. *Interaction of nitrogen with vacancy defects in N+-implanted ZnO studied using a slow positron beam.* **Z. Q. Chen, M. Maekawa, and A. Kawasuso.** 2005, Appl Phys. Lett. , Vol. 87, p. 091910.

184. *Decomposition kinetics of tertiarybutanol and diethylzinc used as precursor sources for the growth of ZnO* . **C. Thiandoume, V. Sallet, R. Triboulet, and O. Gorochov.** 2009, J. Cryst. Growth, Vol. 311, pp. 1411-1415 .

185. *Hydrogen local modes and shallow donors in ZnO.* **G. A. Shi, M. Stavola, S. J. Pearton, M. Thieme, E. V. Lavrov, and J. Weber.** 2005, Phys. Rev. B , Vol. 72, p. 195211.

186. *Hydrogen migration in single crystal and polycrystalline zinc oxide.* **N. H. Nickel.** 2006, Phys. rev. B , Vol. 73, p. 195204.

187. **W. Beyer, II,.** in Hydrogen in Semiconductors. [book auth.] N.H. Nickel. San Diego : Academic, 1999, Vol. 61, p. 165.

188. *Nature of Native Defects in ZnO.* **F. A. Selim, M. H. Weber, D. Solodovnikov, and K. G. Lynn.** 2007, Phys. Rev. Lett., Vol. 99, p. 085502.

189. *One-step growth of ZnO from film to vertically well-aligned nanorods and the morphology-dependent Raman scattering.* **G. W. Cong, H. Y. Wei, P. F. Zhang, W. Q. Peng, J. J. Wu, X. L. Liu, C. M. Jiao, W. G. Hu, Q. S. Zhu, and Z. G. Wang.** 2005, Appl. Phys. Lett., Vol. 87, p. 231903.

190. *Metalorganic vapor-phase epitaxial growth of vertically well-aligned ZnO nanorods.* **W. I. Park, D. H. Kim, S.-W. Jung, and Gyu-Chul Yi.** 2002, Appl. Phys. Lett. , Vol. 80, p. 4232.

191. *ZnO nanorods: synthesis, characterization and applications.* **G.-C. Yi, C. Wang, and W. I. Park.** 4, 2005, Semicond. Sci. Technol., Vol. 20, pp. S22-S34.

192. *ZnO Nanoneedles Grown Vertically on Si Substrates by Non-catalytic Vapor-Phase Epitaxy.* **W.I. Park, G.-C. Yi, M. Kim, and S.J. Pennycook.** 4, 2002, Adv. Mater., Vol. 24, p. 1841.

193. *Early stage growth behavior of ZnO nanoneedle arrays on Al2O3 (0001) by metalorganic chemical vapor deposition.* **J. Y. Park, J. M. Lee,J. H. Je, S. S. Kim.** 2005, Journ Cryst. Growth, Vol. 281, pp. 446-451.

194. *ZnO nanoneedles with tip surface perturbations: Excellent field emitters.* **Y. B. Li, Y. Bando, and D. Golberg.** 2004, Appl. Phys. Lett. , Vol. 84, p. 3603.

195. **M. H. Sukkar, and H. L. Tullerin.** Advances in Ceramics. [ed.] and A. H. Heuer M. F. Yan. Columbus : American Ceramic Society, 1982, Vol. 7, p. 71.

196. *Effect of Annealing in Oxygen Radicals on Luminescence and Electrical Conductivity of ZnO:N Films.* **A. N. Georgobiani, A. N. Gruzintsev, V. T. Volkov, and M. O. Vorob'ev.** 3, 2002, Semiconductors, Vol. 36, pp. 265–269.

197. *Shifting donor-acceptor photoluminescence in N-doped ZnO.* **T. Makino, A. Tsukazaki, A. Ohtomo, M. Kawasaki, and H. Koinuma,.** 7, 2006, J. Phys. Soc. Jpn , Vol. 75, p. 073701.

198. *Comparative photoluminescence study on p-type and n-type ZnO films codoped by nitrogen and aluminium.* **H. Tang, Z.Ye, H. He.** 2008, Optical Materials , Vol. 30, pp. 1422–1426.

199. *Donor–acceptor pair luminescence in nitrogen-doped ZnO films grown on lattice-matched ScAlMgO4 (0001) substrates.* **K. Tamura, T. Makino, A. Tsukazaki, M. Sumiya, S. Fuke, T. Furumochi,M. Lippmaa, C.H. Chia, Y. Segawa, H. Koinuma, M. Kawasaki.** 2003, Solid State Communications , Vol. 127, pp. 265–269.

200. *Characteristics of nitrogen-doped p-ZnO thin films and ZnO/ZnSe p–n heterojunctions grown on a ZnSe substrate.* **I. V. Rogozin, and M. B. Kotlyarevsky.** 2008, Semicond. Sci. Technol. , Vol. 23, p. 085008.

201. *Nitrogen-related recombination mechanisms in p-type ZnO films grown by plasma-assisted molecular beam epitaxy.* **J. W. Sun, Y. M. Lu, Y. C. Liu, D. Z. Shen, Z. Z. Zhang, B. Yao, B. H. Li, J. Y. Zhang, D. X. Zhao, and X. W. Fan.** (2007), J. Appl. Phys., Vol. 102, p. 043522 .

202. *Photoluminescence dependence of ZnO films grown on Si (100) by radio-frequency magnetron sputtering on the growth ambient.* **S.-H. Jeong, B.-S. Kim, and B.-T. Lee.** 2003, Appl. Phys. Lett. , Vol. 82, p. 2625.

203. *Control of conductivity type in undoped ZnO thin films grown by metalorganic vapor phase epitaxy.* **Y. Ma, G. T. Du, S. R. Yang, Z. T. Li, B. J. Zhao, X. T. Yang, T. P. Yang, Y. T. Zhang, and D. L. Liu.** 2004, J. Appl. Phys., Vol. 95, p. 6268.

204. *Photoluminescence study of Sb-doped p-type ZnO films by molecular-beam epitaxy.* **F. X. Xiu, Z. Yang, L. J. Mandalapu, D. T. Zhao, and J. L. Liu.** 2005, Appl. Phys. Lett., Vol. 87, p. 252102.

205. *Hydrogen-related defects in ZnO studied by infrared absorption spectroscopy.* **E. V. Lavrov, J. Weber, F. Borrnert, Chris G. Van de Walle, and R. Helbig.** 2002, PHYSICAL REVIEW B , Vol. 66, p. 165205.

206. *Growth behaviour of well-aligned ZnO nanowires on a Si substrate at low temperature and their optical properties.* **J. S. Jeong, J Y. Lee, J. H. Cho, C. J. Lee, S.-J. An, G. -C. Yi, and R. Gronsky.** 2005, Nanotechnology , Vol. 16, pp. 2455–2461.

207. *Structural and luminescent properties of ZnO epitaxial film grown on Si(1 1 1) substrate by atmospheric-pressure MOCVD.* **Y. Chen, F. Jiang, L. Wang, C. Zheng, J. Dai,Y. Pu, W. Fang.** 2005, Journ. of Cryst. Growth , Vol. 275, pp. 486–491.

208. *The photoluminescence properties of ZnO:N films fabricated by thermally oxidizing Zn3N2 films using plasma-assisted metal-organic chemical vapour deposition.* **D. Wang, Y C Liu, RMu,J Y Zhang, Y M Lu, D Z Shen, and X.W. Fan.** 2004, J. Phys.: Condens. Matter , Vol. 16, pp. 4635–4642.

209. *Microcathodoluminescence spectroscopy of defects in Bi2O3-doped ZnO grains.* **X. L. Sun, L. J. Brillson, Y.-M. Chiang and J. Luo.** 2002, J. Appl. Phys., Vol. 92, p. 5072.

210. *Convergence of the formation energies of intrinsic point defects in wurtzite ZnO: first-principles study by projector augmented wave method.* **J.-L. Zhao, W. Zhang, X.-M. Li, J.-W. Feng, and X. Shi.** 2006, J. Phys.: Condens. Matter , Vol. 18, pp. 1495–1508.

211. *Investigation on the variation of green, yellow, and orange emission properties of ZnO thin film.* **H. S. Kang, J. W. Kim, S. H. Lim, H. W. Chang, G. H. Kim, J. H. Kim,S. Y. Lee.** 2006, Superlattices and Microstructures , Vol. 39, pp. 193–201.

212. *Photoluminescence and cathodoluminescence studies of stoichiometric and oxygen-deficient ZnO films.* **X. L. Wu, G. G. Siu, C. L. Fu, and H. C. Ong.** 2001, Appl. Phys. Lett., Vol. 78, p. 2285.

213. *Effects of growth temperature on the characteristics of ZnO epitaxial films deposited by metalorganic chemical vapor deposition* . **B. P. Zhang, K. Wakatsuki, N. T. Binha, N. Usamic, and Y. Segawa.** 2004, Thin Solid Films , Vol. 449, pp. 12-19.

214. *Determination of the ionization energy of nitrogen acceptors in zinc oxide using photoluminescence spectroscopy.* **L. Wang, and N. C. Giles.** 2004, Appl. Phys. Lett. , Vol. 84, p. 3049.

215. *Donor–acceptor pair transitions in ZnO substrate material* . **K. Thonke, Th. Gruber, N. Teofilov, R. Schönfelder, A. Waag, and R. Sauer.** 2001, Physica B , Vols. 308–310, pp. 945–948.

216. *Kinetics of Radiative Recombination at Randomly Distributed Donors and Acceptors.* **D. G. Thomas, J. J. Hopfield, and W. M. Augustyniak.** 1965, Phys. Rev., Vol. 140, p. A202.

217. *Defects in virgin and N+-implanted ZnO single crystals studied by positron annihilation, Hall effect, and deep-level transient spectroscopy.* **G. Brauer, W. Anwand, W. Skorupa, J. Kuriplach,O. Melikhova, and C. Moisson.** 2006, Phys. Rev. B , Vol. 74, p. 045208.

218. *Characteristics of Schottky contacts to ZnO:N layers grown by molecular-beam epitaxy.* **D. C. Oh, J. J. Kim, H. Makino, T. Hanada, M. W. Cho, T. Yao, and H. J. Ko.** (2005), Appl. Phys. Lett., Vol. 86, p. 042110.

219. *Oxygen vacancies in ZnO.* **A. Janotti, and C. G. Van de Walle.** 2005, Appl. Phys. Lett. , Vol. 87, p. 122102.

220. *Effect of annealing on the properties of (100) ZnO films prepared by chemical vapor deposition utilizing zinc acetate dihydrate.* **L.-C. Chao, H.-T. Hu, S.-H. Yang, and Y.-C. Fan.** 2008, Thin Solid Films , Vol. 516, pp. 6305–6309.

221. *Evolution of visible luminescence in ZnO by thermal oxidation of zinc films.* **Y.G. Wang, S.P. Lau, X.H. Zhang, H.W. Lee, S.F. Yu, B.K. Tay,and H.H. Hng.** 2003, Chemical Physics Letters , Vol. 375, pp. 113–118.

222. *Diffusion of zinc vacancies and interstitials in zinc oxide.* **P. Erhart, and K. Albe.** 2006, Appl. Phys. Lett. , Vol. 88, p. 201918.

223. *Effect of annealing atmosphere on the photoluminescence of ZnO nanospheres.* **Y. Zhang, Y. Liu, L. Wu, H. Li, L. Han, B. Wang, E. Xie.** 2009, Applied Surface Science , Vol. 255, pp. 4801–4805.

224. *ESR of electron irradiated ZnO confirmation of the F+ center.* **J. M. Smith, and W. E. Vehse.** 1970, Phys. Lett. , Vol. 31A, p. 147.

225. *Interactions hyperfines du centre F+ dans ZnO.* **C. Gonzalez, D. Galland, and A. Herve.** 1975, Phys. Status Solidi B , Vol. 72, p. 309.

List of publications

1. *Thermal activation of nitrogen acceptors in ZnO thin films grown by MOCVD,* **J.K. Dangbégnon**, K. Talla, J.R. Botha, accepted for publication in phys. stat. sol. (c).

2. *Metalorganic Chemical vapour deposition of ZnO:Nusing NO as dopant,* **J. K. Dangbégnon,** K. Talla, K.T. Roro, J.R. Botha, accepted for publication in Physica B: Physics of Condensed Matter (DOI: 10.1016/j.physb.2009.09.017)

3. *ZnO grown by Metal Organic Chemical Vapor deposition: effect of substrate on optical and structural properties,* K. Talla, **J. K. Dangbégnon,** M.C. Wagener and J.R. Botha, accepted for publication in Africa Material

4. *Towards p-type ZnO using post-growth annealing*, **J. K. Dangbégnon**, K. T. Roro, and J. R. Botha, phys. stat. sol. (a) **205**, No. 1, 155–158 (2008).

5. *Influence of metalorganic chemical vapour deposition growth parameters on the luminescent properties of ZnO thin films deposited on glass substrates*, K.T. Roro, **J.K. Dangbégnon**, S. Sivaraya, A.W.R. Leitch and J.R. Botha, J. Appl. Phys. **103**, 1 (2008).

6. *Temperature dependent Hall effect studies of ZnO thin films grown by metalorganic chemical vapour deposition*, K T Roro, G H Kassier, **J K Dangbégnon**, S Sivaraya, J E Westraadt, J H Neethling, A W R Leitch, and J R Botha, Semicond. Sci. Technol. **23**, 055021 (2008).

脈